To the Graduate Council:

I am submitting herewith a thesis written by Hal E. Beck entitled " Simulation of Physiological Signal Processing Mechanisms in the Visual Tract." I have examined the final copy of this thesis for form and content and recommend that it be accepted in partial fulfillment of the requirements for the degree of Master of Science, with a major in Electrical Engineering.

Dragana Brzakovic, Major Professor

We have read this thesis
and recommend its acceptance:

Accepted for the Council:

Vice Provost
and Dean of The Graduate School

STATEMENT OF PERMISSION TO USE

In presenting this thesis in partial fulfillment of the requirements for a Master's degree at The University of Tennessee, Knoxville, I agree that the Library shall make it available to borrowers under rules of the Library. Brief quotations from this thesis are allowable without special permission, provided that accurate acknowledgment of the source is made.

Permission for extensive quotation from or reproduction of this thesis may be granted by my major professor, or in his absence, by the Head of Interlibrary Services when, in the opinion of either, the proposed use of the material is for scholarly purposes. Any copying or use of the material in this thesis for financial gain shall not be allowed without my written permission.

Signature Hal E. Beck

Date 21 July 1990

SIMULATION OF PHYSIOLOGICAL SIGNAL PROCESSING MECHANISMS IN THE VISUAL TRACT

A Thesis

Presented for the

Master of Science Degree

The University of Tennessee, Knoxville

Hal E. Beck

August 1990

Acknowledgements

The author would like to express his appreciation to many people who were a part of his graduate school experience. Thanks to the peers and friends who were there every step of the way. He would like to thank committee members Dr. Lou Gross and Dr. Aso Bishop for their patience in tieing together two very different disciplines. Thanks also to Dan McDonald for his support. In addition, thanks to Bud Mully and Bobbie Kennard with whom the author enjoyed working very much.

To Dr. Dragana Brzakovic, the deep respect and gratitude due her can not be fully expressed. The author can only hope that it is recognized.

Finally, to a little girl and her mother that gave the author the added incentive needed to jump the last hurdle.

Abstract

The main objective of this thesis is to investigate some of the basic physiological mechanisms associated with information processing in the primate visual tract and to apply the concepts developed from the investigation to image processing and pattern recognition tasks. The main hypothesis that is pursued is that physiological information processing systems multiplex information in a time-varying output waveform. Computer simulations that incorporate parameters derived from the neural processes and structures of neuron ensembles that give rise to time-varying output signals are investigated. The simulations include shape analysis, shift invariance, and rotation invariance. Examples of the time-varying neuron output waveforms and the time-varying spatial firing patterns are used to demonstrate the information encoding and transmission.

TABLE OF CONTENTS

CHAPTER		PAGE
1.	**Introduction**	**1**
2.	**Visual Pathways**	**4**
2.1	Retinal Grid	5
2.2	The Physiology of the Retina	8
2.2.1	Synapse Types	11
2.3	Receptive Field	12
2.4	Ganglion Cell Characterization	14
2.5	Considerations for Modelling the Dynamic Retina	16
2.6	The LGN of Primates	24
2.6.1	Considerations for Modeling	28
2.7	Midbrain Projections	29
2.8	Visual Cortex	29
3.	**The Neuron**	**32**
3.1	Ionic Currents	33
3.2	Voltage Potential	34
3.3	Propagation of the Signal	35
3.3.1	Graded Potential Changes	36

CHAPTER PAGE

3.3.2 Action Potentials 37
3.4 Information Encoding at the Single Neuron Level 39
3.4.1 Factors Affecting the Amplitude and Frequency of the Action Potential 40
3.5 Modeling the Neuron 43
3.5.1 The Seminal Model - Hodgkin and Huxley 43
3.5.2 An Analog Implementation 47
3.5.3 Discrete Implementations 49
3.6 Neural Circuitry 51
3.7 Learning and Memory 56
3.8 Fundamental Neural Networks 61
3.8.1 Kohonen: Self-Organization 62
3.8.2 A Physiological Model 64

4. A Time-Varying Neuron Model 67
4.1 The Foundations For a Time-Varying Model 67
4.2 The Neuron Model-With Time Delays and Fixed Firing Threshold Level 72
4.3 An Ensemble of Neurons 77
4.3.1 Architecture of the Ensemble 78
4.3.2 Time-Varying Spatial Characteristics of an Ensemble . . . 81
4.3.3 Time-Varying Characteristics of Single Neurons in the Ensemble 102

CHAPTER PAGE

5. Development of a Layered System 107

5.1 Coarse Encoding 108

5.1.1 Architecture of the Second Layer 108

5.1.2 Time-varying Characteristics of the Second Layer 110

5.1.3 Shape Analysis 126

5.2 Fine Encoding 147

5.2.1 Time-Varying Responses in E1 147

5.2.2 Shape Analysis With Fine Resolution 155

5.3 Rotation and Shift Invariance 159

5.3.1 Rotation Invariance 161

5.3.2 Position Invariance 162

5.4 Incorporating Parameters for Learning and Memory 170

5.5 Clustering Activity With Learning and Memory Mechanisms . . 178

5.5.1 The Architecture of the System 178

5.5.2 Learning and Memory For Clustering 179

5.5.3 Clustering Activity 181

6. Conclusions 185

BIBLIOGRAPHY 188

VITA 194

LIST OF FIGURES

FIGURE		PAGE
2.1	Overview of the visual processes.	6
2.2	The structure of the retina.	8
2.3	Schematic representing visual angle.	18
2.4	The structure of the LGN.	25
3.1	The neuron.	33
3.2	Changes in the membrane potential at the hillock.	37
3.3	Hodgkin-Huxley equivalent circuit.	44
3.4	Voltage-controlled oscillator model.	48
3.5	Possible neuron-neuron interactions.	53
3.6	Efferent connections.	55
3.7	Possible circuits.	60
3.8	Kohonen spatial organization for weight adaptation.	62
4.1	Receptive field structure.	79
4.2	Spatial profile of the receptive field.	80
4.3	(a): Input: Half excitatory field coverage.; (b): T = 5 ; (c): T = 6 ; (d): T = 15	86
4.4	(a): T = 16; (b): T = 25; (c): T = 26; (d): T = 35	87
4.5	(a): Input: Half excitatory and inhibitory field coverage; (b): T = 5; (c): T = 6; (d): T = 10; (e): T = 16; (f): T = 26	89

4.6 (a): T = 31; (b): T = 36; (c): T = 45; (d): T = 46 90

4.7 (a): Input: Full excitatory field coverage; (b): T = 5; (c): T = 6; (d): T = 15; (e) T = 16 91

4.8 (a): Input: Full excitatory and inhibitory field coverage; (b): T = 5; (c): T = 6; (d): T = 10 92

4.9 (a): T = 16; (b): T = 26; (c): T = 31; (d): T = 46 93

4.10 (a): Input: Half excitatory and partial inhibitory field coverage; (b): T = 5; (c): T = 6; (d): T = 15; (e): T = 16:; (f): T = 25 . 95

4.11 (a): T = 26; (b): T = 35; (c): T = 36 96

4.12 (a): Input: Full excitatory and partial inhibitory field coverage; (b): T = 5; (c): T = 6; (d): T = 15; (e): T = 16; (f): T = 25 . . 97

4.13 (a): T = 26; (b): T = 35; (c): T = 36 98

4.14 (a): Input: Full excitatory and partial inhibitory field coverage; (b): T = 5; (c): T = 6; (d): T = 15; (e): T = 16; (f) T = 25 . . 99

4.15 (a): T = 26; (b): T = 35; (c): T = 36; (d): T = 45; (e) T = 46 . 100

4.16 Response profiles of E_c (a): Case (a); (b): Case (b); (c): Case (c); (d): Case (d) 103

4.17 Response Profiles of E_c (a): Case (e); (b): Case (f); (c): Case (g); (d): Case (b) middle; (e) Case (d) edge 104

FIGURE **PAGE**

5.1 Response Profiles of E_C in $E2$ (a): case a: Half excitatory field coverage; (b): case b: Half excitatory and inhibitory field coverage; (c): case c: Full excitatory field coverage; (d): case d: Full excitatory and inhibitory field coverage 113

5.2 Response Profiles of E_c in $E2$: (a): case e: Half excitatory and partial inhibitory field coverage; (b): case f: Full excitatory and partial inhibitory field coverage; (c): case g: Full excitatory and partial inhibitory field coverage 114

5.3 (a): Input: Half excitatory and inhibitory field coverage; (b): T = 8; (c): T = 9; (d): T = 14; (e): T = 19; (f): T = 29 116

5.4 (a): T = 30; (b): T = 35; (c): T = 49; (d): T = 50 117

5.5 (a): Input: Full excitatory field coverage; (b): T = 8; (c): T = 9; (d): T = 18; (e): T = 19; (f): T = 28 118

5.6 (a): T = 29; (b): T = 30; (c): T = 38; (d): T = 39 119

5.7 (a): Input: Full excitatory and inhibitory field coverage; (b): T = 8; (c): T = 9; (d): T = 14; (e): T = 29; (f): T = 30 120

5.8 (a): T = 35; (b): T = 36; (c): T = 49; (d): T = 50 121

5.9 (a): Input: Full excitatory and partial inhibitory field coverage; (b): T = 8; (c): T = 9; (d): T = 10; (e): T = 19; (f): T = 20 . . 122

5.10 (a): T = 28; (b): T = 29; (c): T = 30; (d): T = 39; (e): T = 40 123

5.11 (a): Input: Full excitatory and partial inhibitory field coverage; (b): T = 8; (c): T = 9; (d): T = 10; (e): T = 18; (f): T = 19 . . 124

FIGURE **PAGE**

5.12 (a): T = 20; (b): T = 28; (c): T = 29; (d): T = 30; (e): T = 38; (f): T = 39 125

5.13 Response profiles(a): Input: Diameter=13; (b): Input: Diameter=15; (c): Response SI=SE=13, CI=CE=5 to (a); (d): Response SI=SE=13, CI=CE=5 to (b); (e): Response SI=SE=15, CI=CE=7 to (a); (f): Response SI=SE=15, CI=CE=7 to (b) . 127

5.14 Response profiles of E_c to (a): Circle; (b): Square; (c): Cross; (d): Rectangle 129

5.15 Layer $E1$(a): Input: D=13; (b): T=5; (c): T=6; (d): T=10; (e): T=16; (f): T=26 130

5.16 (a): T=31; (b): T=46; (c): T=51 131

5.17 Layer $E2$ (a): T=8; (b): T=9; (c): T=14; (d): T=29; (e): T=30; (f): T=34 132

5.18 (a): T=35; (b): T=41; (c): T=49; (d): T=50 133

5.19 Layer $E1$ (a): Input: square; (b): T=5; (c): T=6; (d): T=10 . . 135

5.20 (a): T=16; (b): T=26; (c): T=31; (d): T=46 136

5.21 Layer $E2$ (a): Input: square; (b): T=8; (c): T=9; (d): T=14; (e): T=29; (f): T=30 137

5.22 (a): T=35; (b): T=36; (c): T=49; (d): T=50 138

5.23 Layer $E1$ (a): Input: cross; (b): T=5; (c): T=6; (d): T=10; (e): T=16; (f): T=26 139

5.24 (a): T=31; (b): T=46; (c): T=51; (d): T=66 140

5.25 Layer $E2$ (a): T=8; (b): T=9; (c): T=14; (d): T=29; (e): T=30; (f): T=35 141

5.26 (a): T=49; (b): T=50; (c): T=55 142

5.27 Layer $E1$ (a): Input: rectangle; (b): T=5; (c): T=6; (d): T=10; (e): T=16; (f): T=26 143

5.28 (a): T=31; (b): T=36; (c): T=45; (d): T=46; (e): T=51 144

5.29 Layer $E2$ (a): T=8; (b): T=9; (c): T=14; (d): T=19; (e): T=29; (f): T=30 145

5.30 (a): T=35; (b): T=49; (c): T=50 146

5.31 Response profiles of E_c in layer $E1$, Inp delay =1: (a): Input: Diameter=13; (b): Input: Diameter=15; (c): Response SI=SE=13, CI=CE=5 to (a); (d): Response SI=SE=13, CI=CE=5 to (b); (e): Response SI=SE=15, CI=CE=7 to (a); (f): Response SI=SE=15, CI=CE=7 to (b) 149

5.32 Layer $E1$ activity, Input delay=1, SI=SE=13: (a): Input; (b): T=5; (c): T=6; (d): T=7; (e): T=10; (f): T=20 150

5.33 Layer $E1$ activity, Input delay=1, SI=SE=13: (a): T=21 ; (b): T=22; (c): T=23; (d): T=25; (e): T=26; (f): T=27 151

5.34 Layer $E1$, Input delay=1, SI=SE=15 :(a): Input; (b): T=6; (c): T=7; (d): T=8; (e): T=9; (f): T=11 152

5.35 Layer $E1$, Input delay=1, SI=SE=15: (a): T=12; (b): T=16; (c): T=17; (d): T=18 153

FIGURE **PAGE**

5.36 Response profiles of E_c in layer $E2$, Input delay=10, E2 Reversed fields: (a): Circle; (b): Square; (c): Cross; (d): Rectangle 156

5.37 Response profiles of E_c in $E2$, Input delay=1, E2 Reversed Fields: (a): Circle; (b): Square; (c): Cross; (d): Rectangle 158

5.38 Response profiles of E_c in layer $E2$, Input delay=1, E2 Non-reversed fields: (a): Circle; (b): Square; (c): Cross; (d): Rectangle 160

5.39 Position invariance, Layer $E1$, Input delay=1: (a): T=10; (b): T=10; (c): T=11; (d): T=11 163

5.40 Position invariance, Layer $E1$, Input delay=1 (a): T=15; (b): T=15; (c): T=16; (d): T=16 164

5.41 Position invariance, Layer $E2$, Input delay=1: (a): T=13; (b): T=13; (c): T=14; (d): T=14 165

5.42 Position invariance, Layer $E2$, Input delay=1 (a): T=16; (b): T=16; (c): T=17; (d): T=17 166

5.43 Response Profiles for Rotation Invariance: (a): Vertical; (b): Horizontal 167

5.44 (a): Input–cross, Spikes in layer $E2$, no learning; (b): Input–cross, Spikes in layer $E2$, with learning; (c): Input–rectangle, Spikes in layer $E2$, no learning; (d): Input–rectangle, Spikes in layer $E2$, with learning 173

FIGURE **PAGE**

5.45 (a): Input–square, Spikes in layer $E2$, no learning; (b): Input–square, Spikes in layer $E2$, with learning; (c): Input–circle, Spikes in layer $E2$, no learning; (d): Input–circle, Spikes in layer $E2$, with learning 174

5.46 The Differences After Learning (a): Square: Max Difference=10; (b): Circle: Max Difference=10; (c): Cross: Max Difference=11; (d): Rectangle: Max Difference=8 175

5.47 Response profiles of E_c (a): Cross no learning; (b): Cross with Learning; (c): Rectangle no learning; (d): Rectangle with Learning176

5.48 Response profiles of E_c (a): Square no learning; (b): Square with Learning; (c): Circle no learning; (d): Circle with Learning . . . 177

5.49 Spike distribution with clustering (a): Circle; (b): Cross; (c): Square; (d): Rectangle 184

CHAPTER 1

Introduction

Engineers in the field of image processing and pattern recognition draw from many sources, including engineering, psychology, computer science, and physiology, to find solutions to the problems they confront. In this thesis, the physiological aspects of visual processing are investigated. The objective is to identify specific physiological mechanisms used for feature extraction, information encoding and transmission, and pattern recognition; and to develop computer simulations of these mechanisms to perform basic image processing tasks.

The main hypothesis of this thesis is that the signal processing mechanisms of physiological neurons encode information in a manner that results in a temporal modulation of the output waveform, and that software simulations of basic physiological neural mechanisms will result in a time-varying waveform that uniquely describes the information encoded by a model neuron unit. The work in this thesis has drawn from three sources to support this hypothesis: physiology, neural network classifiers, and the simulations developed in this work.

The first two chapters of this thesis are devoted to physiology. The issues discussed in each are only those issues that have had a direct bearing on the simulations that are presented here. There are many issues that could have been

included, and, indeed, those discussed could each be extended into a thesis.

In Chapter 2, the structure of the primary visual pathway is discussed. The picture that emerges from this chapter is a highly organized system with multiple levels of processing performed in parallel. Structure and function at each level of processing, from the system as whole to the receptive field of the individual neuron, are shown to be inextricably tied to one another. In Chapter 3, the dynamics of signal processing for individual neuron units is developed. Membrane properties and ionic flow are shown to be basic to the processing carried out on the single cell level. The membrane structure is shown to be a signal processing system in miniature. Learning and memory mechanisms operate on the level of the single neuron with consequences that affect the behavior of the entire system due to the dynamics of information transmission throughout the visual pathway.

At every level the physiological mechanisms and structure involved in visual processing are shown to be compatible with a time-varying output neuron model. Chapters 4 and 5, are devoted to the simulations. Chapter 4 presents the basic neuron model used for all the simulations, including the basic structure of the receptive field. The behavior of an ensemble under various parameter changes is demonstrated. In Chapter 5, the simulations are extended to include some of the structure and functions discussed in Chapter 2. Shape analysis, multiple resolution processing, and rotation and shift invariance are discussed in terms of the time-varying spatial patterns of an ensemble and the time-varying output

waveforms of single cells in the ensemble during a peristimulus interval. In addition, the learning and memory mechanisms are simulated and are shown to modulate the time-varying output waveforms of single cells and to alter the time-varying spatial patterns within an ensemble. The learning and memory rules are used to perform clustering.

In Chapter 6, the work presented in this thesis is summarized and the main contribution is stated. Further development of the basic simulations presented in this work are necessary before a practical application is viable. This work does provide a foundation for some potentially powerful tools in the field of image processing/pattern recognition.

CHAPTER 2

Visual Pathways

The process of designing a neuron model for a neural network is guided by the designer's understanding of the physiological structure and dynamics and the task at hand. The main objective of this thesis is to develop a neuron model whose response is characterized by a time-varying waveform and to incorporate the model into a system for visual processing. Therefore, the physiological structures involved in the major visual processing pathways are discussed and the basis for the model developed in this work is established. Two pathways are investigated. The first pathway is concerned with visual recognition; the second with spatial localization. Each is discussed separately and then the interaction between the two pathways is made apparent.

Tracing the neural pathways of the visual system reveals separate tracts for different cell-types. The cell-types are traced to highly structured processing centers in the visual system, *e.g.*, retina, diencephalus, primary visual cortex, and inferior temporal lobe. Each center has regions which are predominately of one cell-type and other regions which are a combination of cell-types. At every level, each cell-type is found to have its own pathway through the visual system and, presumably, its own function. A highly organized structure is apparent

from the first level of processing, at the retina, to the primary visual cortex.

This discussion begins with a look at the structure of the retina leading to the optic nerve. Five major cell types are involved in the two pathways from the retina to the optic nerve. Photoreceptors, bipolar cells, and ganglion cells connect vertically in the most direct path. Between the photoreceptor and bipolar cells are horizontal cells. Amacrine cells are found in a layer between the bipolar cells and ganglion cells. A strong correlation between structure and function is demonstrated. This correlation is shown to be maintained throughout the visual system.

2.1 Retinal Grid

The characteristics of the retina are discussed in detail since the basic structures and dynamics common throughout the visual system are found here. In addition, the distribution of the cone and rod mosaic of the retina define the acuity of the visual system and, coupled with the retinotopic mapping, the relationship of the visual field to the various processing centers can be understood.

The structure of the primary visual pathway (Fig. 2.1) reveals a great deal about information processing in the retina. The retina has a sharp vertical boundary which passes directly through the fovea. Cells temporal to this line trace ipsilaterally to the brain, while cells nasal to this line decussate at the optic chiasm and trace contralaterally to the brain. A narrow region lying directly

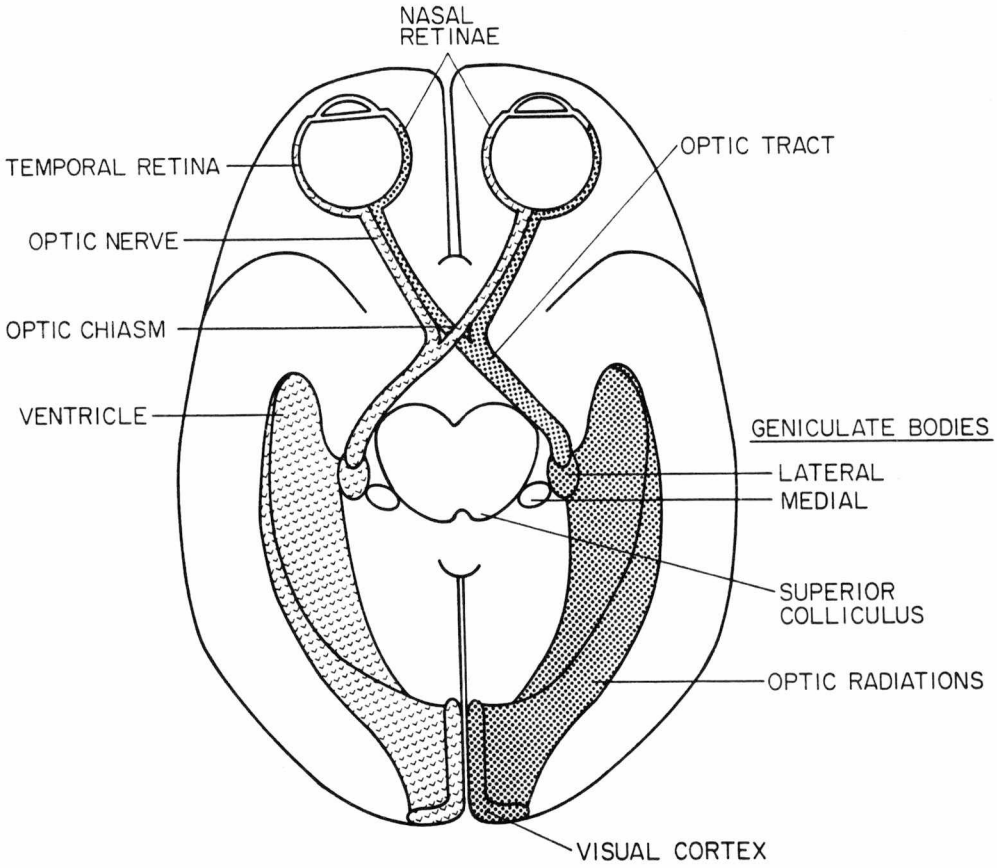


Figure 2.1: Overview of the visual processes.

on this line is composed of a combination of ipsilateral and contralateral cells. In addition to the vertical axis, a horizontal axis passes through the center of the retina. Surrounding this axis are cell isodensity lines with decrementing densities away from the axis center. The entire region, mainly a feature of the nasal side of the vertical axis, is termed the visual streak. Cell bodies are much smaller and much more densely packed here than in the periphery. Along the axis, the number of ganglion cells approaches the number of receptors [1].

The most central region of the retina, the macular region, is further divided into subregions. The inner most region is the foveola, which has a diameter of approximately $0.35mm$. Around this is the fovea, which has a diameter of approximately $1.9mm$. The outer annulus, the macula, has a diameter of approximately $5.5mm$. The foveola and fovea are predominately cone populated regions, estimates of which vary from $100,000$ to $200,000$ cones. The bipolar and ganglion cell processes are displaced to an annulus outside of this region [2]. The function of the cone pathway is visual acuity and color perception. The rods dominate the peripheral areas and their function is low intensity perception; in addition, low spatial frequency perception and motion detection are considered to be functions of the rod dominated regions.

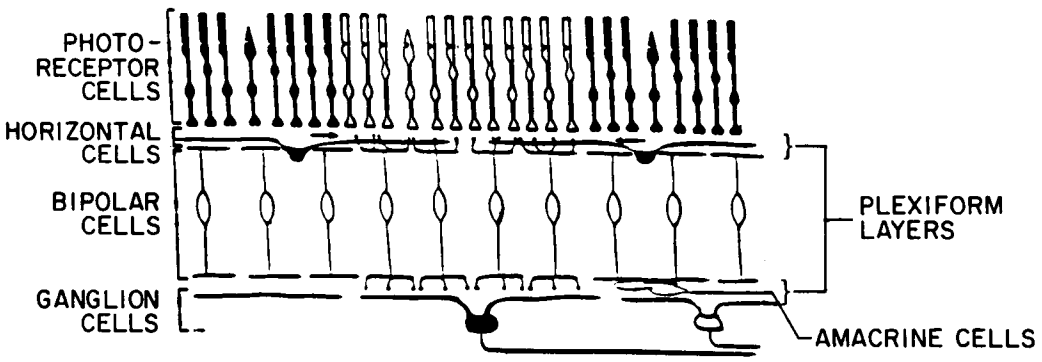


Figure 2.2: The structure of the retina.

2.2 The Physiology of the Retina

The retina is not merely a two dimensional array of rods and cones, but a highly complex structure whose function must be considered in terms of the two dimensional arrangement of the photoreceptors and, also, in terms of the pathways from these photoreceptors to the optic nerve. The information pathway through the retina is discussed first [3]. Second, the two dimensional structure is discussed. The basic structure of the pathway through the retina is shown in Fig. 2.2.

The retina is composed of three nuclear layers and two synaptic (plexiform) layers. Beginning at the most distal part of the retina, rods and cones perform the task of changing light energy into nerve impulses. The mechanism for this process is the breakdown of visual pigments - rhodopsin in the rods and iodopsin in the cones. Thus, the visual nerve impulse begins with a chemical encoding

of light. The length of the cones vary from $85\mu m$ in the fovea to $40\mu m$ in the periphery. The rods vary from $40\mu m$ to $60\mu m$. The nuclei of the rods and cones lie in the outer nuclear layer and their fibers continue into the external plexiform layer. The external plexiform layer is the first synaptic layer. The dendrites of bipolar cells and the processes of the horizontal cells extend into the external plexiform layer and synapse with rod spherules and cone pedicles, the synaptic processes of the rods and cones respectively. Typically, large numbers of photoreceptors converge on a single bipolar cell; although, in the fovea a bipolar may synapse with a single cone pedicle. The horizontal cells spread over relatively long distances connecting large numbers of photoreceptors. The nuclei of the bipolar and horizontal cells are in the inner nuclear layer.

Although there are many types of bipolar cells, three types are typically cited: rod bipolars, which have large dendritic arborizations and synapse only with rod spherules; midget bipolars, which are relatively small and synapse only with cone pedicles; and flat bipolars, which contact only cone pedicles. The axons extend through the internal plexiform layer and into the most proximal retinal layer, the ganglion cell layer, where they form synapses with the dendrites and the somata of the ganglion cells. The bipolar cells synapse with anywhere from a relatively large number of ganglion cells to, in the case of midget bipolars, only a single ganglion cell [3].

The horizontal cells show a wide range of lateral spread and synaptic specificity. It is generally accepted that two types of horizontal cells dominate the

retina: type A, synapsing with a number of cone pedicles, bipolar cells, and other horizontal cells; and type B, synapsing with rods, bipolar cells, and other horizontal cells. The synapse sites on each may be both presynaptic and post-synaptic, transmitting information in both directions [3].

The amacrine cells make up a third cell-type found in the inner nuclear layer. They form complex connections between bipolar axons and ganglion dendrites and somata in the inner plexiform layer [2]. Like horizontal cells, they can be both presynaptic and postsynaptic at all sites [3].

Recent research [4] indicates that the function of different amacrine cells can be determined by the cell shape and the specific neurotransmitter released by each cell; and, in fact, the cell shape and neurotransmitter are interrelated. The results show a large number of amacrine cells - perhaps as many as 30 distinct types. One set of amacrine cells responds to light with an immediate burst of action potentials which fades away with constant stimulation. This transient response is thought to be a mechanism for sharpening the ganglion cell response.

Amacrine cells also have a role in some very selective ganglion cell responses. For example, some ganglion cells are known to be directionally selective. These cells are often seen to resolve spots of moving light that are smaller than one would expect the cells would be able to resolve. A second set of amacrine cells seems to provide an explanation for this phenomenon. The amacrine cell, which releases its neurotransmitter locally to ganglion cells, responds to stimulation with a graded and locally constrained response. This could provide a mechanism

for hyper-acuity by raising the membrane potential closer to the firing threshold.

Another type of amacrine cell connects rod-driven bipolar cells to ganglion cells. The rod driven bipolar cells do not have a direct synapse to ganglion cells; instead, the bipolar cells are linked to the ganglion cells through an amacrine cell. These cells may be the mechanism that allows ganglion cells to function in both low and high intensity light. There are many other amacrine cell types in the neural pathways, the function of most are not presently known.

The ganglion cell layer is discussed in detail in Section (2.4). In the central retina, the predominate ganglion cell type is the midget ganglion. The midget ganglion cells are often linked to a single cone receptor by a single midget bipolar. The same cone may be connected to more than a single bipolar. In the peripheral retina, the predominate ganglion cell is polysynaptic. These cells have wide dendritic fields and can synapse with hundreds of bipolar cells [3].

The distal neurons (receptors, horizontal cells, and bipolar cells) and certain amacrine cells hyperpolarize in response to stimulation in a sustained graded potential. The proximal neurons - amacrine cells and ganglion cells - depolarize in reponse to stimulation with a spike train superimposed on the changing potential [3].

2.2.1 Synapse Types

There are two prominent types of synapses in the retina. Each is found in both plexiform layers. The first type, ribbon synapses, are characterized by

a negatively charged ion dense ribbon in pre-synaptic cytoplasm surrounded by a cluster of synaptic vesicles. Multiple post-synaptic junctions are found along ribbon synapses. The second type of synapse is the conventional synapse, characterized by a cluster of vesicles in the pre-synaptic terminals near the presumed synaptic sites. A third, less prominent synapse, is the basal synapse which is characterized by electron-dense material found on both pre-synaptic and postsynaptic membranes, as well as in the synaptic cleft. There are no ribbons or clusters of synaptic vesicles associated with basal synapses.

Synapses found in the outer plexiform layer are: basal synapse at receptor to bipolar (flat bipolar), ribbon synapse at receptor to bipolar (invaginating bipolar), ribbon synapse at horizontal to receptor and horizontal to horizontal. Synapses found in the inner plexiform layer are: ribbon synapse at bipolar to amacrine and bipolar to ganglion, conventional synapse at amacrine to bipolar, amacrine to ganglion, and amacrine to amacrine [3]. A more in depth and sometimes contradictory review is given in [5].

2.3 Receptive Field

The response of every neuron in the retina can ultimately be traced back to a localized region of photoreceptors. The links may be direct pathways or may be indirect pathways through lateral processes. This region is known collectively as the receptive field of the neuron. The receptive field of neurons higher in the

visual tract is composed of neurons from lower levels and at the same level as the particular neuron. Thus, the response profiles of these cells are the result of the cumulative inputs from a complex composite of cells. The shape of a receptive field is roughly circular and is made up of a central area, corresponding to the direct pathway, surrounded by an annulus, corresponding to the lateral pathway.

The interactions in the receptive field are discussed for the pathway involving invaginating midget bipolar cells in the fovea. Light hyperpolarizes the photoreceptors causing a decrease in the amount of inhibitory transmitter released at the ribbon synapses. The bipolar cell is less inhibited and depolarizes. This results in an increase in the amount of transmitter released at the ribbon synapses, at the center of the receptive field structure, causing the ganglion cell to fire at an increased rate. At the same time, the surround responds in an antagonistic manner. The decreased amount of transmitter released by the hyperpolarized photoreceptor causes the horizontal cells to hyperpolarize; less excitatory transmitter is released to the bipolar cell and it responds with less activity. This type of arrangement is of an on-centered bipolar receptive field, the term coming from the depolarization of the bipolar due to the central stimulation and the hyperpolarization due to the surround. An off-center arrangement is similar, except the bipolar is a flat bipolar and responds in the opposite manner to the invaginating midget bipolar. Analogous paradigms hold for ganglion cells [3] with the input from amacrine cells providing mechanisms for the **W**, **X**, and **Y** cell characteristics, which are discussed in Section (2.4).

Two other horizontal cell synapses play a role in the surround activity. The horizontal cells also synapse through ribbon synapses with the photoreceptors, providing a feedback loop and depolarizing the photoreceptors. Ribbon synapses extend the lateral range of the horizontal cell receptive field.

2.4 Ganglion Cell Characterization

Extensive work has been done in the area of retinal ganglion cell classification. The classification of ganglion cells, as well of the other cells found in the retina, can become very involved and cumbersome. The different classification schemes result from different measurement techniques and from the choice of parameters used to characterize the cell. The choice of taxa in the following comes from the arguments presented in [1,6] in which the cells are categorized into **W**, **X**,and **Y** cells. The usefulness of this scheme also lies in its adaptability to a large range of species' visual systems and is reflected in the extensive reference to these categories in phsiological research.

The **X** and **Y**cells can be characterized by two antagonistic concentric receptive fields; each cell being either on or off centered, reflecting the cells response to the nature of the stimulus (light or dark). The **X**-cells sum the illumination on their receptive fields in a linear fashion. Their response can be characterized by a single Difference Of Gaussian (**DOG**) operator with optimal tuning for high spatial frequency stimuli. Functionally, the cells serve acuity tasks.

The conduction velocities are slower than the **Y**-cell velocities.They are the predominant cell in the retinal centralis. The **Y**-cells have a non-linear response to light, *i.e.*, the **Y**-cells' response can be characterized by the **DOG** operator with additional summing from local overlapping subunits. These subunits can be modeled as half-wave rectifiers summing locally (thus the nonlinear response to stimulation). **Y**-cells respond to low spatial resolution for pattern vision and to high frequency flicker for detection of movement. They also have the fastest conduction velocities and are found to be the predominate cell in the periphery of the retina.

W-cells are not as clearly defined as the other two and, in fact, this class has been a catch-all for any cell not exhibiting either **X** or **Y** cell characteristics. They seem to be used in ambient vision. Perhaps, they serve to focus the gaze or to perform some low level resolution processing. In addition, they do not seem to be as important in regards to human vision (as far as current research shows).

As a comparative note, much of the work done with retinal cell ganglion cells has been done with cats and monkeys. It is interesting to note that the differentiation between **X** and **Y** cells is much more marked, both spatially and functionally, in the monkey than in the cat. In addition, **W**-cells are much less prominant in the monkey than the cat. Comparison with other species' visual systems reveals the development of perceptual systems from the vantage point of evolution. A developmentally directed review of the literature could also add

a great deal to the understanding of our perceptual system, but is not pursued in this thesis.

The evidence is overwhelming for separate neural pathways of each cell type to cortical regions associated with visual processing, which lends support to the concept of separate cell function and parallel processing. By next examining these pathways, some insight into possible processing schemes can be gained.

2.5 Considerations for Modelling the Dynamic Retina

The cone mosaic is a grid of photoreceptors that samples, spatially and temporally, the visual field, and as such, defines the spatial limits of acuity from a sampling theory point of view. The pattern and spacing of cones in the central most region of the retina are discussed in terms of spatial frequency and visual angle. The constraint is that the eye remains static.

Data on the foveal area varies with the technique used to isolate and mount the retinal material and the age of the individual from which the retina came. In addition, approximations of the photoreceptor shape, foveal shape, and mosaic spacing (hexagonal or rectangular) affect the final estimations.

An exhaustive study of the foveal cone mosaic has been done in [7]. This study provides a breakdown of the data based on age. The average diameter of the rod-free region is about $680\mu m$ in the middle-age adult and the average receptor width is $1.0\mu m$ *to* $1.25\mu m$. The density ranges from 42 cones per

$100\mu m$ at 37 years old to 32 cones per $100\mu m$ at 72 years old. All assumptions are based on a hexagonal packing of the cones. Counts in the central most $250\mu m$ are considered to be the most accurate. The photoreceptor densities are calculated by:

$$total\ number\ of\ cones\ in\ a\ given\ area = \frac{\pi r^2}{\frac{6a^2}{\sqrt{3}}}(\mu m)^2, \tag{2.1}$$

where a is the average cone center-to-center distance divided by 2, and r is the radius of the region under investigation. The average cone center-to-center distance is the reciprocal of a divided by 2. The density is given by:

$$density = \frac{total\ number\ of\ cones\ in\ a\ given\ area}{total\ area\ (mm^2)}. \tag{2.2}$$

In this region, the density ranges from around 180.0×10^3 *to* 210.0×10^3 cones per mm^2 [7]. From this data, the relationship of the outside world to the retinal image can be defined.

Physiologists and psychophysiologists define visual acuity in terms of neuronal responses to textured images which can be classified in cycles per degree of visual angle. Fig. 2.3 is a simplified schematic for the purpose of discussing visual acuity. Assuming a sinusoidal stimulus, the number of cycles of the sine function crossing one degree of visual angle gives the spatial frequency of the stimulus. In reference to Fig. 2.3, x is the distance from the nodal point along the visual axis to the retina ($17mm$), y is the eccentricity of the image due to the optics of the eye, and θ is the visual angle. The model assumes that the visual axis divides the fovea into symmetric parts. The visual angle is then calculated

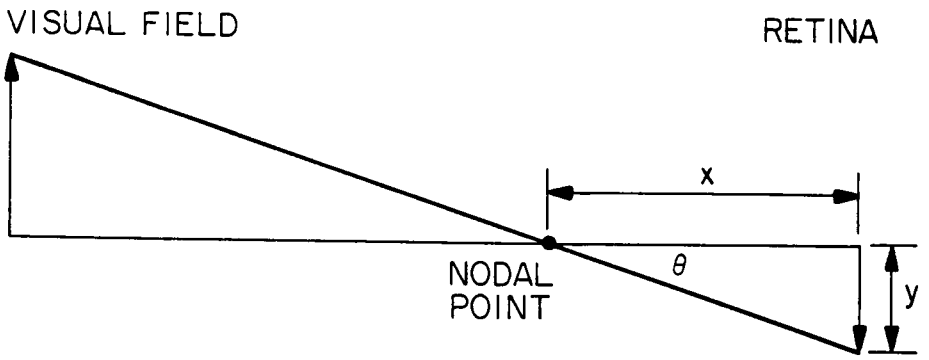


Figure 2.3: Schematic representing visual angle.

by:

$$\theta = tan^{-1}(\frac{y}{17}),$$

The average distance between the centers of two adjacent photoreceptors is approximately $2.33\mu m$, which corresponds to a visual angle of 0.00785^0 or approximately $0.5arc - min$.

From sampling theory, the highest resolvable spatial frequency, the cut-off frequency (f_c), is $\frac{1\ cycle}{arc-min}$, or $\frac{60\ cycles}{visual\ degree}$. This, in fact, is the approximate upper limit on visual acuity. The visual angle subtended by the central most $250\mu m$ is approximately 1.0 degrees of visual angle; the angle subtended by the $680\mu m$ diameter is approximately 2.3 degrees.

According to sampling theory, any spatial frequency (f_a) higher than the cut-off frequency will add energy to the lower frequencies and, in the case of a sinusoidal grating, will be seen as a frequency $f_a - f_c$. This is known as the alias-

ing problem. From the photoreceptor spacing, aliasing is expected for any spatial frequency higher than $\frac{60\ cycles}{degree}$. This does not seem to be the case, however. For example, in sinusoidal grating tasks, frequencies higher than $\frac{60\ cycles}{degree}$ are simply not resolved [8]. Two possible solutions to this puzzle are the constant movements of the eye – optokinetic nystagmus, saccades and slow drift, and neural interactions – time delays, receptive field characteristics, and refractory periods.

The above discussion assumes a static retinal image, a situation that will cause blurring due to the characteristics of neurons. Instead, the eye is constantly in motion, *e.g.*, saccades, slow drift, and optokinetic nystagmus, each one supporting a different task but ultimately providing the same effect – bringing the retinal image from the peripheral retina to the fovea, followed by high resolution visual inspection.

A discussion of the role of saccadic eye movement in visual inspection is given in [9,10]. The author's work is in response to earlier work by Kelly [11,12,13] in which it was established that the natural eye drift frequency is between 0.05 $\frac{deg}{s}$ *to* 0.2$\frac{deg}{s}$. This is the experimentally determined optimal detection frequency for images under a continuous velocity and a stabilized retina. Kelly hypothesized that saccades are too fast for such detection tasks. In [9,10] the authors determined that, for specific stimuli, saccades continue even after the retinal image is brought to the fovea. In fact, small saccades, together with drift movements and tremors of the eyes form a continuous, involuntary, pattern of oculomotor activity. The specific stimuli are low spatial and low temporal

frequencies or high temporal frequencies (flicker). For low spatial frequencies ($0.5\ \frac{cycles}{degree}$), saccades as large as 1 *degree* in amplitude are seen. An example of a pattern of low spatial frequency and low temporal frequency is a luminous step. The observed saccadic movement is a continuous change in fixation from one side of the step to the other. A high frequency pattern is an array of flickering lines. The observed saccadic movement in both cases is small amplitude saccades. The optimal saccade should be half the period of the grating – which is the approximate frequency of the saccades for both of these patterns. The authors conclude that for near threshold tasks, the eye uses all movement resources at its disposal.

In addition to spacing and eye movements, time delay differences between cells also affect an analysis of the sampling dynamics of the eye. Recent studies have called into question the commonly accepted definition of *receptive field* which assumes a representable impulse response as a function solely of position relative to a central point. Instead, the relationship between the surround and center strengths, surround delay with respect to the central response, and the extent of the surround can all vary with temporal frequency [14]. Data from primate recordings is presented in [15] and a model is derived from the data. In this model the mechanisms for the x-type of ganglion cell response are shown to be available at the outer plexiform layer and, in fact, are generated at the bipolar cell.

Considering only the cone network in the area of the fovea, the spatial profile

of bipolar cell receptive fields is well known and is described in the following and is taken largely from [14]. Recall that the bipolar cell has two regions of excitability, termed together as the bipolar cell's receptive field. The dendrites of the bipolar cell synapse in the outer plexiform layer with two types of cells (cones and horizontal cells). The cones comprise the center of the bipolar's receptive field. The response due to the cones is the first term in Eq. (2.3). The horizontal cells comprise the surround of the bipolar cell. The response due to the horizontal cells is the second term in Eq. (2.3). Together, the cones and horizontal cells sum across their expanse, beginnig at the bipolar dendrites, and produce the well known DOG bipolar cell response profile (BR):

$$BR(i,j) = \frac{A}{\sqrt{2\Pi}\sigma_c} e^{\frac{-(i^2+j^2)}{2\sigma_c^2}} - \frac{B}{\sqrt{2\Pi}\sigma_s} e^{\frac{-(i^2+j^2)}{2\sigma_s^2}}, \tag{2.3}$$

where A and B are the center and surround strengths, respectively, i and j are the locations in the receptive field represented by a 2-D array and the origin at the center, and σ_c and σ_s are the center and surround space constants, respectively. Also as mentioned, there are two forms of the DOG which have been recorded at the bipolar level. The on-centered X-cell response is from summation due to the cones and resulting in a positive sensed gaussian and the summation due of the horizontal cells and resulting in a negative sensed gaussian. The signs of A and B are reversed in the response of the off-centered X-cell. The retinal mosaic is completely covered by both forms of bipolar cells, independently, and defines the values of parameters A, B, σ_c, σ_s. The values for σ_c and σ_s dictate the limits of spatial acuity as constrained on the system at the bipolar level.

The convolution integral describes the processing from the cones to the bipolar cells.

$$f(x,y)\otimes g(x,y) = \int_{-\infty}^{\infty}\int_{-\infty}^{\infty} f(\alpha,\beta)g(x-\alpha,y-\beta)d\alpha d\beta. \qquad (2.4)$$

Neurological recordings from single bipolar cells indicate that the cells integrate over their receptive fields, as modeled by the convolution integral. As indicated in Fig. 2.3, the image array is 'flipped' with respect to a coordinate system orthogonal to the visual axis. The image projected onto the cones is represented by $f(\alpha,\beta)$; the DOG filter is represented by $g(x-\alpha,y-\beta)$.

Invaginating midget bipolar cells synapse in sublamina a of the inner plexiform layer, which is where the on-centered responses have been measured. The flat bipolar cells synapse in sublamina b of the inner plexiform layer. The time responses of each are similar to the charging and discharging of a capacitor and the spatial responses are modeled by the difference of gaussians. The time constant for the center response is 10 ms and the time constant for the surround is 20 ms. The surround is delayed in relation to the center by 3 ms. The space constant ratio is 1.75. The center spread for the on-centered cells is $80''$ and the off-centered cells is $150''$. The time dependent response is:

$$R(t) = C(1-e^{\frac{-t}{10}}) - S(1-e^{\frac{(t-3)}{20}}), \qquad (2.5)$$

where C and S are the relative center and surround strengths.

The Y-type of response is modeled by pooling the response of a number of bipolar cells in the inner plexiform layer, taking the derivative with respect to

time, and rectifying the negative signals. In addition, the y-type response is transient, not sustained. The dyad, a composite of the processes at the synapse, provides a mechanism for a derivative operation in the bipolar cells. The recursive synapse from the amacrine cell to the bipolar cell, if inhibitory and with a strong enough synapse would perform the derivative operation. The radius of the bipolar cell field for a given ganglion cell is 100 μm [15].

The number of cells in a given area indicates the amount of receptive field overlap between neurons. In the rod-free central portion of the retina, for each cone pedicle there are two to three bipolar cells, 0.6 horizontal cells, 0.7 amacrine cells, and 0.9 ganglion cells. The synaptic pedicles of these cones are located in an annular zone surrounding the central region. Each cone in the central region may be connected to both an invaginating bipolar cell and to a midget bipolar cell [16].

The objective of citing the above data is to provide the building blocks for modelling the interactions in the retina which include time delays, signal decays and receptive field characteristics to capture the time-varying characteristics of neural behavior. In addition, the sampling dynamics of the physiological system have been discussed to emphasize both the spatial and the temporal factors inherent in the physiological signal processing system. In fact, each feature is directly related to the others.

2.6 The LGN of Primates

The Lateral Geniculate Nucleus (LGN) of the thalamus is located in the diencephalon. Most ganglion cells leaving the retina converge on relay cells of the LGN on the way to the primary visual cortex. The nucleus is retinotopically organized, and, as with many other regions in the visual tract, the LGN has a disproportionate amount of area dedicated to foveal processing. For a detailed discussion of the retinotopic mapping outlining the isoelevation and isoazimuth lines projected from the visual field see [17]. In addition, the magnification factor per angle of the visual field is discussed in terms of the mapping from the retina to the striate cortex.

As with other structured areas, different taxa are used to describe and delineate the various layers of the LGN. One such taxa identifies four developed areas, two parvocellular layers (PI and PE) and two magnocellular areas (MI and ME), and two less developed layers (SI and SE). This is shown in Fig. 2.4. Under this taxa, the two parvocellular layers are further subdivided into leaflets corresponding to the central region of the fovea. Each is highly specific in terms of input. The ME layer and PE layer receive only inputs from the contralateral eye. The MI layer and PI layer receive inputs only from the ipsilateral eye [18,19].

LGN neurons receiving input from the retina can be classified based on X- or Y- type responses. The parvocellular areas receive mainly, if not solely, X-

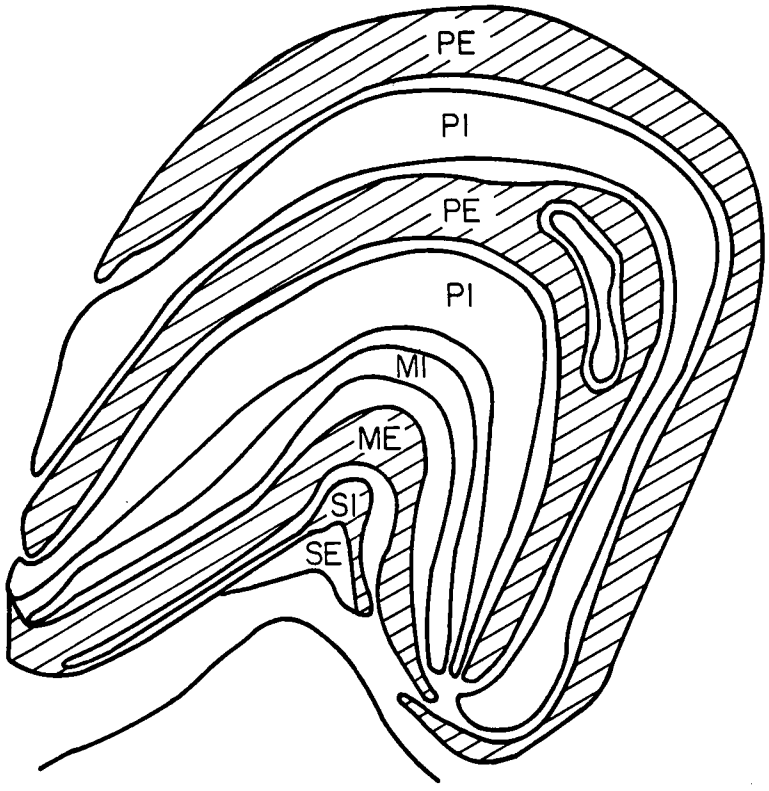


Figure 2.4: The structure of the LGN.

type inputs, and the magnocellular areas receive Y-type inputs. The dorsal and ventral pairs of parvocellular layers segregate the on-centered and off-centered neurons, respectively [18]. The faster conducting Y-cells are traced to the larger magnocellular cells in the LGN; the larger cells allowing for faster conduction velocities.

The neurons in the LGN have receptive fields somewhat similar to the ganglion cells of the retina and the cell response is often characterized, as are ganglion cells, as having a DOG response profile, *e.g.* [20]. One difference in the receptive field response is that LGN cells have a much stronger antagonistic surround. It is proposed that fields of ganglion cells provide the basis for the receptive field structure by converging on single LGN cells. In addition, there are a large number of interneurons converging on a single neuron. One hypothesis is that inhibitory interneurons are responsible for the strong antagonistic surround. There are two types of intrinsic neurons [21]. Both have a center-surround receptive field similar to relay cells carrying information from the LGN to striate cortex. These cells seem to be the primary mediators of inhibition in the X-pathway. In terms of signal processing, these cells attenuate lower frequencies and tune LGN cells to specific spatial frequencies. A second set of interneurons, having cell bodies in the perigeniculate nucleus, mediate the average discharge of the LGN cells. In terms of modeling, these cells could possibly monitor the threshold level of individual cells and keep the system from saturating [21].

A second theory of the structure of the LGN receptive fields is given in [22].

This theory takes into account recent evidence for an excitatory annulus outside the limits of the antagonistic surround. Evidence is presented for overlapping ganglion receptive fields comprising the entirety of the receptive field response. The mechanism hypothesized for generating the center-surround profile is the interaction between the on and off pathways. This mechanism is questionable in light of [23], but the outer annulus is significant. The outer surround is of the same polarity as the central response and is termed a disinhibitory input. A minimum delay time of 80 $ms.$ was observed for this added input. It is suggested that the receptive field is organized to sharpen the spatial tuning of the ganglion cells. Independent of the accuracy of the proposed receptive field mechanism, the outer annulus is quite significant. A detailed account of LGN cells with the outer surround, or side-lobes, is given in [24], along with a further delineation of the X and Y cell classification.

The afferent and efferent pathways of the LGN become very involved. Each projection hints to a new piece of information involved in the assimilation and recognition process. Some afferents originate outside the visual system, suggestive of feedback from behavioral and emotional centers. There are feedback loops from interneurons, the brainstem, and other non-visual regions of the cortex. Feedforward and feedback loops are found between area 17 (a prominant processing center in striate cortex) (IVα) and the parvocellular area of LGN; a similar loop exists with area 17 (IVβ) and the magnocellular area [20]. The feedforward connections maintain a high degree of retinotopic organization, as

shown in [25]. The central most part of the parvocellular layers in dLGN are clearly labeled through retrograde transport of horseradish peroxidase when the foveal processing region of striate cortex is injected. Cells in the interlaminar zone and laminar zone which do not fit into either the X or Y classification scheme project to layers 4 and 5 of area 19 of the prestriate cortex. Some of the afferents to these cells can be traces to the Superior Colliculus region [1]. Other cells terminate in the dLGN – another possible explanation for the observed inhibitory phenomenon [18].

2.6.1 Considerations for Modeling

The separation of the X and Y pathways indicate that at least two pathways are processing information in parallel. In addition, the relative time constants associated with each cell type indicate that processing goes from coarse analysis to fine analysis. Recall that the Y cells have a shorter latency period than X cells. In fact, the Y cells are 20 to 30 ms faster than the X cells. The Y cells are responsible for spatial localization and, probably, low level recognition. The Y cells drive the X cell processing by bringing objects to the foveal region for processing by the X cells. The response latency varies with the stimulus – indicating that the neural signal encodes more than location and relative intensity [26].

2.7 Midbrain Projections

A second division of the optic tract is the mesencephalic pathway. The majority of retinal ganglion cells project either to this region or to the LGN, but not to both. The superior colliculus (SC) is the prominant visual center in the midbrain. As in the LGN, there is a clear division of cell-types.

The majority of cells are of the W-type, second are the Y-type. There is little supportive evidence for X-cell projection to the SC. The Y and W cells are found to terminate in separate regions, thus suggesting the possibility of parallel processing. Cells projecting from this area to area 17 of the visual cortex are characterized by complex properties, broadly-tuned orientation specifics, and a high degree of binocularity.

Some X-cells are found in the midbrain. They are predominately in the pretectal nucleus in the midbrain. W-cells project to this region directly from the retina.

2.8 Visual Cortex

Again, there is a strong separation of X and Y cell pathways, indicating another possible layer of parallel processing. In addition, numerous feedback loops have been traced to this region. The following diagram depicts some of the primary pathways and feedback loops.

Area 17 of the primary visual cortex is considered the dominant region for

visual processing. This area has been divided into layers. Layers four and up are characterized by a lack of orientation or direction selectivity, circular receptive fields, and color selectivity (Y-cell characteristics). Layers two and three are characterized by line orientation, sensitivity to slow movement, and high spatial resolution sensitivity (X-cell characteristics).

Two parallel pathways have been identified from the retina to the visual cortex. One path is from the retina, to the LGN, and on to the striate cortex. The second path is from the retina, to the SC, the posterolateral thalamus, and on to the visual cortex. The first pathway is viewed as functionally dedicated to high spatial resolution vision; the second pathway is viewed to be responsible for body orientation, spatial appreciation, and limited pattern discrimination. In other words, the X- and Y- cell tracts, respectively.

The signal processing characteristics of striate cortex has been extensively investigated. The impulse response of striate cortex reveals a profile that resembles a 2-D Gabor filter [27]:

$$G(x,y) = exp(-\pi[(x-x_0)^2\alpha^2 + (y-y_0)^2\beta^2])exp(-2\pi i[u_o(x-x_0) + v_o(y-y_0)]), \tag{2.6}$$

where x_0 and y_0 are the spatial parameters, u_0 and v_0 are the frequency modulation parameters, and α and β are the space constants. It should be noted that the impulse response of cells in striate cortex is obtained by stimulating the retina, and, thus, reveals the cumulative processing upto and including striate cortex.

Striate cortex maintains the retinotopic organization that has been discussed throughout this chapter. One feature of striate cortex is that it is organized into interlaced ocular dominance columns that are organized in orientation specific columns (hypercolumns) that are approximately 0.5×0.05 mm in dimension. There is a complete set of orientation specific cells covering a full 180^0 range within a 0.5 mm range. In addition, there appears to be spatial frequency columns within the striate hypercolumns. The data is inconclusive as to the exact frequency incrementations and to the physiological mechanisms supporting the columns. It is of interest to note that the Gabor equation describes the various orientations and frequency sensitivities of the cells in striate cortex. The concept of multi-resolution processing is apparent from striate data.

CHAPTER 3

The Neuron

The structure and function of neural networks vary greatly; however, basic to each is a fundamental building block, a mathematical model which approximates the function of a physiological neuron or an ensemble of neurons. The neuron is, in fact, a fundamental building block of the physical nervous system which, itself, has a wide variety of structures and functions. The degree to which the mathematical models approximate the actual neuron vary from model to model, but the basic function is the same – to encode and transmit information. The neuron is shown diagrammatically in Fig. 3.1. The following discussion is in reference to this figure. In brief, the neuron receives signals at the synapses located at the dendrites. The signals are integrated at the cell body and the net effect is transmitted down the axon to the axon terminals, where the signal is transmitted to other neurons or to receptors. The mechanisms of signal transmission is a voltage potential across the cell membrane which changes in response to chemical and electrical changes in the extracellular fluid surrounding the neuron. Signal transmission is explained in terms of ion concentration gradients and an electric field set up by the concentration gradients [28].

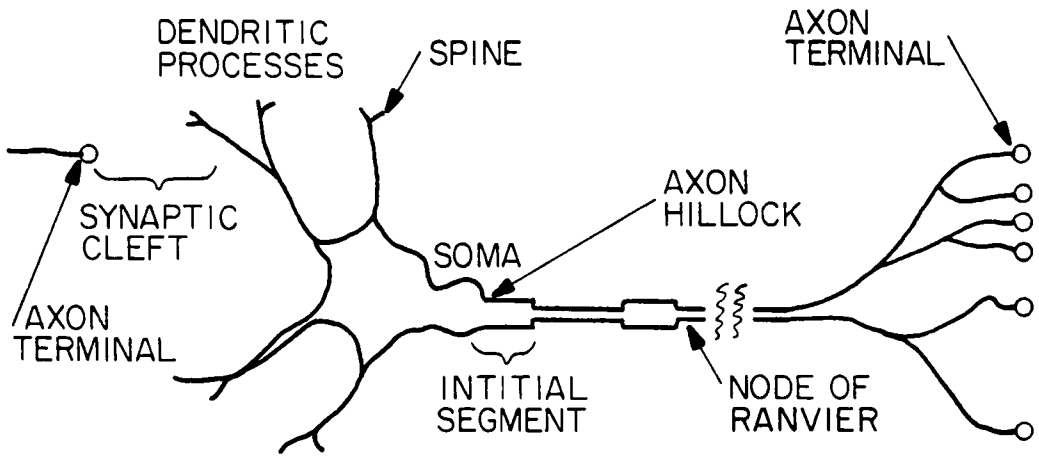


Figure 3.1: The neuron.

3.1 Ionic Currents

Three main ions are found in the intracellular and extracellular fluids surrounding a neuron cell membrane: Na^+, K^+, and Cl^-. Their concentration gradients across the cell membrane are the result of a dynamic process that begins with the neuron at rest (in a steady state condition). At this time, the intracellular fluid has a higher concentration of potassium ions than the extracellular fluid, while the extracellular fluid has a higher concentration of sodium and chloride ions than the intracellular fluid. The plasma membrane is a semipermeable membrane with a much higher permeability to potassium and chloride ions than to sodium ions. As a result of the concentration gradient and the

membrane permeability, potassium ions are constantly diffusing out of the cell and sodium ions are constantly diffusing into the cell. In the process of ion movement, an electric field is created. The net result is that sodium is being driven into the cell by two mechanisms: the electric field and by its concentration gradient; potassium is being driven out of the cell by one mechanism – its concentration gradient, and into the cell by a second mechanism – the electric field. To maintain the steady state condition, an active-transport system continually pumps sodium from the intracellular fluid to the extracellular fluid and pumps potassium from the extracellular fluid to the intracellular fluid [29].

3.2 Voltage Potential

The voltage potential across the axon memebrane in the steady state is $-70mV$ (resting potential), with the extracellular fluid as the reference point. The equilibrium potential of sodium by itself is approximately $+60mV$, and the equilibrium potential for potassium by itself is approximately $-90mV$. The membrane resting potential is maintained at a potential much closer to the equilibruim potential of potassium than that of sodium by two mechanisms. One, an active-transport system which removes three sodium ions from the cell for every two potassium ions that it brings into the system and, two, by the permeability characteristics of the membrane, which is 50 to 75 times more permeable to potassium than to sodium [29].

3.3 Propagation of the Signal

The steady state conditions are maintained until either electrical or chemical forces act on the extracellular fluid surrounding the neuron. Any change is processed by the neuron which then transmits a signal proportional to the amount of change. The response of an isolated neuron serves to demonstrate the local mechanisms by which a neuron processes incoming signals and passes the resultant signal down its axon to the axon terminals.

At a synapse, a junction between two neurons, a signal is transmitted from the presynaptic neuron to the postsynaptic neuron. The signal can be passed as an electrical signal through local currents flowing directly to the postsynaptic neuron, or as a chemical signal in the form of neurotransmitters released from the presynaptic axon terminals and binding to receptor sites on the postsynaptic neuron. This opens specific ion channels in the postsynaptic membrane and is reflected by a change in the membrane potential. The first is commonly seen in densely populated areas of unmyelinated neurons, *e.g.* regions of the central nervous system. The second is the most common means of transmitting signals between neurons. The response of the neuron depends on the type of neuron and the type of signal received. Some neurons respond only with graded potential changes and others can respond with a graded potential change accompanied by a spike train (action potentials). In either case, the potential change depends on whether the incoming signal is an inhibitory stimulus or an excitatory stimulus.

3.3.1 Graded Potential Changes

The graded potential change is explained by local currents along the axon membrane. Recall (Section 3.2) that the intracellular fluid is at $-70mV$ with respect to the extracellular fluid and that there is a much higher concentration of sodium ions in the extracellular fluid and a much higher concentration of potassium ions in the intracellular fluid. An excitatory stimulus changes the permeability of the membrane to sodium ions allowing an influx of positive ions. The membrane slightly depolarizes at the point of stimulation and local currents are set up in both intracellular and extracellular fluids. In the extracellular fluid, current flow is away from the more positive resting membrane potential and toward the stimulated site; in the intracellular fluid, current flow is away from the depolarized site toward the surrounding more negative resting potential. In each case, the charge carriers are ions in solution. Membrane permeability works against local currents by allowing charge carriers to leak across the membrane. As a result, small currents quickly die out. Unless the distance to the receptor site is small, the signal will be completely attenuated. The amount of current generated is dependent on the magnitude of depolarization. If a large number of synapse sites are stimulated or a single site is stimulated at a high frequency, the degree of depolarization will be high and so will the amount of local current generated [29]. Inhibitory stimuli hyperpolarize the cell membrane making it much more difficult to generate local currents or to drive a graded poential high enough for an action potential (the second mechanism for signal transmission) to occur [3].

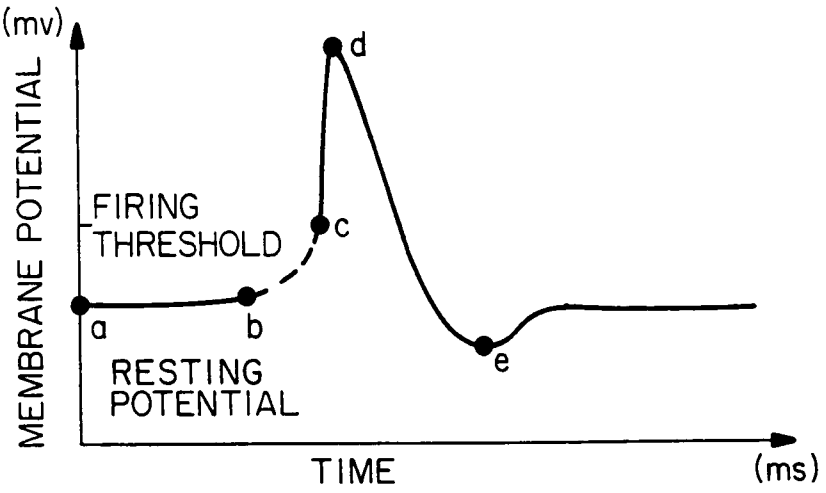


Figure 3.2: Changes in the membrane potential at the hillock.

3.3.2 Action Potentials

The action potential is the most common mechanism for transmitting information by a neuron. Many of the dynamics of an action potential are similar to those seen during a graded potential change. The following is a general description of the changes in the membrane potential generating an action potentail. The membrane potential changes involved in an action potential are shown in Fig. 3.2. The membrane is at the resting potential (a) until the neuron is stimulated (b), at which time the membrane permeability to sodium drastically increases and sodium ions rush into the cell. The increase in sodium permeability causes the cell membrane to depolarize, which in turn increases the cell permeabilty in a positive feed-back loop. This feed-back loop is not set into motion unless more sodium ions enter the cell than there are potassium ions leaving the

cell. This happens when the membrane is depolarized to about $15mV$ above the resting potential (c). The action potential is an all-or-none event. That is, if the membrane is not depolarized to the threshold level, the action potential will not take place; at the same time, once the action potential is initiated, it fires completely. Once the cell fires, the sodium channels close and a special set of potassium channels open (d). The diffusion of potassium ions out of the special potassium channels causes the concentration level of potassium to fall below the steady state level. This is seen in the hyperpolarization of the cell membrane (e). Action potentials are triggered at adjacent sites the full length of the axon. This is a result of local currents set in motion at each action potential. The local currents are strong enough to depolarization the membrane to the threshold level. The direction of signal propagation is controlled by refactory periods at each action potential site.

A site can not produce a second action potential for some time after it has fired. This period is called the absolute refactory period and lasts about as long as the sodium permeability is in the high state. Following this period, there is a time in which only very strong stimuli can elicit an action potential. This period is termed the relative refractory period and lasts up to $15ms$. Not only does the absolute refactory period control the direction of signal propagation, but it also limits the maximum rate of action potentials.

One other factor is involved with action potentials which needs to be discussed. In Fig. 3.1, there are points labeled *nodes of Ranvier*. Many axons

are wrapped in an insulating material called myelin. The nodes of Ranvier are gaps in the myelin sheath. The local currents flow from node to node producing action potentials. This method of signal propagation is much faster than firing at each point along an axon. Conduction velocities can vary from 1 mi/h to 400 mi/h, depending on the diameter of the axon and on whether or not the axon is myelinated.

3.4 Information Encoding at the Single Neuron Level

Functionally, the changes in membrane potential are encoding input signals to the neuron. Interpreting the cellular changes which regulate the affect a given stimulus has on a postsynaptic neuron provides an explanation as to how information is encoded in a neuron. The interpretation depends on whether one assumes that the important information is transmitted by the frequency of firing, patterns of firing, the magnitude of the action potential, or merely on the presence of an action potential; various models have been constructed to study the amount of information contained in each. For both analytic reasons and because of a lack of a complete understanding of the neural processes, the models incorporate simplifications and generalizations about local factors which affect the magnitude and firing frequency of the neuron. Some factors that play a role in encoding information at a single neuron level are discussed in the following.

3.4.1 Factors Affecting the Amplitude and Frequency of the Action Potential

At the most basic level, the postsynaptic neuron is an integrator which sums all the signals, in space and in time, that affect its membrane. If the summation raises the membrane potential above a threshold level, an action potential is generated. The neuron continues integrating over time until the graded potential again reaches a suprathreshold level and another action potential is generated. Intracellular and extracellular forces impose conditions on the neuron that affect the rate of action potentials, magnitude of action potentials, the pattern of action potentials, and even whether or not an action potential will be generated. Each change reflects information about the state of the neuron and, hence, contains information about the input signals.

One factor is the rate at which graded potentials are attenuated. In the case of large graded potentials, the decay time can be much longer than the refractory period after an action potential. If this happens, a single suprathreshold stimulation can produce more than a single action potential. Although the action potential is an all-or-none event, the amplitude of the action potential is not always of the same magnitude. The ion concentration and the state of the cell membrane determine the final amplitude [29].

At the other end of the neuron, the axon terminals, the amount of neurotransmitter released into the synaptic cleft is affected by both graded potentials and action potentials [3]. One factor which determines how much a synapse af-

fects the postsynaptic neuron is the location of the synapse. It has been generally accepted that the nearer to the initial segment (Fig. 3.1), the more impact the synapse will have at the postsynaptic membrane [29]. A somewhat more elaborate, and contradictory, view is presented in the discussion on physiological mechanisms of learning and memory storage (Section (3.7)).

A fourth ion, Ca^{+}, exists in the extracellular fluid and it has been found to be instrumental in the release of neurotransmitters; consequently, a change in the amount of calcium ions in the extracellular fluid will also affect the impact a presynaptic potential will have on a postsynaptic neuron. Depolarization at the axon terminal opens voltage-sensitive channels in the terminal membrane. The calcium from the extracellular fluid diffuses into the presynaptic terminals and causes the release of neurotransmitter into the synaptic cleft [29]. Voltage-sensitive channels are also present on the postsynaptic membrane and allow for calcium to diffuse across the postsynaptic membrane. This mechanism also provides the basis for a theory that counters the generally accepted notion that most of the important activity at a synapse takes place at the midsection of the postsynaptic synapse. In this theory, the high resistance properties in distal dendritic spines of the post-synaptic membrane are cited as evidence for a large contribution made in those regions to the graded potentials [30]. The function of the calcium channels is discussed in more detail in the Section (3.7). Many other factors affect the manner and amount of information encoded at the single neuron level.

It is generally accepted that the pertinent input information is contained in the firing frequency of the neuron [31,29]. The same factors affecting the graded potential changes affect the firing frequency, *i.e.*, chemical and electrical forces which produce a change in the extracellular fluid surrounding a neuron, especially at synapse sites.

Recently, a theory suggesting that the pertinent information transmitted by a neuron is in the pattern of firing, *i.e.*, the firing frequency, interspike distances, and latency to firing, and not merely in the frequency of firing [32,33,34,35]. According to this view, signals in the visual system are processed according to a multiplex filter model in which pertinent stimulus parameters are transmitted simultaneously in the spike train. Thus, a temporal modulation of the spike train results from the signal processing mechanisms of the neuron membrane. The authors use digital signal processing, statistics, and information theory to quantify the information content in the output waveforms of neurons. They prove that the information content is at least twice that contained in the firing frequency and that the different stimulus parameters are carried in different parts of the neuron output. If this theory proves to be a more accurate description of information encoding, current theories of visual processing will have to be rethought with particular attention to time as a factor in the model. This is basic to the model developed in Chapter 4.

3.5 Modeling the Neuron

Hodgkin and Huxley [36,37] developed an equivalent electric circuit to model the behavior of the neuron membrane along the axon. This model serves as a basis for many other models and so will be discussed here as a representative neuron model. The objective of this thesis is not to develop an exact model of a single neuron, but to develop a neuron model and a structure for an ensemble of neurons which will serve as a reference point for neuron models used in neural networks. In addition, basic models based on simplifications of the Hodgkin-Huxley model (H-H model) are discussed.

3.5.1 The Seminal Model - Hodgkin and Huxley

The equivalent circuit of a single neuron, as presented in [36], is shown in Fig. 3.3. In this circuit, I_{Na} is the current due to sodiom ion movement, g_{Na} is the variable coefficient of membrane permeability for sodium, and E_{Na} is the equilibrium potential for sodium. Similar variables are shown for potassium (K) and, for a group of *other* ions, collectively , I_l. The capacitance, C_m, is the membrane capacitance due to the charge build up as discussed in the physiological description of the neuron. The conductances, g_{Na} and g_K, are functions of time and membrane potential. Recall that depolarization of the membrane causes a rapid, transient increase in sodium permeability. The potassium permeability also increases, but at a much slower rate.

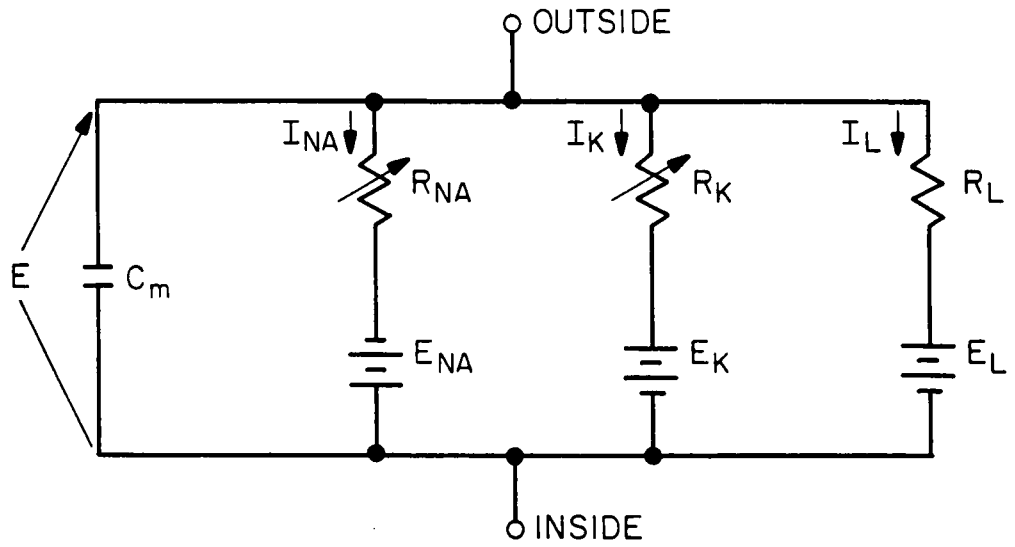


Figure 3.3: Hodgkin-Huxley equivalent circuit.

The equations describing the current are

$$I = C_m \frac{dV}{dt} + I_i, \tag{3.1}$$

where I is the current density, I_i is the ionic current density, V is the displacement of the potential from the resting potential, and C_m is the membrane capacitance per unit area. The ionic current density is composed of the three sources already mentioned.

$$I_i = I_{Na} + I_K + I_l \tag{3.2}$$

Each individual current is described in terms of the forces acting on the specific ions, as discussed in the previous section. For sodium, the current equation is

$$I_{Na} = g_{Na}(V - V_{Na}), \tag{3.3}$$

where V is the difference between the membrane potential at a particular state of activation and the absolute value of the resting potential ($V = E - E_r$), V_{Na} is the difference between the equilibrium potential of sodium and the absolute value of the resting potential ($V_{Na} = E_{Na} - E_r$), and g_{Na} is the conductance of the membrane reflecting the membrane at a particular state of activation. The concuctance term, g_{NA}, is defined so as to reflect the changes in permeability:

$$g_{Na} = m^3 h \overline{g}_{Na},$$

$$\frac{dm}{dt} = \alpha(1-m) - \beta_m m,$$

$$\frac{dh}{dt} = \alpha(1-h) - \beta_h h,$$

where m represents the proportion of activating ions inside the membrane, $(1 - m)$ represents the proportion of activating ions outside the membrane, h and $(1-h)$ are similarily defined for inactivating ions. The directional transfer rates from outside the cell membrane to inside the cell membrane are represented by α_M and α_h; the directional transfer rates from inside the cell membrane to outside the cell membrane are represented by β_M, and β_h.

Similar terms have been developed for currents due to potassium ions and due to the other ions. The resulting current equation is given by

$$I = C_m \frac{dV}{dt} + \overline{g}_K n^4 (V - V_K) + \overline{g}_{Na} m^3 h (V - V_{Na}) + \overline{g}_l (V - V_l), \qquad (3.4)$$

where $\frac{dm}{dt}$, $\frac{dh}{dt}$, and g_{Na} are defined above,

$$\frac{dn}{dt} = \alpha_n(1-n) - \beta_n n,$$

$$g_K = \overline{g}_K n^4,$$

where α_n and β_n are rate constants, n is a dimensionless quantity that varies between 0 and 1, and $\overline{g}_k$ is a constant with dimensions $\frac{mhos}{cm^2}$. The relationships for α and β with the membrane potential were determined experimentally.

$$\alpha_n = \frac{0.01(V+10)}{(exp^{\frac{V+10}{10}} - 1)},$$

$$\beta_n = 0.125 exp^{\frac{V}{80}},$$

$$\alpha_m = \frac{0.1(V+25)}{(exp^{\frac{V+25}{10}} - 1)},$$

$$\beta_m = 4 exp^{\frac{V}{18}},$$

$$\alpha_h = 0.07 exp^{\frac{V}{20}}, \text{and}$$

$$\beta_h = \frac{1}{(exp^{\frac{V+30}{10}} + 1)}.$$

The above equations describe the behavior of the neuron during an action potential. The process of propagated action potentials is a little more involved. The current equation for a propagated action potential becomes

$$\frac{a}{2R_2\theta^2}\frac{d^2V}{dt^2} = C_m\frac{dV}{dt} + \overline{g}_K n^4(V - V_K) + \overline{g}_{Na} m^3 h(V - V_{Na}) + \overline{g}_l(V - V_l), \quad (3.5)$$

where a is the radius of the axon, R is the resistance of the axoplasm, and θ is the velocity of conduction.

Hodgkin and Huxley have laid the ground work for modeling a single neuron based on ionic currents. In light of the physiological discussion of signal transmission in the neuron, a model based on ionic currents provides a reasonable

first approximation to neuron behavior. For an extended mathematical treatment of the neuron based on Hodgkin and Huxley see, for example, [38]. In [39,40], various analog circuits modeling the behavior of a neuron are given; the bases for many of the models comes from the Hodgkin and Huxley model.

3.5.2 An Analog Implementation

The model presented in [40] discusses various simplifications of the Hodgkin-Huxley equations to develop a hardware model of the neuron. This model assumes that the pertinent output information is contained in the phase of the output signal. The cell body of the neuron is modeled as a voltage-controlled oscillator (VCO) and the neurotransmitter activity at the synapse is modeled as an RC circuit (Fig. 3.4).

The neurotransmitter activity is modeled by a low-pass filter with a diode in series to simulate the action potential threshold level. The output signal, V_s, is related to the input signal by a differential equation

$$V_s + RC\frac{d(V_s)}{dt} = V_{in}, \tag{3.6}$$

where V_{in} is the clipped output voltage from the diode.

The cell body is modeled by a voltage-controlled oscillator (VCO) in which the phase of the output signal is modulated by the input signal. From basic communication theory [41], a frequency modulated signal can be represented by

$$\psi(t) = Acos[\theta(t)], \tag{3.7}$$

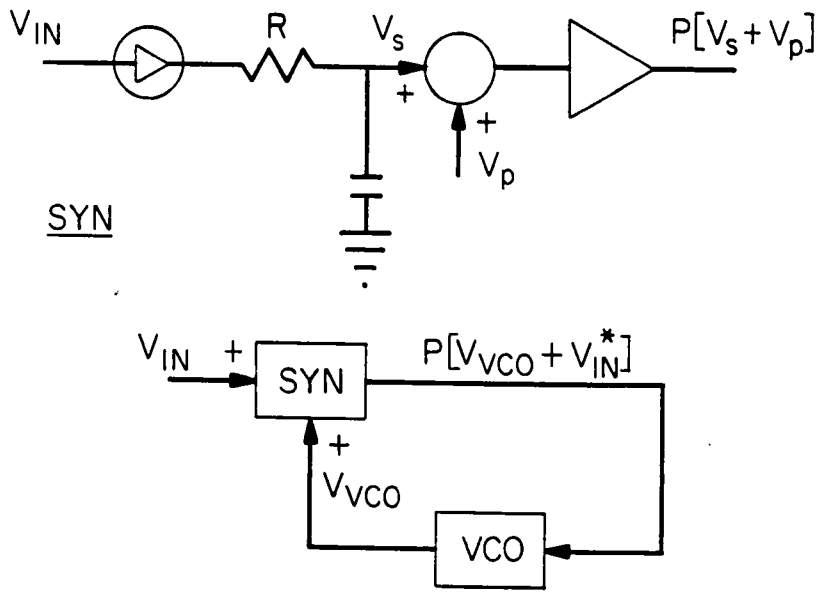


Figure 3.4: Voltage-controlled oscillator model.

where A is a constant amplitude, $\theta(t)$ is the phase angle. The instantaneous frequency ω_i of the modulated signal is linearly related to the input signal $f(t)$ by:

$$\frac{d\theta}{dt} = \omega_i = \omega_c + k_f f(t), \tag{3.8}$$

where ω_c is the center frequency, and k_f is a scalar constant times the input signal $f(t)$. The phase angle is derived from integrating Eq. (3.8)

$$\theta(t) = \omega_c t + k_p \int_0^t f(\tau) d\tau + \theta_0. \tag{3.9}$$

The important information in terms of neural modeling is the instantaneous frequency which provides a means of analysing the output of the neuron.

The cell body model is a VCO with a feed-back loop. The output is defined

in terms of phase, $(\theta(t))$:

$$\frac{d\theta(t)}{dt} = \omega_o + P[V_s + V_v(x(t))], \tag{3.10}$$

where ω_o is the center frequency, V_s is the output from the synapse model, and $V_v(\theta(t))$ is the VCO output with phase $\theta(t)$. The function $P[]$ is defined as the hyperbolic tangent. As discussed in Sec. (3.4), the state of a neuron at any given time affects the way in which it will respond to an input signal. This is modeled by putting the VCO output in a feedback loop with the input signal.

The basic assumptions about this model are that the magnitude of the output spike is constant and that the firing frequency contains the pertinent information. The basic VCO unit is extended to networks of neurons that model the behavior of biological clocks. Biological clocks show not only frequency responses but frequency modulated responses. The VCO's and the equations developed in the preceding allow for patterned responses when the VCO's are arranged in specific configurations or circuits.

3.5.3 Discrete Implementations

As with the other models, mathematical functions are used in software simulations to represent various aspects of the physiological neuron. The mathematical functions chosen are usually simplifications of the H-H model and, hence, are not an attempt at a strict representation of the physiological model. The simplifications inherent in the choice of the mathematical functions are designed to tailor the neural response to fit a specific information encoding paradigm. It

becomes immediately apparent that the behavior of the network as a system is the primary focus of most of the software models.

The basic building blocks common to most software network models are discussed in [42]. Three factors that directly address the issue of information encoding at the processing unit level are: the state of activation, an output function, and an activation rule. The main focus in these models is with information encoding on a system level.

One component from the system level is pertinent to the present discussion. The composite state of activation of all processing units at a time t is a spatial pattern of activity reflecting what the system is processing. For this reason, all processing unit parameters are developed to form a meaningful, stable spatial pattern of activation states over the entire system. The state of activation at a time t is represented by $a_i(t)$, where the subscript designates the particular unit. The values range from binary values, designating only on/off states, to unbounded continuous values, where the magnitude determines the amount of affect the unit will have on other units in the system. The output function, $o_i(t)$, is an operator that maps the activation state into an output signal. This operator is generally governed by a threshold level, θ, that attenuates low activation states. Finally, the activation rule determines activation states at a time $t+1$ and is a function of $a_j(t)$ and the net input, $\sum_i o_i(t)\omega_{ij}$, into unit j at time t. The parameter ω_{ij} is defined as the synapse strength between the j^{th} neuron and all impinging neurons, i. The activation rule can map the activation states into

binary levels or continuous levels. When continuous levels are used, a typical function used is the sigmoid function

$$a_j(t+1) = \frac{1}{1+e^{-\sum_i o_i(t)\omega_{ij}+\theta}}. \tag{3.11}$$

Frequently, the output function maps the activation function directly to the output, $o_j(t) = a_j(t)$.

From Eq. (3.11), the simplifications of the physiological neuron become obvious. First, the primary function of the neuron is integration of all the input signals. Second, all chemical, ionic, and membrane dynamics are encapsulated in a single term, ω_{ij}. The time constants of the physiological neuron are ignored, except in a broad sense. The time scale adopted results in a time-averaged representation of the firing frequency, thus, the sigmoid function. On the local level, the information is encoded in a discrete real value between 0 and 1. The sigmoid function imposes an upper bound to simulate the effects of saturation and the limitations on firing frequency imposed by the refractory period. Beyond this, little resembles the physiological neuron and, in fact, the neuron model resembles more an ensemble than a single neuron.

3.6 Neural Circuitry

A model describing the behavior of a single neuron is of interest in as much as it can be applied to a pool of interacting neurons. The central nervous system is composed of thousands of neurons, some synapsing with as many as

ten thousand other neurons. From what once appeared to be a confusing jumble of massively interconnected neurons, a highly organized structure is emerging based on morphology, pharmacology, topology, and function. One fact that is becoming apparent is that structure and function are closely related. This is evident even at the single neuron level. Consider, the solitary neuron model previously discussed. The structure of the dendritic arborization lends itself to the primary function performed by a neuron. Neurophysiological studies have revealed a substantial amount of structure throughout the central nervous system. The challenge becomes one of discerning the function of a given region based on structural clues. At the same time, modeling the structure and function of a given region often suggests further neurophysiological research.

Possible neuron - neuron interactions are represented schematically in Fig. 3.5. In the case of a group of neurons, structure is defined by the physical organizational of the group of interacting neurons. The likelihood of a neuron which has a single synapse with a second neuron to generate an action potential is very low. In this case, the first neuron generates a graded potential in the second neuron and serves in a facilitory role to the second neuron; additional subthreshold stimulation that sums to a suprathreshold level will generate an action potential. In the opposite extreme, a neuron may have multiple synapses with a second neuron. In this case, a single neuron is capable of generating an action potential in a second neuron. At the axon terminal, synaptic knobs are much more densely packed in the central region of the arborization than in the

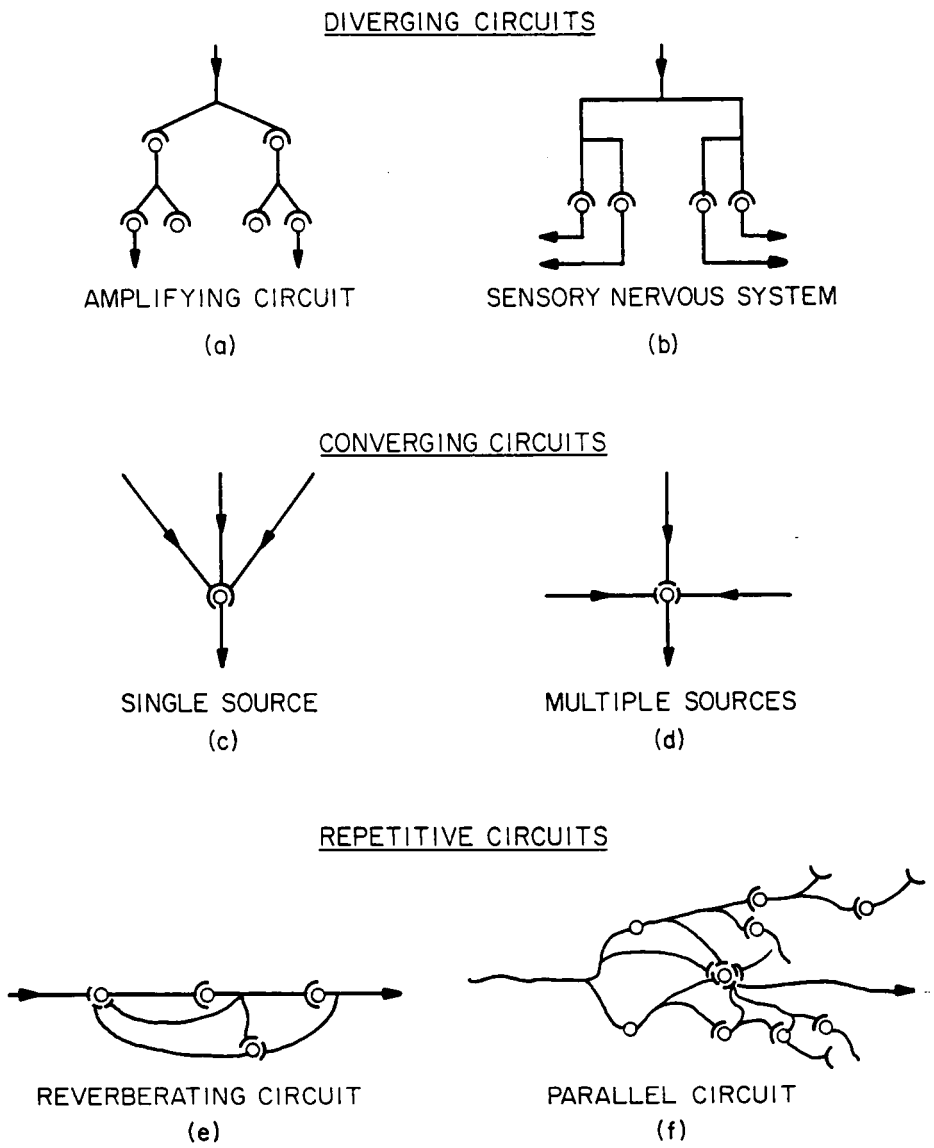


Figure 3.5: Possible neuron-neuron interactions.

peripheral regions. According to conventionally held theories, a second neuron located within this central area has a much higher probability of generating an action potential [31].

Three major classes of neuron configurations found in the nervous system have been identified in [31]. Variations of these three configurations are found in many of the neural network models. The first class has two variations and is shown in Figs. 3.5 (a) and (b) and is characterized by diverging circuits. Fig. 3.5 (a) is an amplifying circuit and is found in skeleton muscle control sytems. An incoming signal synapses with one or more neurons which in turn each synapse with one or more neurons. This pyramiding of neurons may continue for numerous layers and the impact of a single neuron is propagated to multiple sites. Fig. 3.5 (b) shows input signals being directed to various pathways. This type of configuration is common in the sensory nervous system.

One class of diverging circuits needs mention at this point. Examination of regions of neurons has revealed a structure that is so common that it seems to be one of the most fundamental structures in the nervous system. The structure is a topographical ordering of neurons in a specific region [43] and is found throughout the nervous system of most species. The connections in Fig. 3.6 show only the efferents from a single neuron, although a similar pattern of connections exists for all the neurons in the region. The inner circle consists of excitatory synapses and the outer circle consisits of inhibitory synapses. Examples of this structure are: the projection of the retina on the striate cortex, the tonotopic

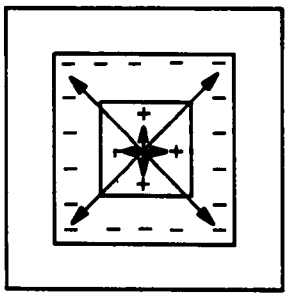


Figure 3.6: Efferent connections.

organization of the cochlea, the somatosensory cortex, and local sensory-receptor organization. The functionality of this structure is dependent on the region. The organization of touch receptors exploits the lateral interaction to localize a stimulus [29]. The same organization is used in the visual system to enhance features.

The second class also has two main variations. Together they represent the class of converging circuits. One result of converging arborizations is that a single neuron can have a very strong impact on another neuron (Fig. 3.5(c)). A different converging circuit (Fig. 3.5 (d)) provides a means for decision making based on signals that are physically widely separated.

Two variations of the third class, repetitive circuits, are shown in Fig. 3.5 (e) and (f). A single input signal generates a series of pulses at the output. The circuit of Fig. 3.5 (e) generates an output continuously until the neurons fatigue. The output can last seconds, minutes, or a life time. These circuits are representative of clocks maintaining rhythmic activities of the central nervous

system, such as in respiration, or rhythmic muscular activities, such as walking. The circuit in Fig. 3.5 (f) is a parallel circuit in which a single input generates a series of pulses in a single output neuron. There is a delay at each synapse due to the physical movement of neurotransmitter across the synaptic cleft. The number of synapses in each loop determines the amplitude and frequency of the action potential of the output neuron. Unlike the reverberating circuit, the parallel circuit does not run to fatigue but runs only until the signal has propagated through all of the loops [31].

All of the mentioned circuits are descriptive of actual neural circuitry. Some of the circuits are fairly close approximations to neural circuitry found in lower forms of life. While higher life forms show evidence of similar circuitry, the actual circuitry involves a great many more components, including feed-forward and feed-back pathways that are not clearly understood.

3.7 Learning and Memory

Learning and memory are generally described in terms of elicited behaviors or in terms of the recollection of ideas, images, etc. In this discussion, learning and memory are described in terms of specific chemical, electrical, and structural changes at the cell level, often at the cell membrane, in response to stimulation. In addition, neural circuitries which could facilitate the learning process are discussed. In the process, it is shown that the mechanisms that come into play

during learning are often sufficient to explain memory.

One of the earliest theories of learning was presented by Hebb [44]. He theorized that the synaptic strength between two active neurons is increased in response to repeated or persistent presynaptic and postsynaptic firing. The mechanism postulated was that synaptic knobs on an active axon develop or increase in size when in contact with the dendrites of a second active cell. Although the mechanism is not entirely accurate, the concept that synapses are modifiable with experience has been a major contribution that remains as the basis for theories of learning and memory. The term used to describe this is *synaptic plasticity.*

Relatively recently, a specific biochemical process has been investigated as a possible mechanism for modified Hebb-like learning. This process is discussed in terms of known neural circuitry in the hippocampus [45]. In brief, the mechanism is described in the following. Short bursts of high frequancy stimulation can change the functional and structural properties of synapses. A functionally descriptive name has been applied to the changes: long-term potentiation (LTP). The structural changes that result are an increase in the number of receptor sites and changes in the shape of the dendritic spines. The changes are highly localized and show varying degrees of synaptic facilitation. In addition, the initiation of the process requires a cooperative effort on the part of a number of afferents.

The mechanism is explained by three substances found in the neuron: calcium, calpain, and fodrin. High frequency stimulation of synapses sharply in-

creases the amount of dendritic intracellular calcium. As mentioned in the Section (3.4), voltage-sensitive channels in the dendritic membrane open in response to membrane depolarization. The intracellular calcium, in turn, activates a proteolytic enzyme, calpain, which has a substrate, fodrin, in the membrane of the neuron. The proteolytic activity exposes hidden transmitter receptors in the membrane. The result is seen in the growth of dendritic spines in the distal parts of the dendrites and, thus, an increase in the synaptic efficacy.

It has been proposed in [46] that this basic mechanism can account for both strengthening and weakening of synapses. Experimental evidence indicates that there is a postsynaptic threshold firing level that determines when morphological changes are made, both to increase and decrease the synaptic efficacy. In addition, data acquired during eye-suture studies of cats indicates that the threshold level is not constant but floats, apparently in relation to the average cellular activity. These three factors, it is proposed, provide a viable model of learning, memory, and memory decay.

Discovery of this mechanism has led to further investigations into the functional properties of dendritic spines. As discussed in Section (3.4), it has generally been accepted that the nearer a synapse to the axon hillock the more impact it will have on the postsynaptic neuron. A new model is developing that places as much importance on the more distal parts of the dendrite as on the middle parts of the dendrites. Distal spines are often much smaller than proximal spines. As a result, their input impedance is much higher and much larger

voltage changes are generated when current flows through them. In addition, it appears that spines can serve as both input and output sites. When stimulated strongly enough to act as an output site, they often affect neighboring spines in much the same way as an afferent synapse. In light of the functional changes attributed to dendritic spines, changes in the structure of the dendrite may correspond to memory [45].

Neural circuitry supports the learning mechanism described above ([45]). Recall that the combinatorial affect of a number of afferents is generally necessary for an action potential to be generated. This fact paired with the postsynaptic changes, as mentioned above, has lead to the development of a model of neural circuitry that models learning and memory. Lynch proposes that postsynaptic changes must be accompanied by changes on the presynaptic neuron. Specifically, as the number of receptor sites increases, it is logical to assume an increase in the afferent pathways.

In [45], two circuit types are discussed in terms of memory storage and retrieval. Both are in the class of converging circuits discussed in Section (3.6). The first circuit is termed a combinatorial circuit and is shown in Fig. 3.7 (a). It is argued that memory is distributed in the structure of the neuronal interactions and that combinatorial circuits are necessary for this to occur. In this type of circuit, an input circuit makes only limited contact with other neurons and can only produce graded potentials in the targeted neuron. In order for an action potential to be generated a large number of neurons would have to synapse

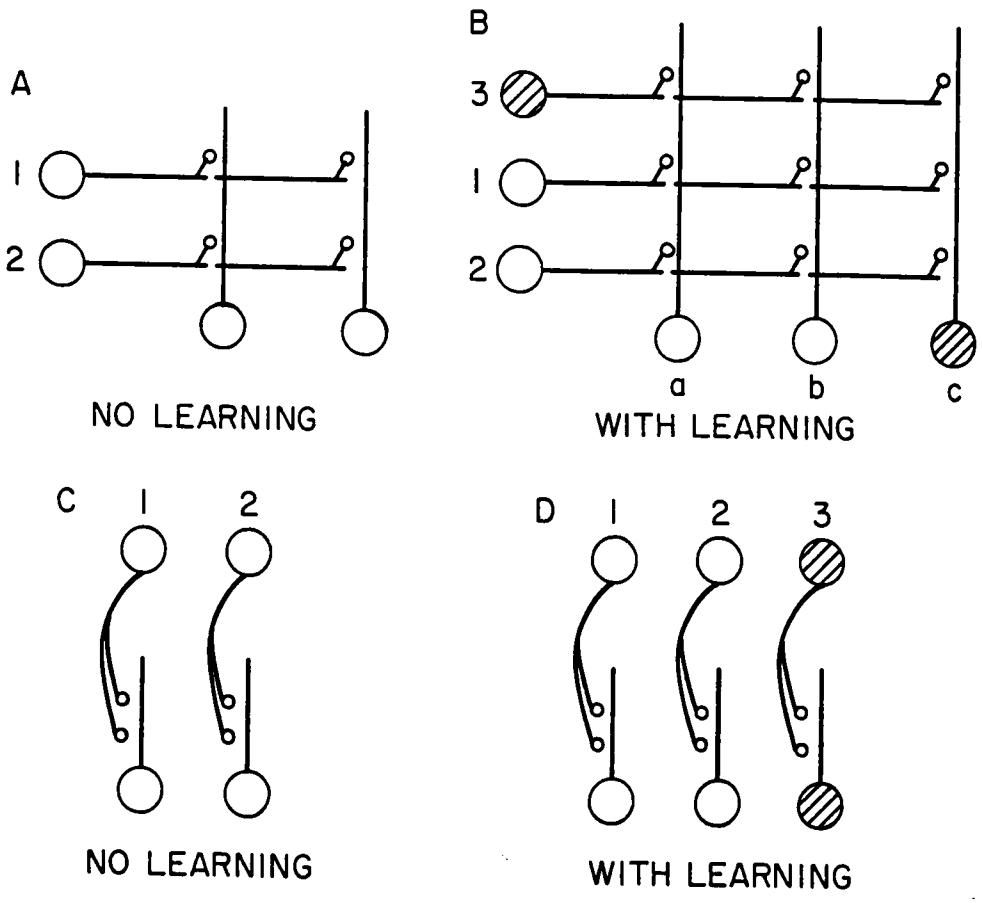


Figure 3.7: Possible circuits.

with the target neuron closely in time to one another. Additional synapse sites, acquired through learning, provide a mechanism by which a larger combination of afferents can stimulate the effernt dendrites. Furthermore, the extended dendrites could be accessed by newly generated afferent arborizations (Fig. 3.7 (b)). The second circuit is termed a topological circuit and is shown in Fig. 3.7 (c). This circuit provides a mechanism by which topologically dependent processes can learn.

3.8 Fundamental Neural Networks

The popularity of neural networks makes a comprehensive review impractical. Most of the networks found in the literature today can be traced to the work of a relatively small number of researchers, and the models discussed here are chosen because of their relevancy to the research presented in this thesis. Each of the models discussed in this section demonstrate a specific physiological phenomenon that must be addressed in any model of physiological processing that involves higher processing. Associated with each model are the basic elements discussed in Sections (3.5 and 3.6); specifically, these elements are mathematical functions describing activation states, output states, and rules of activation. In addition, each model has a specific architecture, or circuitry. Together, the mathematical functions and architecture determine the structure of memory and the mode of learning.

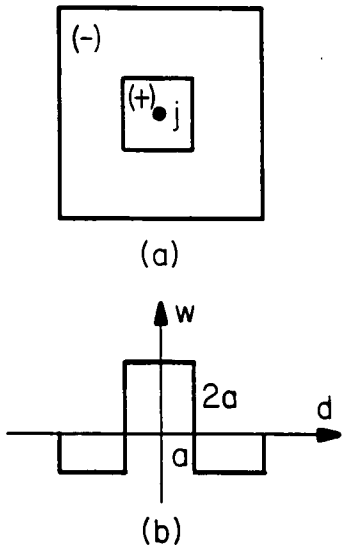


Figure 3.8: Kohonen spatial organization for weight adaptation.

3.8.1 Kohonen: Self-Organization

The organization of neurons, in both the peripheral and central nervous system, shows both spatial and functional structure. An example from the peripheral nervous system of a structure repeated throughout both systems is the organization of touch receptors. One function of the receptors is to localize the source of stimulation. The spatial organization is shown in Fig. 3.8 (a). The concentric squares represent the extent of neurons that synapse with the neuron labeled j. This region is called the *receptive field* of neuron j. The receptive fields of the neurons overlap with each other but are not shown in the figure. A profile of possible synapse types across the receptive field is shown in Fig. 3.8 (b).

Associated with this type of structure in the cerebral cortex is an ordering of particular regions. The ordering is often spatial, as found in the topological mapping of the retina on to the striate cortex. The ordering can also be according to measurements of the feature space. The most commonly cited example of this is the columnar organization of area 17 in the cerebral cortex. Kohonen's model addresses the issue of whether the ordering is genetically predetermined or whether it is a developmental phenomenon resulting from a Hebbian-type learning paradigm.

Kohonen's clustering algorithm groups data in regions of an output array according to the probability density function of the input data. The algorithm utilizes a feedforward network. The signal propagates from the input, $X(t)$: $(x_1, x_2, ..., x_n)$, through a connectivity matrix, $W_{ij}(t)$, to an output array $O(i, j)$. At each presentation, the output node which is the most similar to the input, calculated as the minimum distance, d,

$$d = min[\Sigma_i(x_i - W_{ij})^2], \text{for all} j, \tag{3.12}$$

is chosen as the node for learning.

Learning is regulated by local teachers and is based on correlation between the weight values and the input vector values. Each weight associated with the nodes with the minimum distance d from the input, and all weights connecting the output nodes to the input in a neighborhood of the most similar node, are

updated according to the following

$$W_{ij}(t+1) = W_{ij}(t) + \alpha(t)(x_i(t) - W_{ij}(t)), \tag{3.13}$$

where $\alpha(t)$ is a monotonically decreasing gain term that decreases both the magnitude of the learning increment and the size of the neighborhood included in the learning process. After learning, the output layer is organized into regions reflecting the probability density functions of the input signals. Simulation demonstrates that structure in the physiological system could come from active processes as part of stimulus-response pairings from interactions with the environment and not necessarily as a result of a genetically dictated ordering.

3.8.2 A Physiological Model

The following neuron model [47] is a much closer approximation to a physiological neuron than the model used in well known neural networks. The membrane potential changes with time according to the following:

$$\frac{dU_i}{dt} = \begin{cases} \frac{-U_i}{T_R} + \omega\varrho[\Delta t_i]\sigma[A_i(t)] & \text{if } U_F \leq U_i(t) \leq U_T, \\ \frac{-U_i}{T_R} & \text{otherwise.} \end{cases} \tag{3.14}$$

The first term $\frac{-U_i}{T_R}$ reflects the decay of the membrane potential over time due to ionic transport and membrane resistances. The second set of terms, $\omega\varrho[\Delta t_i]\sigma[A_i(t)]$, accounts for both refractory periods and the afferents to cell i from lateral and feedforward pathways. The term ω is a coupling coefficient

which scales the link strength between neurons. The term $\varrho[\Delta t_i]$ is given by

$$\varrho[\Delta t_i] = U_T \Theta(\Delta t_i - T_F)(1 - G_i(\frac{\Delta t_i - T_F}{\frac{T_F}{2}}), \tag{3.15}$$

where U_T is the threshold level above which the neuron fires, $\Theta(\ )$ is a step function which maintains membrane insensitivity to afferents during the absolute refractory period, and $G(\frac{\alpha}{\tau}\ )$ is a memory function describing the effects of past firings and is given by $exp(-\frac{\alpha}{\tau})$. Both the total refractory, T_F, and relative refractory, $\frac{T_F}{2}$, are included in the term $\varrho[\Delta t_i]$. The last term $\sigma[A_i(t)]$ is a sigmoid that limits the maximum firing rate and accounts for lateral, S_{ik}, and feedforward, R_{ij}, connections

$$A_i(t) = \sum_k S_{ik} G_K(\frac{\Delta t_k}{T_u}) + \sum_j R_{ij} G_K^R(\frac{\Delta t_k^R}{T_u}). \tag{3.16}$$

The conditional statements refer to the refractory membrane potential, U_F, and the firing threshold, U_T. These equations describe the membrane potential at the axon hillock, incorporating the input signal decay from the synapse to the hillock, and the time delays imposed by the spatial extent of the dendritic arborizations.

The changes in synapse strengths are based on Hebbian learing rules and are given by

$$\frac{dS_{ik}}{dt} = \begin{cases} -\frac{S_{ik}(t) - S_{ik}(0)}{T_S} + \Omega G_k \frac{\Delta t_k}{T_m} k(G_i, G_k) & \text{if } S_u \geq |S_{ik}| \geq S_i; \\ -\frac{S_{ik}(t) - S_{ik}(0)}{T_S} & \text{otherwise.} \end{cases} \tag{3.17}$$

The first term allows the synapses to relax to their original values over time. The term Ω is a scaling function. Since Hebbian learning rules are based on both

presynaptic and postsynaptic activity, the term $k(G_i, G_k)$ allows for increasing the link strength only between highly active neurons and decreasing the link strength if either the presynaptic or the postsynaptic activity is below a specified level of activity. This model is much closer to the physiological neuron and has been shown to respond in a similar manner under certain simulations. In addition, the output is shown to have temporal responses that approximate that of the physiological neuron.

CHAPTER 4

A Time-Varying Neuron Model

In the preceding chapters, the foundations for the time-varying neuron model, which is the heart of this thesis, have been developed. The basic physiological signal processing mechanisms of individual neurons have been discussed in detail and these mechanisms have been shown to be common throughout the visual tract. From this, the single unit neuron model is developed in the following. The structures found in the visual tract, including the structure of specific centers and the overall structure of the primary visual pathway, have also been discussed in detail, and from this, the development of neuron ensembles is drawn in the following. In addition, some basic paradigms used in neural networks have been discussed. These basic paradigms form the foundation from which the design objective of the software simulations – to simulate basic physiological signal processing mechanisms with potential utility in image understanding – is based.

4.1 The Foundations For a Time-Varying Model

Historically, much of the research in neural networks has considered the time-varying changes of the output signal and membrane characteristics only in terms of very coarse time scales. And, in fact, the 'neuron' models reflect the behaviors

and characteristics of ensembles of neurons more than that of single physiological neural units. This is reflected in the discrete models commonly used in which the output of a neuron has been modeled in terms of the average firing rate. In addition, rules governing changes in the synaptic efficacy have been designed to support this underlying assumption, *i.e.*, changes in synaptic efficacy increase/decrease the average firing rate. The primary function of individual neurons has been thought to be the integration of input signals. If the integration reaches a threshold value, the neuron fires and the signal is transmitted to other neurons. Viewed in this manner, temporal membrane characteristics at both the dendrites and axons need not be modeled specifically – but only in a global sense. The coarse time scale is all that is necessary for this interpretation of the neuron function.

These simplifications of the actual physical system are supported by classical interpretations in neurophysiology of neuron output and stem from the inability of neurophysiologists to interpret time-varying responses in any meaningful way other than by estimating the spike count within the peristimulus interval. Recently, however, investigators have found relatively small time-scale changes in the output signal and in dendritic membrane characteristics that are pertinent to information encoding, signal transmission, and learning in physiological systems. Two separate types of studies (*e.g.*, [33,34,35,45,46]), both suggestive of the same conclusion, are used in the development of the neuron model in this work. The conclusion is that temporal characteristics at the output, synapse,

and dendritic membrane are necessary components in even simplified models if one wishes to more fully exploit the information processing capabilities designed in neural systems, or even if one merely wishes to gain further insight into the workings of the brain. The spatial structure and equations describing neruon interactions based on spatial dimensions do not account for the cited characteristics of the signal processing dynmics.

The work of [35] in neurophysiology has been directed at deciphering the information encoded in the neuronal output in terms of the time-varying characteristics of the output waveform, as discussed in Section (3.4). In response to visual stimuli, the temporally modulated output waveform of neurons in the inferior temporal region is shown to uniquely encode each member of a set of orthogonal input signals. Furthermore, the decomposition of the output waveform into a set of orthogonal basis vectors and the corresponding coefficients are used to quantify the amount of information in the principal components of the waveform. The information content in the first four principal components is shown to be much greater than spike count alone. Furthermore, the additional information in the waveform is shown to be correlated with the input signal and is utilized by the physiological system in the recognition process. The important contribution for this thesis is a physiological basis for a neuron model that supports a time-varying view of neuron activity.

A second set of seemingly unrelated work, Section (3.7), also seems to point in the same direction. This work focuses on changes in the dendritic membrane

and provides a physiological mechanism for learning [45,46]. Calcium ions are shown to be involved in both short term and long term changes in the membrane characteristics at specific sites along the membrane that alter the synaptic efficacy. Implied in this work is a definition of learning: local changes, either short term or long term, in membrane characteristics that affect the temporal modulation of the output signal. Long term changes in the membrane structure, changes in which calcium is the catalyst, are defined as memory. Although a small time-scale is not necessary for modelling these processes, the affect of the processes is evident only in a small time-scale window of the output signal. The important contribution for this work is a physiological basis for incorporating in the neuron model synaptic and dendritic processes involving calcium ion currents.

Small changes in the dendrite at the spines are shown to result in significant changes in the membrane potential at the axon hillock by Rall [49,50] and Rinzell [51]. These changes are related to learning and are modeled by resistance changes in the spine stem that attenuate the voltage changes from the synapse site, at the spine head, to the membrane along the cell body. This work provides a model that supports the importance of membrane changes that have previously been ignored. In the work presented in this thesis, these small changes are shown to change the waveform of the output response of the neuron.

The model used in this work is based on two main assumptions motivated by the work mentioned above. The first assumption is that the time-varying out-

put of the neuron represents a more accurate representation of the information encoding process performed by neurons than does a time-average response interpretation. As a more accurate representation, information processing in a neural network will more closely resemble the processing done by the brain and, as can be shown with basic signal processing principles, a great deal more information can be encoded and transmitted in this manner than with a time-average response model. The second assumption is that the time-varying response is generated by known processes at the synapse and within the dendritic membrane, and, in fact, modeling the recently identified physiological mechanisms of learning and memory requires incorporating these known processes in a neural model.

The learning mechanisms extend the Hebbian learning rules of increasing synaptic efficacy to a participation in the temporal modulation of the neural waveform. This is done through incorporating associated time delays and time constants with the temporal and spatial summation within the dendritic membrane. In addition, a process has been identified that extends the Hebbian notion of localized learning to long term memory changes by providing a mechanism for permanent structural changes in the membrane. The time-varying signal characteristics extend the local processes to global pattern recognition processes by multiplexing pertinent stimulus parameters onto a single spike train. The model developed in this thesis is discussed in the following, with reference to the physiological analogs for the parameters and processes.

4.2 The Neuron Model-With Time Delays and Fixed Firing Threshold Level

The objective in this section is to incorporate the neuron characteristics necessary for a time varying pattern of impulses as the neuron output. This section focuses on the model parameters pertaining to the membrane changes at the axon hillock. It is shown that the pertinent stimulus parameters are encoded in the temporal characteristics of the output signal. The specific features and their incorporation in the model are discussed in the following. The basic 'neuron unit' incorporates characteristics from both single physiological neurons and ensembles of physiological neurons. Each component of the unit model is included specifically for the purpose of eliciting a time-varying response from the unit and from ensembles of the units. This is demonstrated by the output of individual neurons in the ensemble in response to stimuli in different points in the receptive field. In addition, the response of an ensemble of neurons to the same stimuli is discussed. The main contributing elements to the time-varying behavior are time delays, membrane leakage, graded potentials, non-attenuated spikes, and a refractory period between spikes.

In a coarse sense, the neuron is modeled as an integrator which sums the graded potentials, elicited by input signals, along its membrane. The integration is referenced, ultimately, to the axon hillock; although, potentials along the membrane are pertinent to learning and memory. The hillock is an important

reference point when viewing the neuron as an integrator for two reasons. It is at this point that the membrane potential must reach a threshold value before the neuron can fire. Once the neuron fires at the hillock the signal propagates virtually unchanged down the length of the axon. In addition, any temporal characteristics in the neuron output can be observed at this point.

The integration has a time dimension and three spatial dimensions. The intralayer and interlayer brachiations of neuron dendritic and axonic processes determine the spatial extent for summation. Integration continues throughout the peristimulus interval. The membrane characteristics reflect the irregular timing of different synapses at different synapse sites and the possible multiple synapses at a single site during the peristimulus interval. The electrotonic distance and the timing of the firing of a presynaptic neuron are reflected in the postsynaptic membrane.

Each presynaptic neuron, designated by the subscript j, that synapses with the postsynaptic neuron, designated by the subscript i, has associated with it a specific firing efficacy, f, which is a multivariant variable:

$$f_j = g(\Delta t_{ji}, \omega_{ji}(t)) \tag{4.1}$$

The first term is a time delay indicating the amount of time it takes for the signal to reach the axon hillock once the j^{th} neuron fires. The value of Δt_{ji} is dependent on the geometry of the dendrite and is modeled by the distance to the hillock from the afferent neuron. The second term, $\omega_{ji}(t)$, is a term that encompasses two physiological factors. The first is the amount of neurotransmitter released

from the j^{th} neuron when the signal reaches that neuron's axon terminal. The amount of transmitter released varies with pre- and post-synaptic firing and with calcium ion concentration in the intracellular and extracellular fluid. The calcium ion concentration gradient is affected by pre- and post-synaptic firing and post-synaptic membrane potential. A second factor pertains to the voltage-controlled ion channels and is often modeled as an electrical resistance (Section 3.5). Local ion currents flow across this resistance and cause a voltage drop. The voltage drop is the change in the local membrane potential, which then sets up more local ion currents, and so forth. The resistance value is controlled by pre- and post-synaptic firing and calcium ion concentration in the intracellular and extracellular fluid. If the input signal hyperpolarizes the postsynaptic membrane the sign of ω_{ji} is negative to indicate inhibition; if the input signal depolarizes the postsynaptic membrane the sign of ω_{ji} is positive to indicate excitation. The physiological significance of the sign was discussed in Section (2.3) and it's significance in terms of the model is discused in Section (4.3). In Section (5.4), the change of $\omega_{ji}(t)$ over time is discussed in terms of the pre- and post-synaptic firing and calcium ion concentrations that are relevant to the physiological learning and memory mechanisms.

The integration at the axon hillock reflects the cumulative affect of the graded potentials that propagate from the synapse sites. The signals are assumed to be transmitted by local ion currents and the associated decayed graded potentials. Properties of the membrane cause the signals to be attenuated as they are prop-

agated along the membrane toward the hillock. Two mechanisms are responsible for the attenuation. First, the dendritic membrane is a semi-permeable membrane that is porous to specific ions. Ions passively move across the membrane due to concentration gradients that are associated with changes in the membrane potential. The increased potential at a point on the membrane activates voltage-controlled ion channels which further affect the membrane potential. It should be noted that voltage-controlled ion channels have been used as an explanation for both hyperpolarization and depolarization of the membrane (Chapter 2). In addition, an active ion pump is constantly moving ions across the membrane. Both mechanisms are driving the neuron membrane toward its resting potential and are reflected in the model as an exponential decay term. The membrane potential at the hillock, $AP_i(t)$, of neuron i due to the effects of the afferents is

$$AP_i(t) = \sum_j \delta(t_j - \Delta t_{ji}) * e^{\frac{-\Delta t_{ji}}{\tau}} * \omega_{ji}(t), \tag{4.2}$$

where each term is supported by a physiological analog. The dirac delta function δ determines the time delay from the time since neuron j fires, t_j, and the time it takes the signal to reach the hillock of axon i, Δt_{ji}. The exponential term, $e^{\frac{-\Delta t_{ji}}{\tau}}$, decays the graded potential over the time interval Δt_{ji}. The last term, $\omega_{ji}(t)$, is as before. The signal is attenuated from one time step to another due to ionic movements, as stated in the preceding. The total membrane potential at the hillock, $MP_i(t)$, at time t is

$$MP_i(t) = AP_i(t) + MP_i(t-1) * e^{\frac{-1}{\tau}}. \tag{4.3}$$

Two properties of the axon hillock that affect the integration are incorporated in the model. The first property is that the neuron will fire only when the membrane potential has reached a threshold level, $\theta_i(t)$. The driving force of the membrane potential at the hillock is assumed to be completely spent when the neuron fires. The membrane at other points maintains the potential that has been generated. Thus, if $MP_i(t) \geq \theta_i(t)$, neuron i fires and $MP_i(t) = 0.0$. Upon firing, the signal is transmitted to other neurons. The second membrane property included in the axon hillock is the absolute maximum firing rate (Chapter 2) which is determined by the refractory period Δt_{ref}. The refractory period is modeled as a constant period of time, under the assumption that the axon fires in an all-or-none manner to a maximum value from which the potential then decays.

When the neuron fires it immediately begins the refractory period. During the refractory period the membrane potential at the hillock continues to be affected by the the signals propagating from other points on the membrane. These signals are assumed to decay at a faster rate, at the hillock, than when the neuron is not in the refractory period. It is also assumed that the dendrite continues to integrate during this period. The membrane potential accumulates at one electrotonic distance from the axon hillock and, while $t_j < \Delta t_{ref}$, the total membrane potential at this point is as follows:

$$MP_{ref}(t) = AP_i(t) + MP_i(t-1) * e^{\frac{-2}{\tau}} \tag{4.4}$$

where the rate of decay is one time step faster than the non-refractory decay

rate.

This neuron model is used to build a network of neurons to study physiological processing and to perform basic visual processing tasks. The architecture of the ensemble is taken from a structure commonly observed in the nervous system of primates, including the visual pathway (Chapter 2).

4.3 An Ensemble of Neurons

An ensemble of neurons is defined as a layer of interconnected neurons with a common afferent layer and a common efferent target layer. The synaptic efficacies are assumed fixed; thus, the preceding equations which do not reflect the behavior of the neuron at any point except at the hillock are valid. In addition, $\theta_i(t)$ is assumed fixed. In the following discussion, a single layer of neurons, $E1(k,l)$, represents the first layer of processing for an input, $I(g,h)$. The input layer is a two dimensional binary array containing an arbitrary shape. The signal path is feedforward for the interlayer pathways. The signal path is both feedforward and feedback for the intralayer pathways. The receptive field of a neuron is described in detail to emphasize two components of the receptive field, spatial and time, that are paramount to understanding the behavior of an ensemble.

4.3.1 Architecture of the Ensemble

Layer $E1$ is an $NE1 \times NE1$ array of neurons with receptive field structure defined as follows. For each neuron, i, at location (k,l) in $E1(k,l)$, there is an $SI_i \times SI_i$ neighborhood in $I(g,h)$ that composes the first feedforward receptive field of i. Likewise, for each neuron, i, in $E1(k,l)$, there is an $SE_i \times SE_i$ neighborhood in $E1(k,l)$ that composes the intralayer receptive field of i. The two receptive field components, together, define the receptive field of the neuron. The interlayer receptive fields are defined by: a point (g,h) in I is an element of the receptive field of neuron i in $E1$ if $|D_{ji}| \leq int(SI_i/2)$, where $D_{ji} = max(|k-g|, |l-h|)$ (Fig. 4.1). Points outside of this neighborhood have no direct synaptic links to neuron i. In this way, the entire input space is sampled, with a one to one mapping of each receptive field center to a unique position in $I(g,h)$ and each point in $I(g,h)$ has a mapping to a unique receptive field center in $E1(k,l)$, although they may be included in the receptive fields of many points in $E1(k,l)$. The intralayer receptive fields are defined by: a point (k,l) in $E1$ is an element of the receptive field of neuron i in $E1$ if $|D_{ji}| \leq int(SE_i/2)$, where $D_{ji} = max(|k-k_i|, |l-l_i|)$, see Fig. 4.1. Points outside of this neighborhood have no direct synaptic links to neuron i.

Each neighborhood has a structure composed of a center-surround (**C-S**) architecture that, along with the time delays and decay constants, defines the point spread profile of the neuron. The C-S connections from I are defined first. The surround is an $SI_i \times SI_i$ annulus with strength w_{is} and the center is a

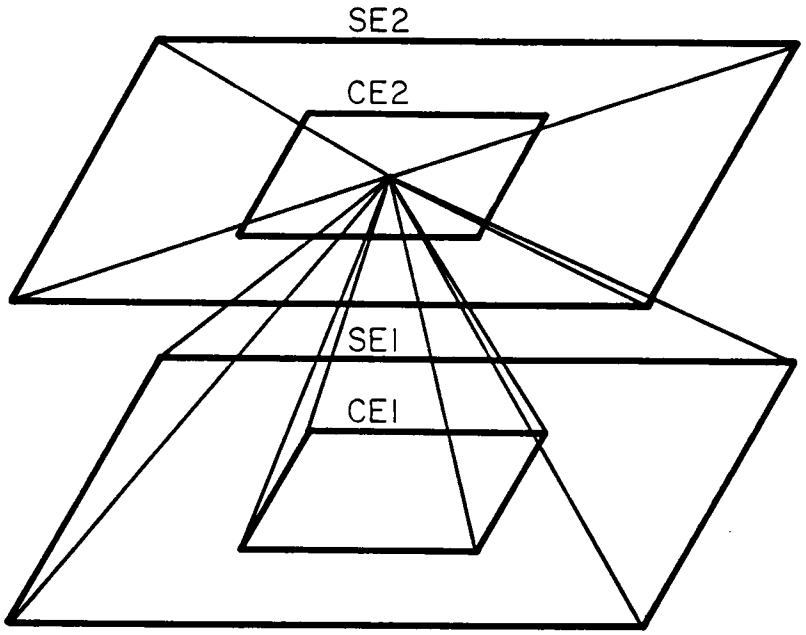


Figure 4.1: Receptive field structure.

$CI_i \times CI_i$ neighborhood with strength w_{ic}. The C-S connections within $E1$ are defined similarly. The surround is an $SE_i \times SE_i$ annulus with strength w_{es} and the center is a $CE_i \times CE_i$ neighborhood with strength w_{ec}. All connections are assumed to be unchangeable in strength and linkage in this section.

The spatial profile of a typical receptive field is shown in Fig. 4.2. The impulse response of a non-weighted receptive field, due to a single point stimulation at each point in the receptive field, is the decayed magnitude dependent on the time constant in the neuron model equations. The amplitude at each point is the effective amplitude felt at the axon hillock. Therefore, the shape of the impulse response is a function of both the geometry of the receptive field and the electrotonic distance of the afferent.

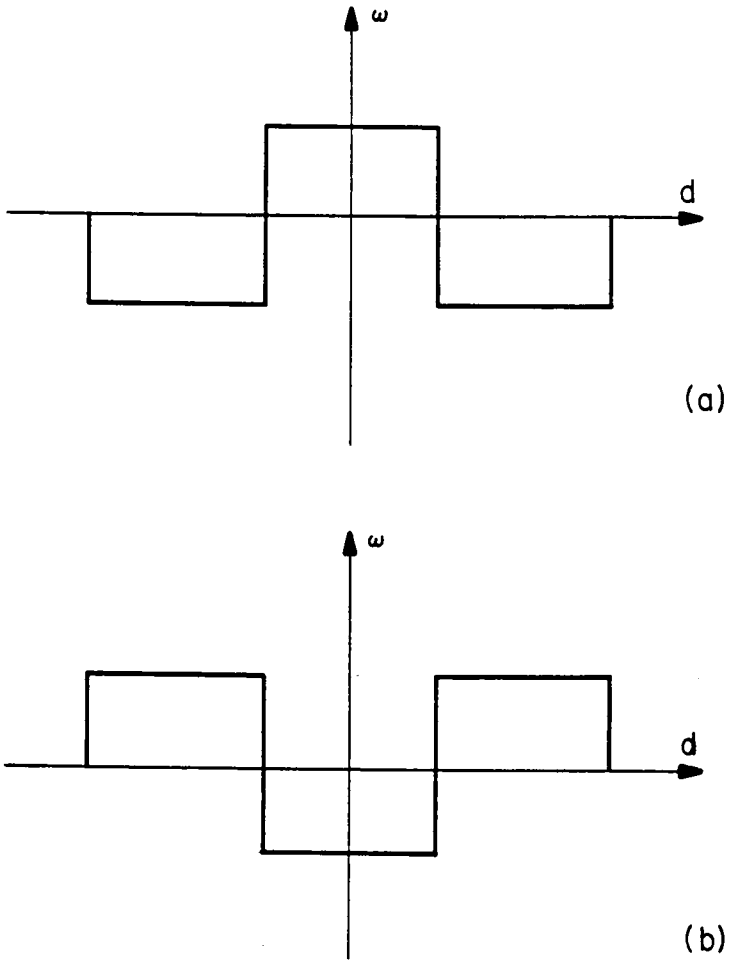


Figure 4.2: Spatial profile of the receptive field.

4.3.2 Time-Varying Spatial Characteristics of an Ensemble

The impulse response, the spatial frequency response tuning curves, and the contrast sensitivity tuning curves of a neuron vary with the experimental conditions, *i.e.*, the frequency, spatial and temporal, of the stimulus (Chapter 2). This may be a result of the architecture and dynamics of the neuron layers or the result of eye-scanning strategies. It has been determined that the eye scans an image characterized by a specific spatial frequency at a rate compatable with Nyquist frequency. The mechanisms are not fully understood. The numerous dynamic scanning mechanisms of the eye are not modeled in this stage of this work. Another complicating factor is that constant stimulation of a neuron causes saturation and the neuron ceases to function. Considering the preceding, the behavior of the ensemble is investigated under two different time-sampling frequencies. In the first case, the input is pulsed to $E1$ each Inp_{delay} $ms.$ interval after the initial presentation. In the second case, the input is constantly presented to $E1$. In each case the sampling frequency chosen must not result in neurons firing at their maximum firing rate as a result of direct synapses with the input otherwise the information from the lateral interactions is lost. The neuron may fire at the maximum rate with the additional input of the lateral inputs.

In the first case, the inclusion of Inp_{delay} allows for the membrane potential to be predicted. This enables a cause-effect relationship to be established between changes in the ensemble parameters and the behavior of the ensemble. Thus,

in order to demonstrate the possible functioning of an ensemble of neurons and to adjust the ensemble parameters, some assumptions have been made about the maximum stimulus time frequency. A delay period of 10 $ms.$ for a 1 $ms.$ presentation of a point of light has been chosen as one of the experimental conditions. The reason for this choice is that the refractory period is 5 $ms.$, leaving a window of 5 $ms.$ in which the neuron could fire due to intralayer synapses. In addition, a significant part of the summation interval has passed, including intralayer summations, prior to the next presentation of the input. Under this constraint, receptive fields of various sizes have been tuned. The tuning process is based on assumptions about the behavior of neurons with respect to the spatial relationship of the neuron and it's input from I, $i.e.$, cells can be characterized by their behavior at the edge location of an object in the input and by their behavior under full field coverage by an object in the input. Small receptive fields are assumed to be more accurate at detecting edges in high spatial frequency inputs and large receptive fields are assumed to be more accurate at detecting edges in low spatial frequency inputs. Also, an inhibitory input can completely cancel an excitatory input. The behavior of $E1$ with $Inp_{delay} = 1$ is investigated after the behavior of $E1$ with $Inp_{delay} = 10$ is fully developed.

Considering the preceding, the response of a single layer of neurons with tuned receptive fields is discussed. Tuned receptive fields are chosen in this section since there is a preponderance of evidence pointing to tuned receptive fields

up to and including striate cortex. The tuning has been guided by physiological descriptions and the work of Marr and Hildreth [48]; values for the pertinent parameters are given in Table 4.1. The following discussion reflects this bias.

The input is a binary image with an intensity value of 0 for the background and an intensity value of 1 for the stimulus. The stimuli are chosen to cover specific regions of the receptive field of the neuron at the center of $E1$, denoted by E_c. The regions covered are defined in the following 7 cases: case (a) one-half of the excitatory region, case (b) one-half of the excitatory and inhibitory regions, case (c) the full excitatory region, case (d) the full excitatory and inhibitory region, case (e) one-half the excitatory region and a small area of the inhibitory region, and cases (f and g) two examples of the full excitatory region with different inhibitory region combinations. The seven cases, along with the spatial time-varying firing patterns of $E1$, are shown in Fig. 4.3 through Fig. 4.15. The results from these stimuli show pictorially the concept of "tuned" receptive field and can be used to explain and predict the neuron responses to more complex, or less optimal, stimuli and the response of receptive fields which are not tuned.

The initial signal from I synapses with the neurons in $E1$ after a time delay of Δt_{ji} (Eq. 4.2) which is as follows:

$$\Delta t_{ji} = D_{ji} + \Delta t_{layer}, \tag{4.5}$$

where D_{ji} is the geometric distance mentioned above and Δt_{layer} is the inter-layer/intralayer time delay. At this step Δt_{layer} is Inp_{delay}. Neurons that fire during the period of time that their receptive fields are integrating the excitatory

Table 4.1: Tuning Parameters: Receptive Field Sizes and Weighting.

Size	*small* 1	*medium* 2	*large* 3
SI	9	13	15
CI	3	5	7
ω_{SI}	-0.11	-0.068	-0.045
ω_{CI}	0.27	0.19	0.091
SE	9	13	15
CE	3	5	7
ω_{SE}	-0.23	-0.55	-0.55
ω_{CE}	0.21	0.21	0.33
τ	4.3	4.3	4.3
Δt_{layer}	4	4	4
$\Delta t_{layer}(intra)$	3	3	4
Δt_{ref}	5	5	5
Inp_{delay}	10	10	10

inputs, a time dependent on the size of the receptive field, immediately begin a refractory period; at the same time, the intralayer signals propagate along intralayer pathways. After a time period of Δt_{ji} (Eq. (4.5)), where Δt_{layer} is now the intralayer time delay, neurons with residual membrane potentials close to $\theta_i(t)$ and receiving sufficient intralayer input, fire. This process continues until the layer settles, given a long enough stimulus interval, into a periodic spatial and temporal pattern of firing.

The following 12 figures demonstrate the time-varying spatial firing patterns established by a specific tuned receptive field in response to various stimuli, stimuli chosen to pictorially demonstrate the tuning characteristics and lateral pathways. In the figures, the background is shown as white, corresponding to 0 intensity in the input, and the stimuli is shown as black, corresponding to 1 in the input. Likewise, the neurons that are firing are shown as black and the quiescent neurons are white. All time steps correspond to ms intervals and discontinuities in the time steps indicate time steps in which no neurons are firing. The Δt_{layer} distance from $I(g,h)$ is 4 and the Δt_{layer} distance within $E1$ is 3. In Figs. 4.3 and 4.4, case (a), half excitatory region coverage, is shown. The input is 3 units in the x-direction by 5 units in the y-direction, positioned such that one-half of excitatory region of the receptive field of E_c is covered. At $T = 5$ the center three neurons fire. These neurons are receiving input from all 8 synapse sites at $D_{ji} = 1$ and one from the synapse site at $D_{ji} = 0$. One time step later, at $T = 6$, six neurons, whose receptive fields map to the boundary of

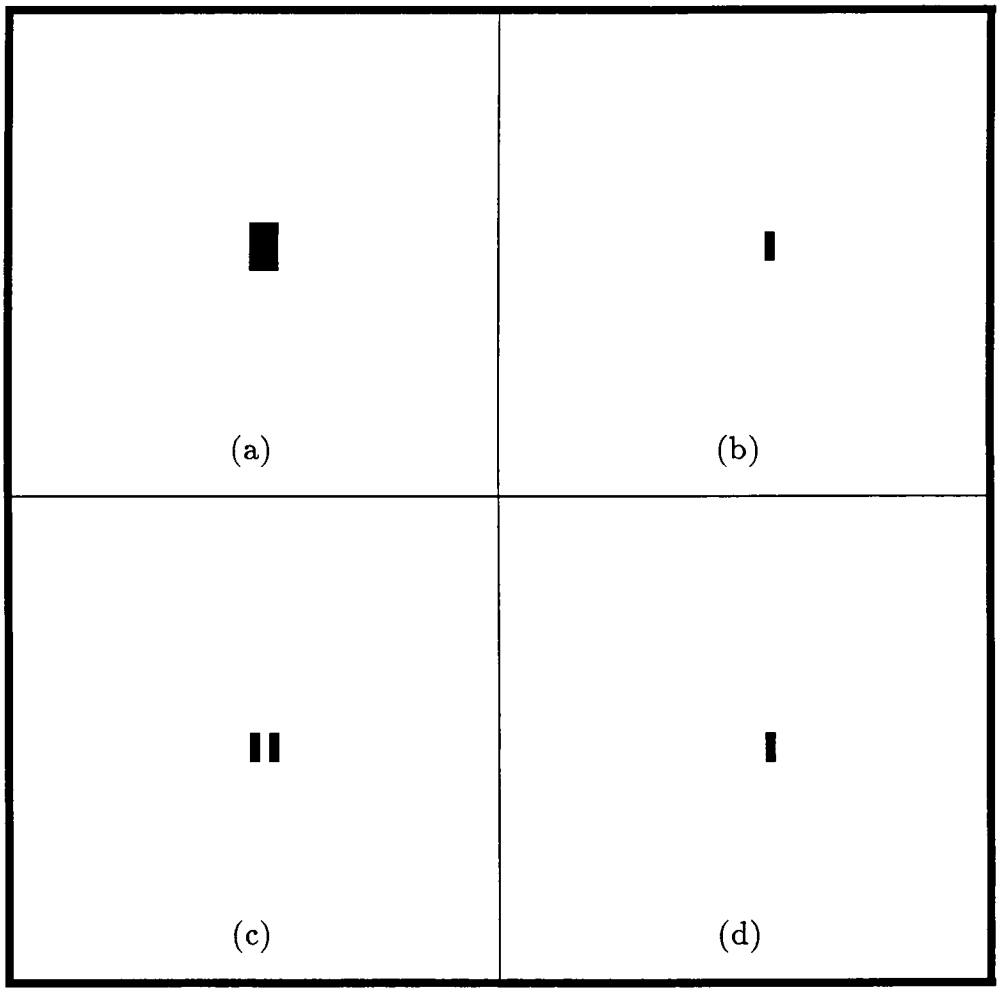


Figure 4.3: (a): Input: Half excitatory field coverage.; (b): T = 5 ; (c): T = 6 ; (d): T = 15

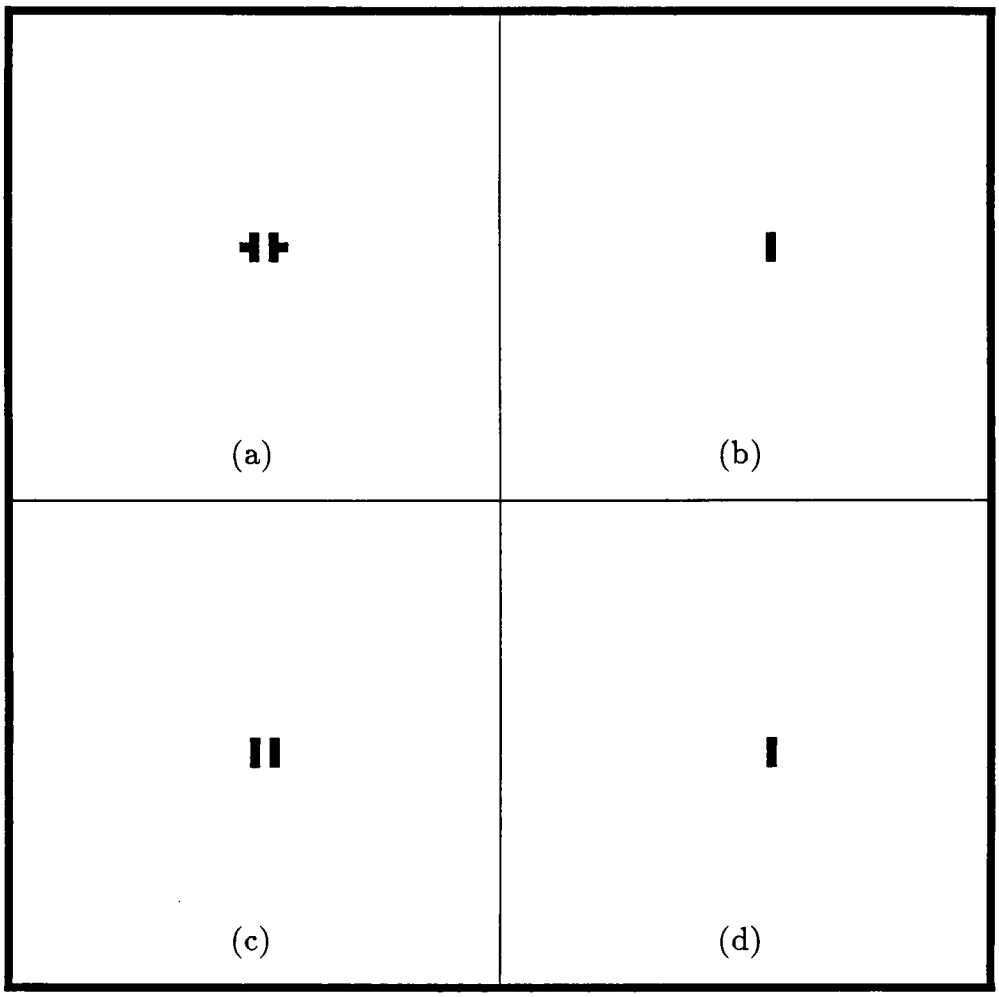


Figure 4.4: (a): T = 16; (b): T = 25; (c): T = 26; (d): T = 35

the input stimulus, fire. They received one input at $T = 4$ from the synapse site at $D_{ji} = 0$, five inputs at $T = 5$ from synapse sites at $D_{ji} = 1$, and a minimum of 6 inputs at $T = 6$ from synapse sites at $D_{ji} = 2$. The lateral excitatory synapses are not strong enough to elicit a firing during the time interval $T = 8 - 11$. At $T = 16$, the residual membrane potentials from the intralayer excitatory synapses are strong enough to elicit firing in the two neurons on either side of the boundary after the input signal reaches these neurons.

In Figs. 4.5 and 4.6, case (b), is shown. The input is 7 units in the x-direction and 13 units in the y-direction. This corresponds to coverage of one-half of both the excitatory and inhibitory regions of E_c. The signal does not propagate outside the dimensions of the input stimulus, but oscillates within those boundaries. The lateral-intralayer excitatory synapses are responsible for the firings at $T = 10$ and 31. Neurons along the edge of the stimulus remain quiescent after their initial firing due to the cumulative effects of the interlayer inhibitory synapses and the lateral-intralayer inhibitory synapses. These inhibitory synapses are also responsible for the irregular firing patterns over the peristimulus interval.

In Fig. 4.7, case (c) is shown. The input is 5 units in the x-direction and 5 units in the y-direction. This corresponds to coverage of the full excitatory region of E_c. The firing pattern is extremely regular and is confined to the dimensions of the input stimulus. The interlayer inhibitory synapses and the lateral-intralayer inhibitory synapses restrict the lateral propagation of the signal within $E1$.

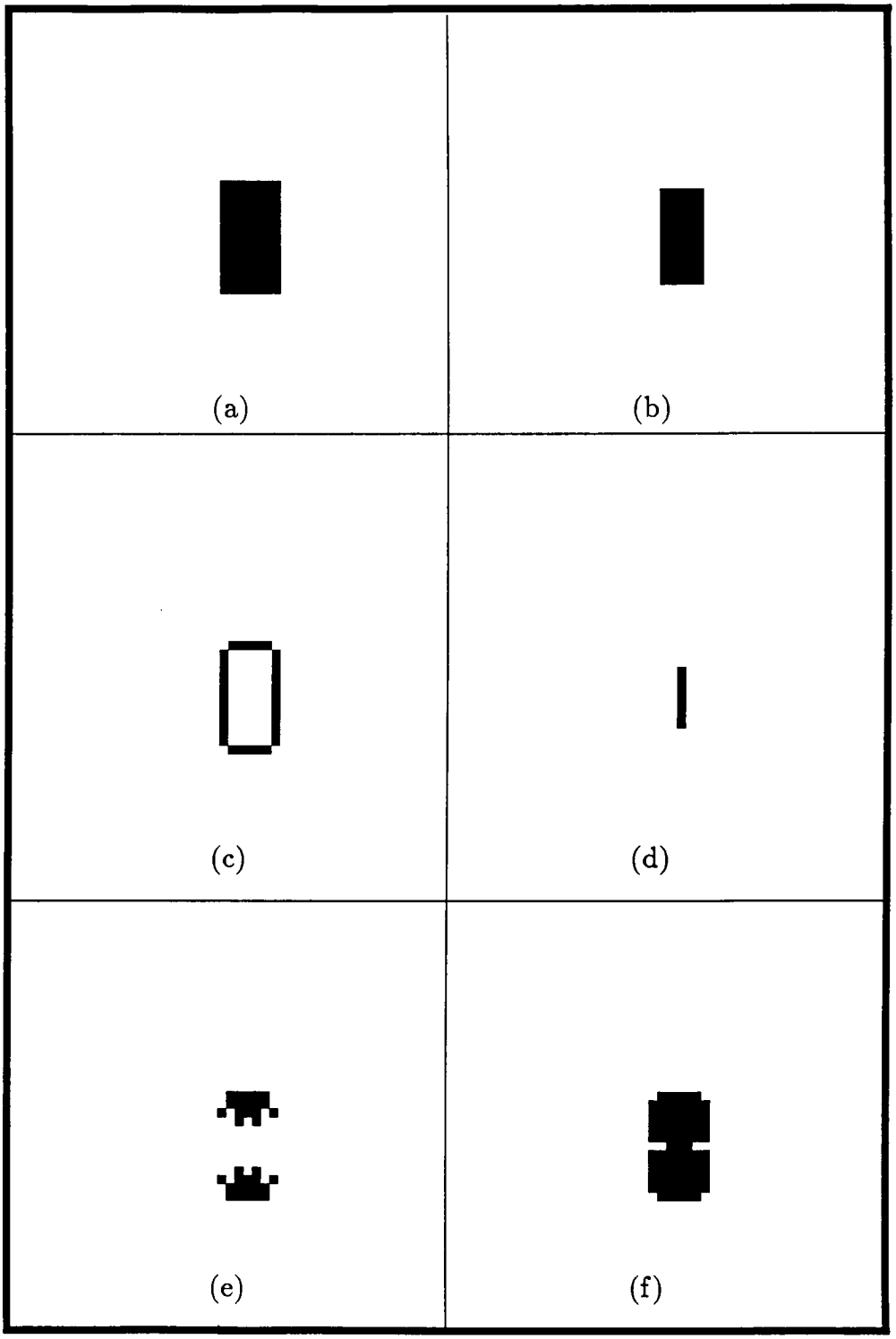


Figure 4.5: (a): Input: Half excitatory and inhibitory field coverage; (b): T = 5; (c): T = 6; (d): T = 10; (e): T = 16; (f): T = 26

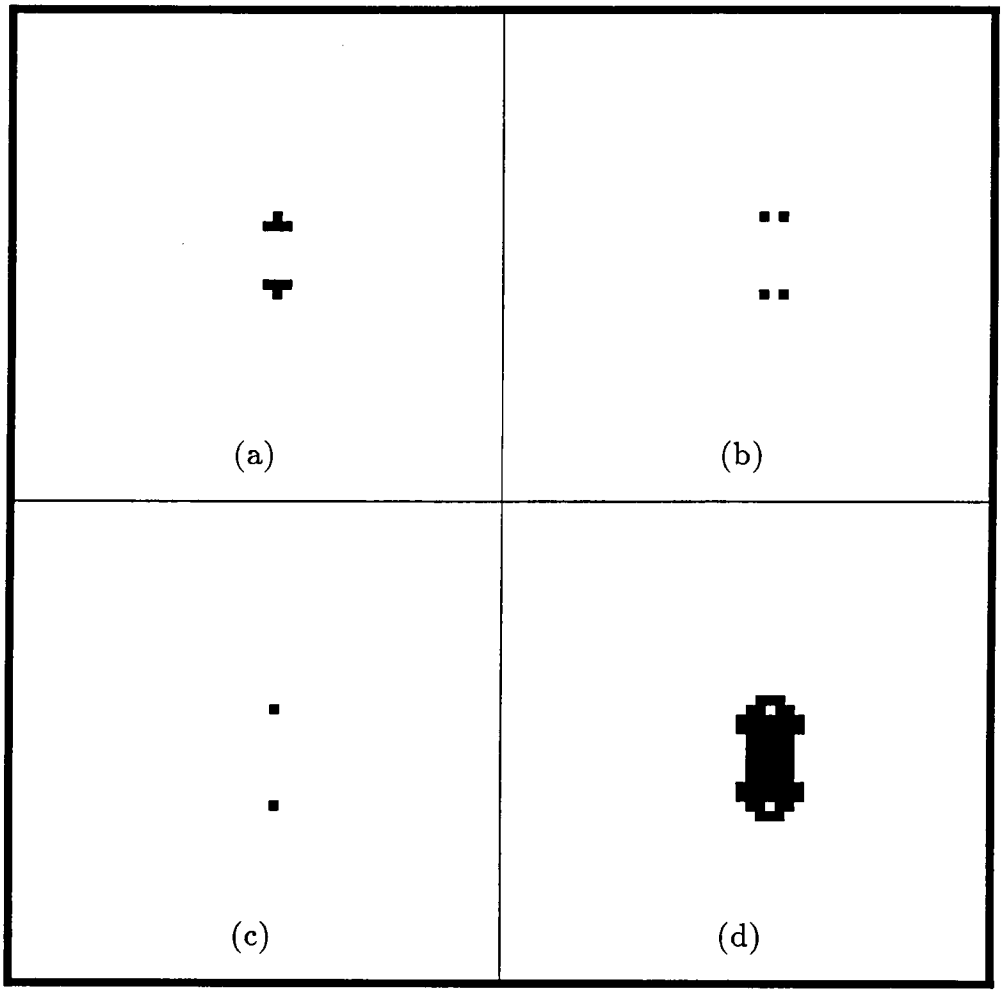


Figure 4.6: (a): T = 31; (b): T = 36; (c): T = 45; (d): T = 46

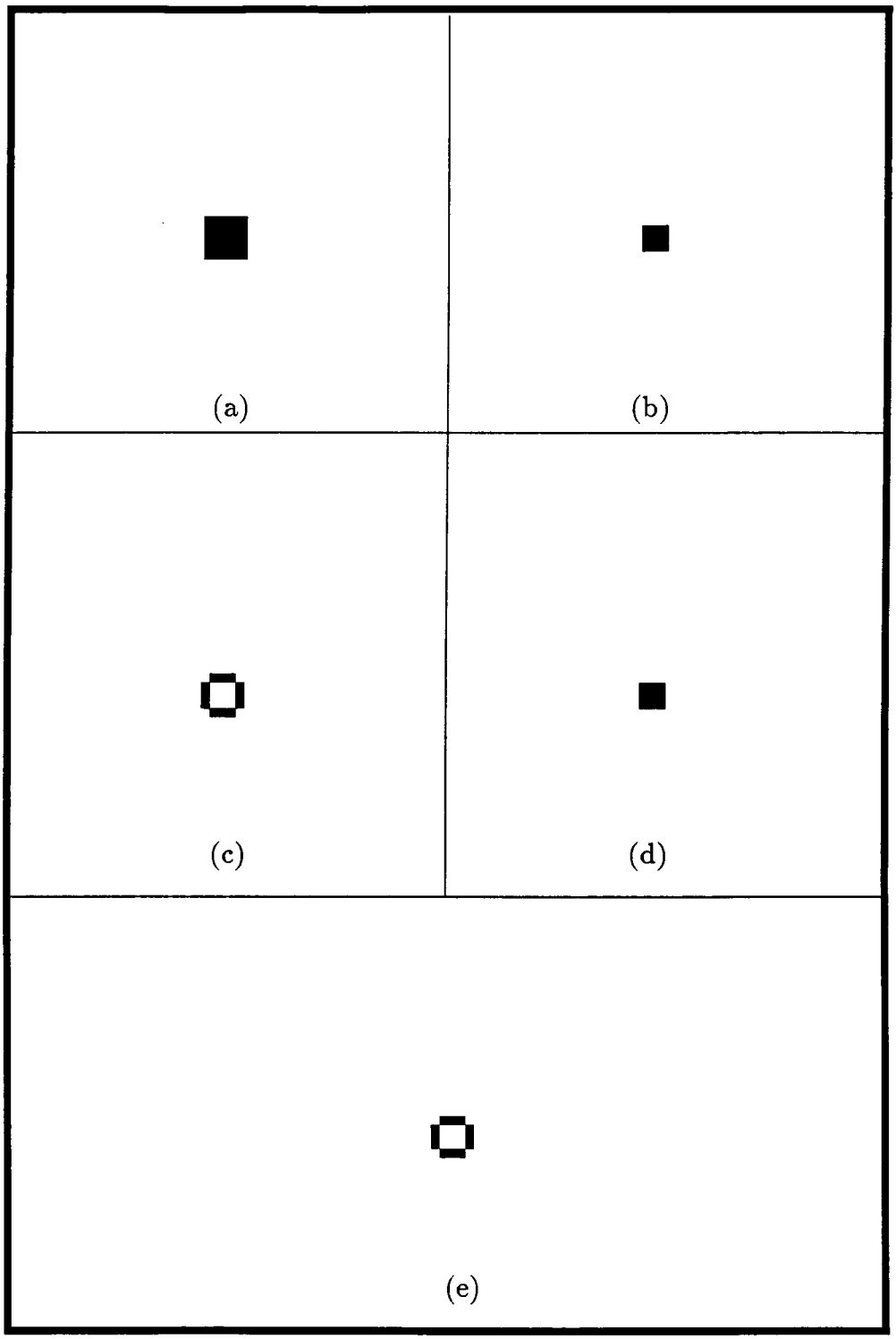


Figure 4.7: (a): Input: Full excitatory field coverage; (b): T = 5; (c): T = 6; (d): T = 15; (e) T = 16

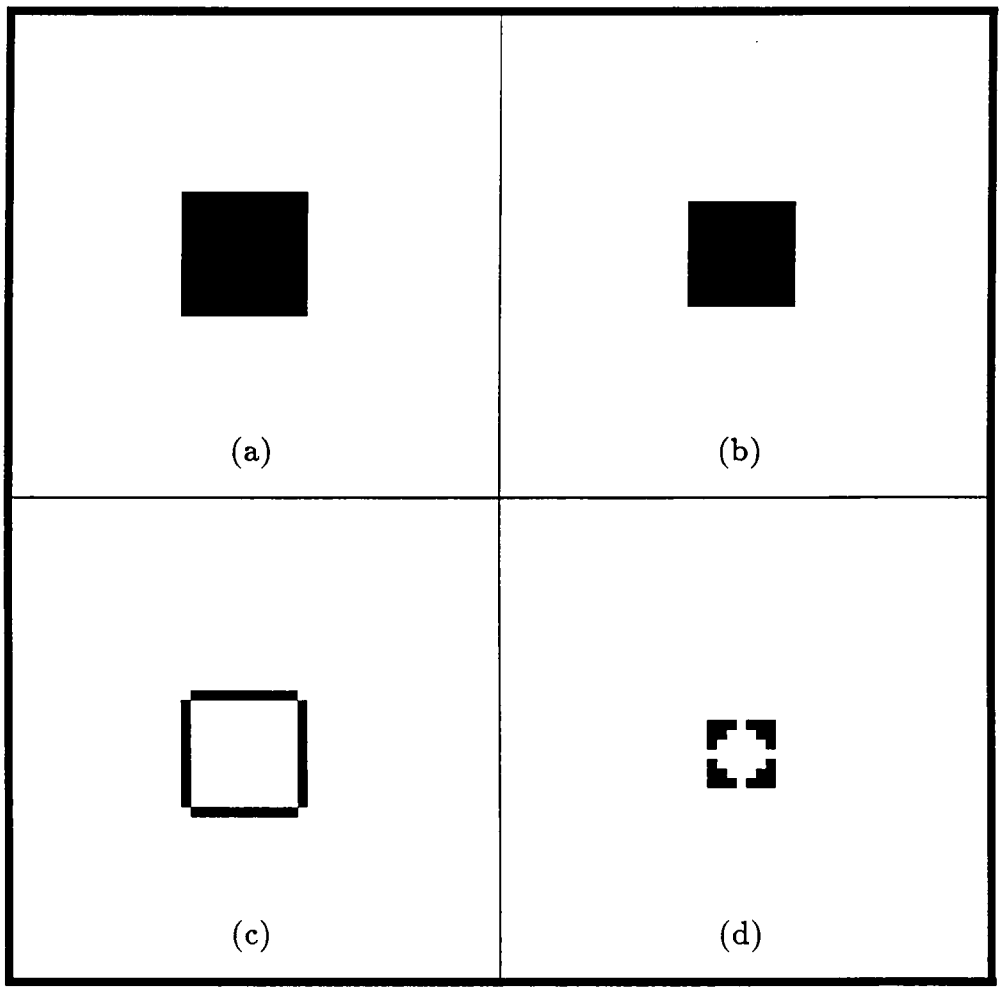


Figure 4.8: (a): Input: Full excitatory and inhibitory field coverage; (b): T = 5; (c): T = 6; (d): T = 10

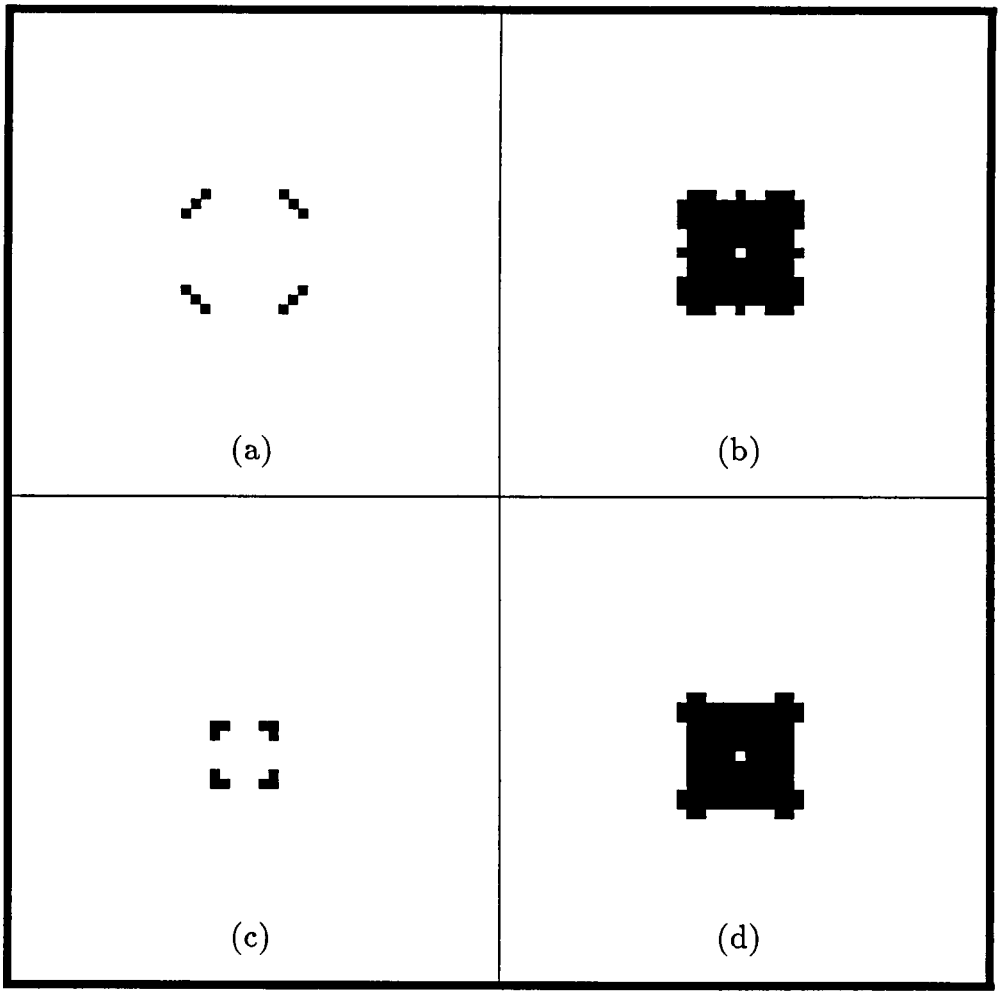


Figure 4.9: (a): T = 16; (b): T = 26; (c): T = 31; (d): T = 46

In Fig. 4.8 through Fig. 4.9, case (d) is demonstrated. The input is a 13×13 square that covers E_c's entire inhibitory and excitatory receptive field. At $T = 10$, the lateral $E1$ connections converge to a ring inside those firing at $T = 6$. E_c is completely quiescent after the initial firing. The boundary neurons with one half of the excitatory and inhibitory regions involved, those along an edge of the input, are not completely quiescent due to the cumulative effects of the interlayer excitatory synapses and the lateral-intralayer excitatory inputs, but are firing at a low frequency. Compare this with Figs. 4.5 and 4.6, case (b), in which the boundary neurons are completely quiescent after the initial firing.

Figures 4.10 through Fig. 4.15 demonstrate the effects of partial inhibitory involvement. Neurons with relatively large proportions of inhibitory involvement may become completely quiescent after a period (*e.g.*, along edges or at a central point of the stimuli). In Figs. 4.10 and 4.11, case (e), the neurons outside the stimuli boundary fire at alternating 10 ms intervals due to alternating effects of the inhibitory and excitatory intralayer inputs. A similar effect is seen in Figs. 4.12 and 4.13 and Figs. 4.14 and 4.15, cases (f) and (g). Each settles into a periodic pattern after the inhibitory and excitatory inputs have run their course at least once. In some instances it takes a much longer peristimulus interval before the pattern becomes periodic than that shown in this section.

The firing patterns within this simple configuration change spatially over time. Time delays strongly affect the firing patterns. A lateral-intralayer excitatory synapse during the refractory period may or may not elicit a spike

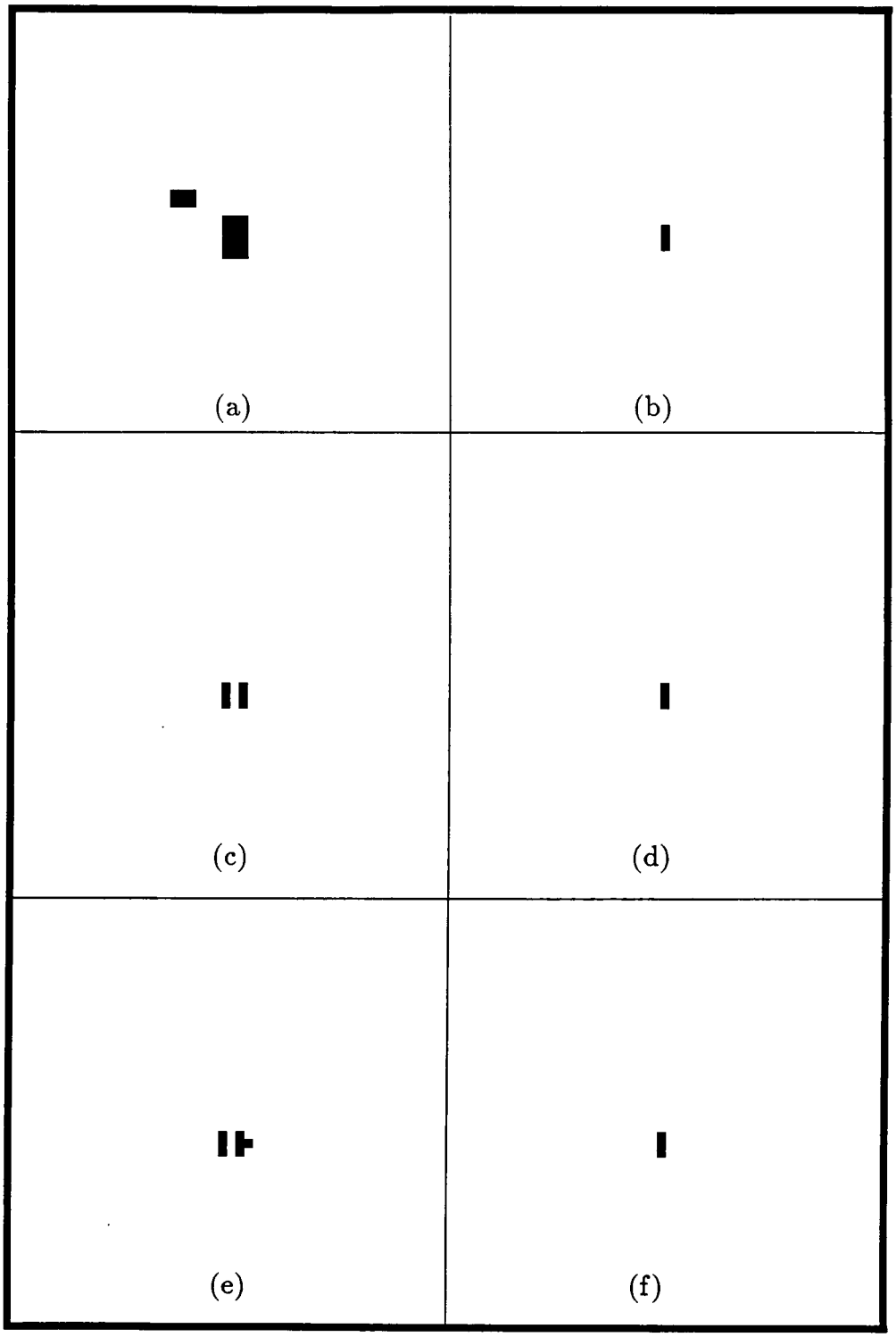


Figure 4.10: (a): Input: Half excitatory and partial inhibitory field coverage; (b): T = 5; (c): T = 6; (d): T = 15; (e): T = 16:; (f): T = 25

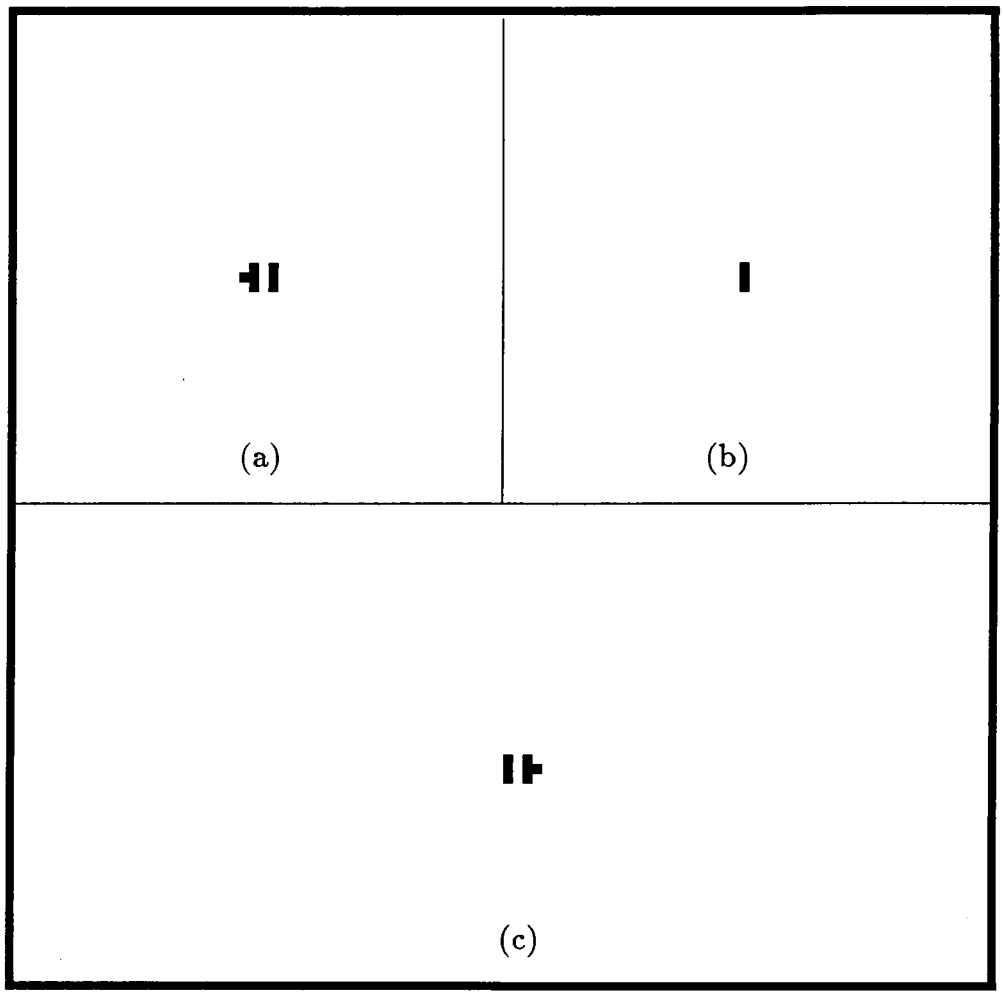


Figure 4.11: (a): T = 26; (b): T = 35; (c): T = 36

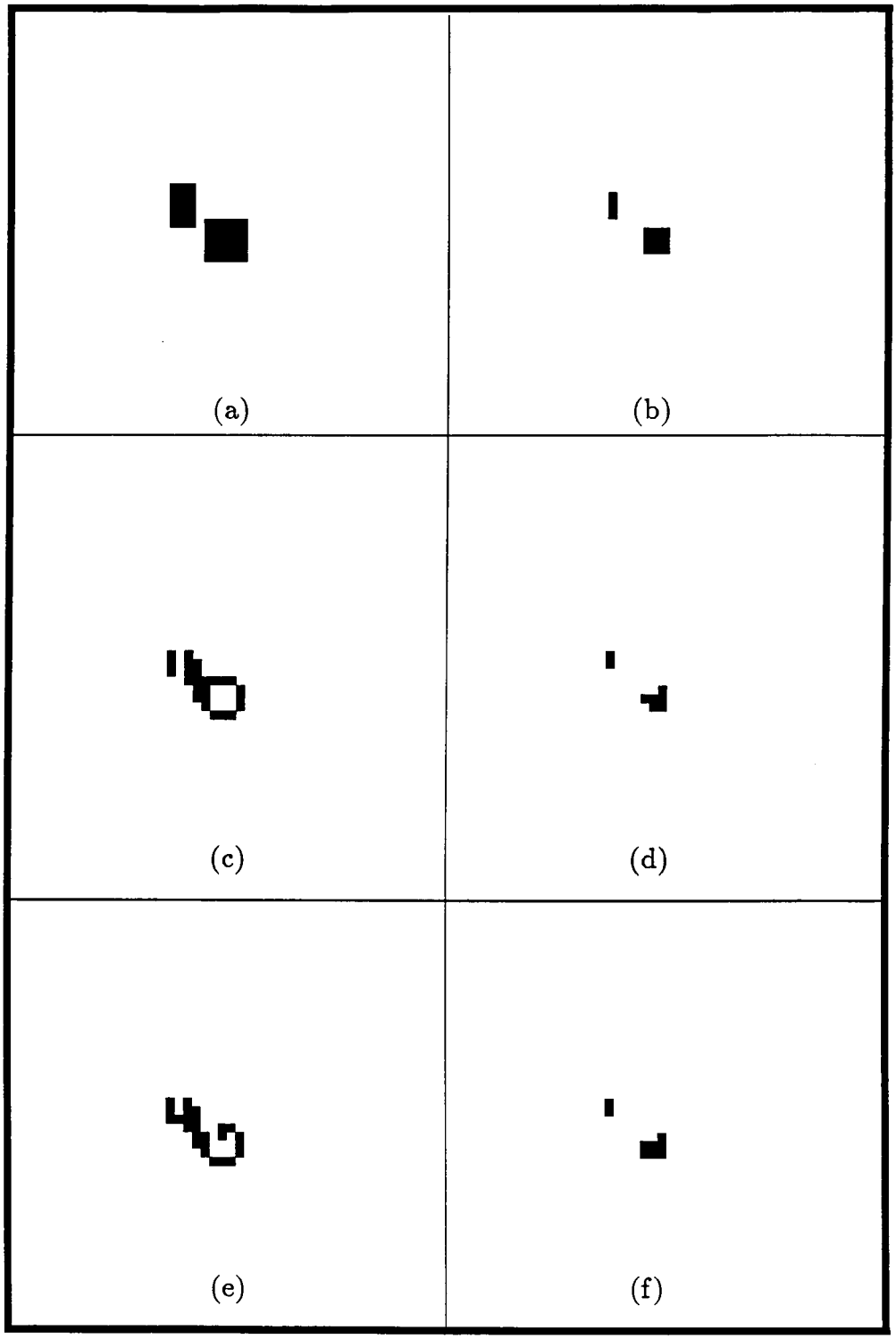


Figure 4.12: (a): Input: Full excitatory and partial inhibitory field coverage; (b): T = 5; (c): T = 6; (d): T = 15; (e): T = 16; (f): T = 25

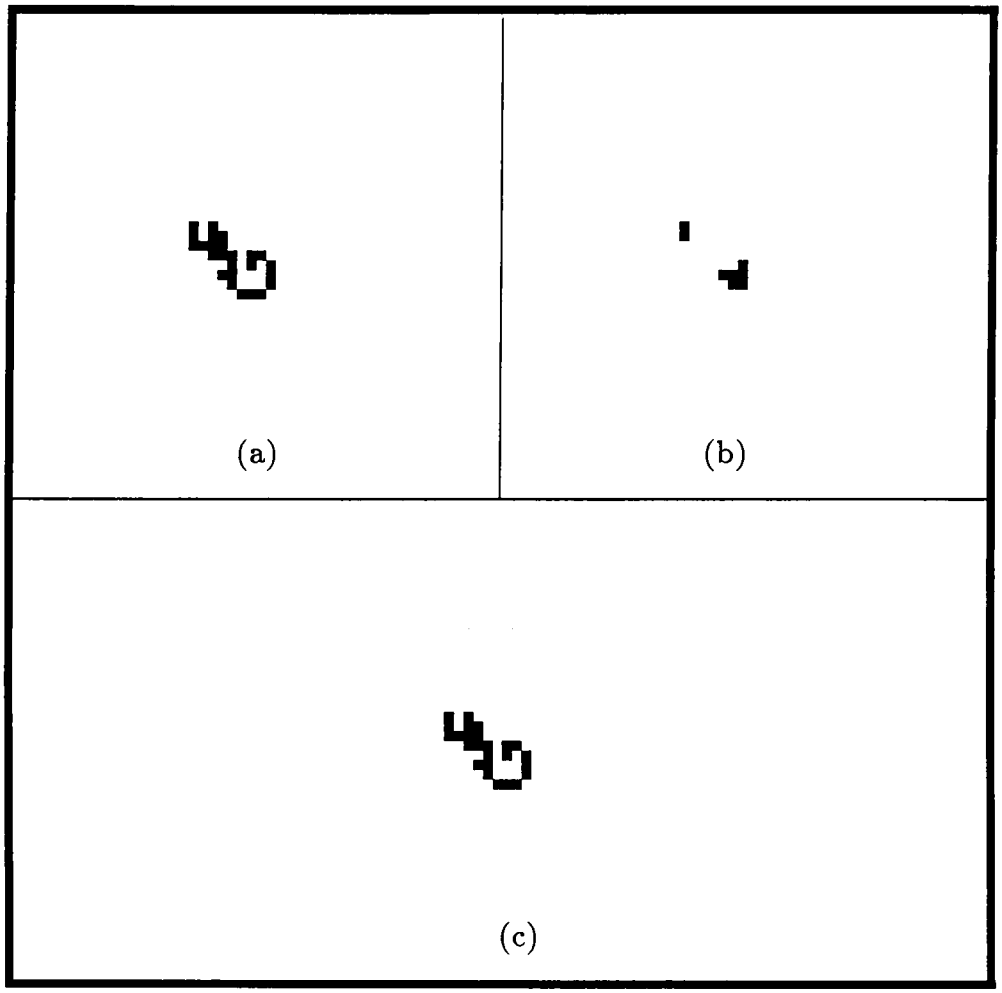


Figure 4.13: (a): T = 26; (b): T = 35; (c): T = 36

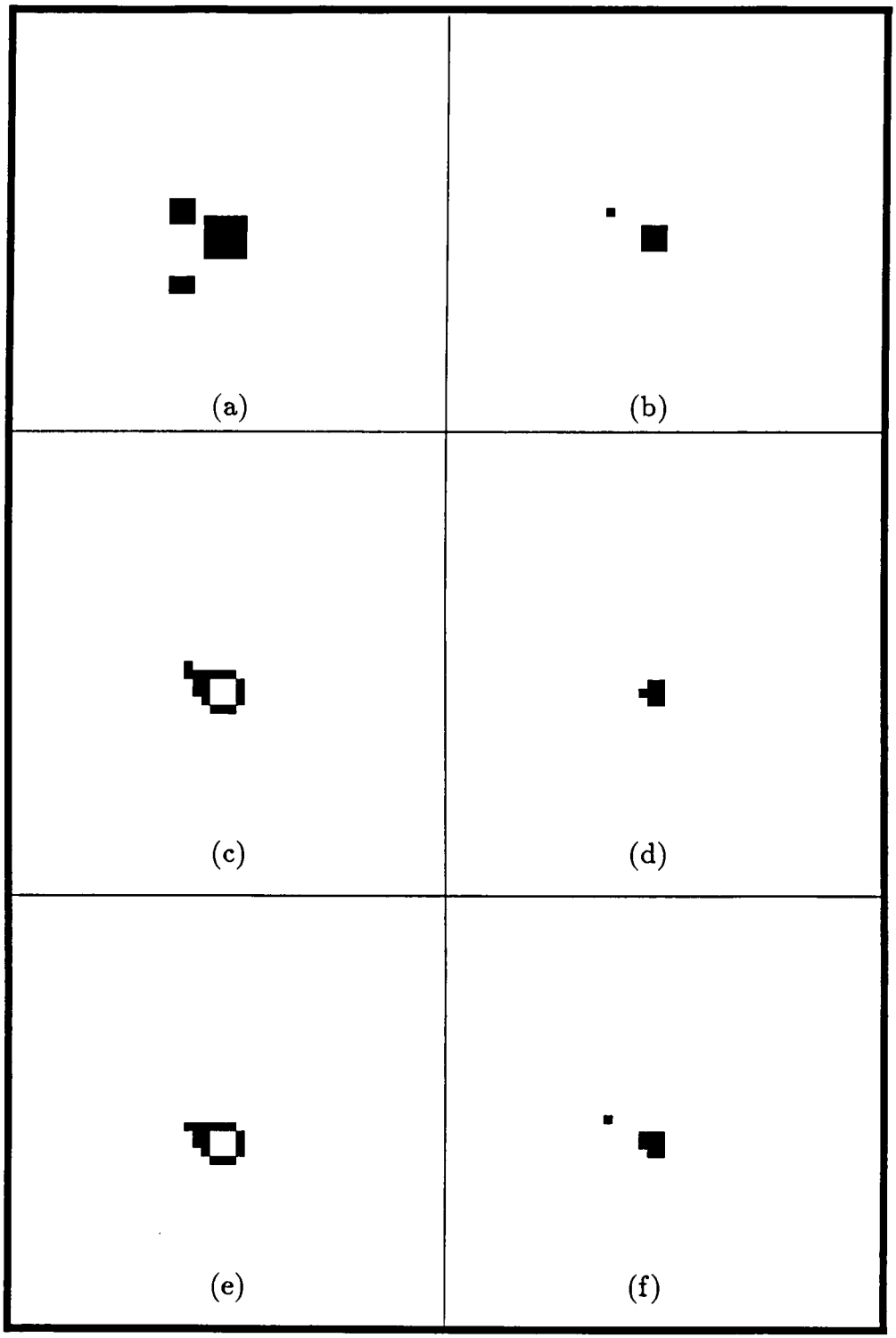


Figure 4.14: (a): Input: Full excitatory and partial inhibitory field coverage; (b): T = 5; (c): T = 6; (d): T = 15; (e): T = 16; (f) T = 25

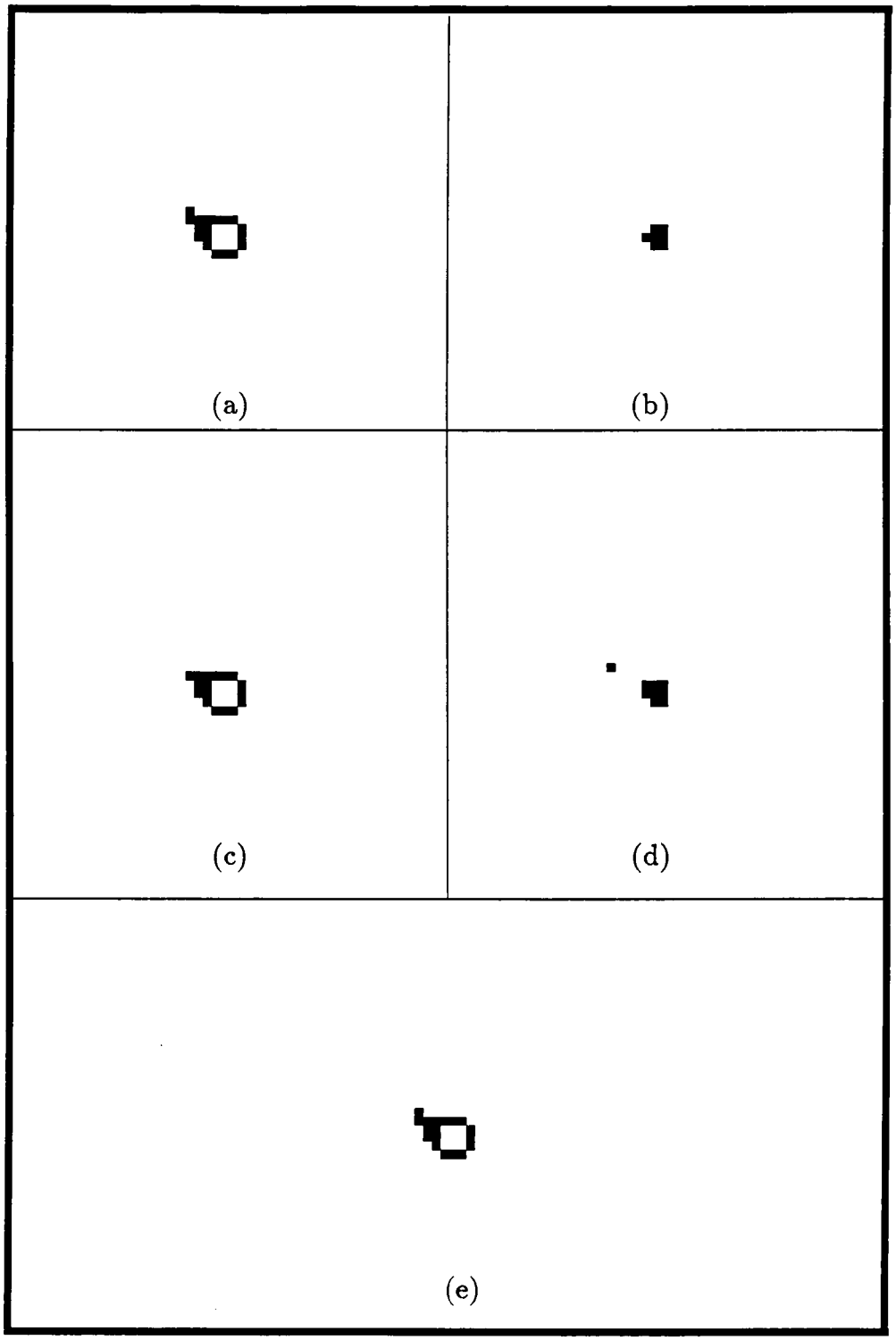


Figure 4.15: (a): T = 26; (b): T = 35; (c): T = 36; (d): T = 45; (e) T = 46

post-refractory. A lateral-intralayer inhibitory synapse that coincides, in time, with an excitory synapse, may completely cancel the excitatory effects. The time delays in this stage have been adjusted to obtain a large amount of activity within layer $E1$ for a simple set of inputs.

These firing patterns suggest that either shape or texture can be encoded by the neurons by adjusting the receptive field size in relation to the size of the input stimulus and by the amount of convergence from one layer to the next. Large receptive fields, which may consist of a neuron many layers removed from the input-convergence of finer resolution receptive fields, may encode shape. Smaller receptive fields, which also may be many layers removed from the input layer-without a large amount of convergence, may encode texture. The following discussion will focus on shape, extrapolations to texture follow logically by viewing the stimuli as elements of a textured surface. The ensemble behaviors are due to the tuning of the receptive fields of each neuron to specific sized stimuli, and the response of an ensemble to textured inputs, composed of various shapes and sizes, is revealed, in part, by it's response to an element of texture.

The preceding examples pictorially demonstrate the encoding of stimulus parameters from a given stimulus, which is seen in the two-dimensional time-varying firing pattern. This can be extended to one dimension by examining the output of a single neuron. The output of each neuron, viewed in time, is the response profile of the neuron. Each response profile is a mapping of the input seen, directly or indirectly, by the neuron during the peristimulus interval and,

thus, reflects in one-dimension the encoding of local stimulus parameters.

4.3.3 Time-Varying Characteristics of Single Neurons in the Ensemble

The main thesis in this work is that the time-varying response of a neuron contains the pertinent stimulus parameters necessary for recognition and that known physiological mechanisms are instrumental for the signal processing that produces the time-varying response. This has been demonstrated in a very coarse sense with the time-varying spatial firing patterns. It is further, and more definitively, demonstrated in the analysis the response profiles of E_c for each of the 7 cases already mentioned. The profiles of this single neuron contain highly localized information and do not contain enough information for shape or texture analysis for the given input set. This follows from the previous development of the tuned receptive fields. The neurons in $E1$ are tuned to encode local input parameters. An analysis of the $E1$ response profiles shows only localized encoding (Figs. 4.16 and 4.17). The pertinent features of the response profile are the latency time to firing, the inter-spike times, and the frequency of firing (Chapter 3). These features are discussed in the response profile of E_c and in subsequent sections.

In cases (a), (c), (e), (f), and (g); corresponding to half excitatory field coverage, full excitatory field coverage, half excitatory coverage and partial inhibitory coverage, full excitatory coverage and partial inhibitory coverage, and a second

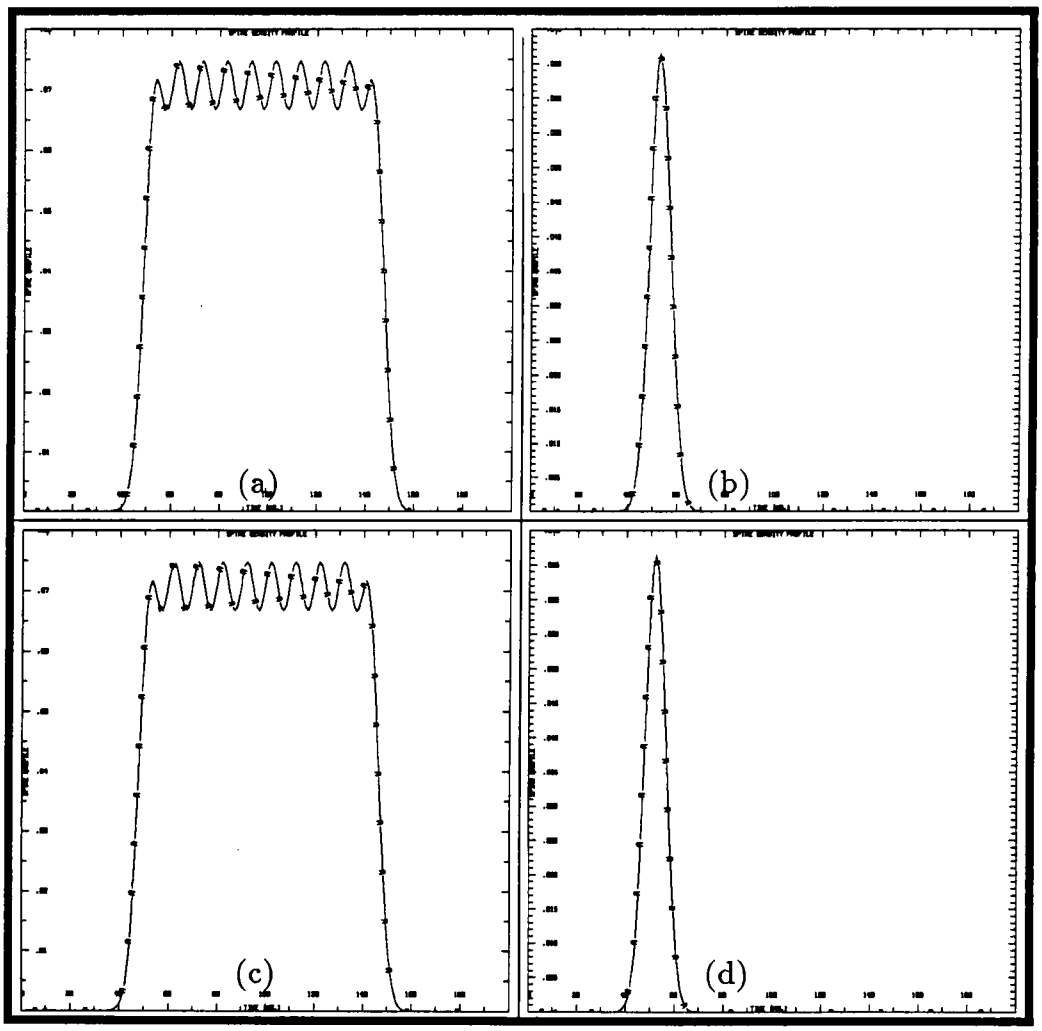


Figure 4.16: Response profiles of E_c (a): Case (a); (b): Case (b); (c): Case (c); (d): Case (d)

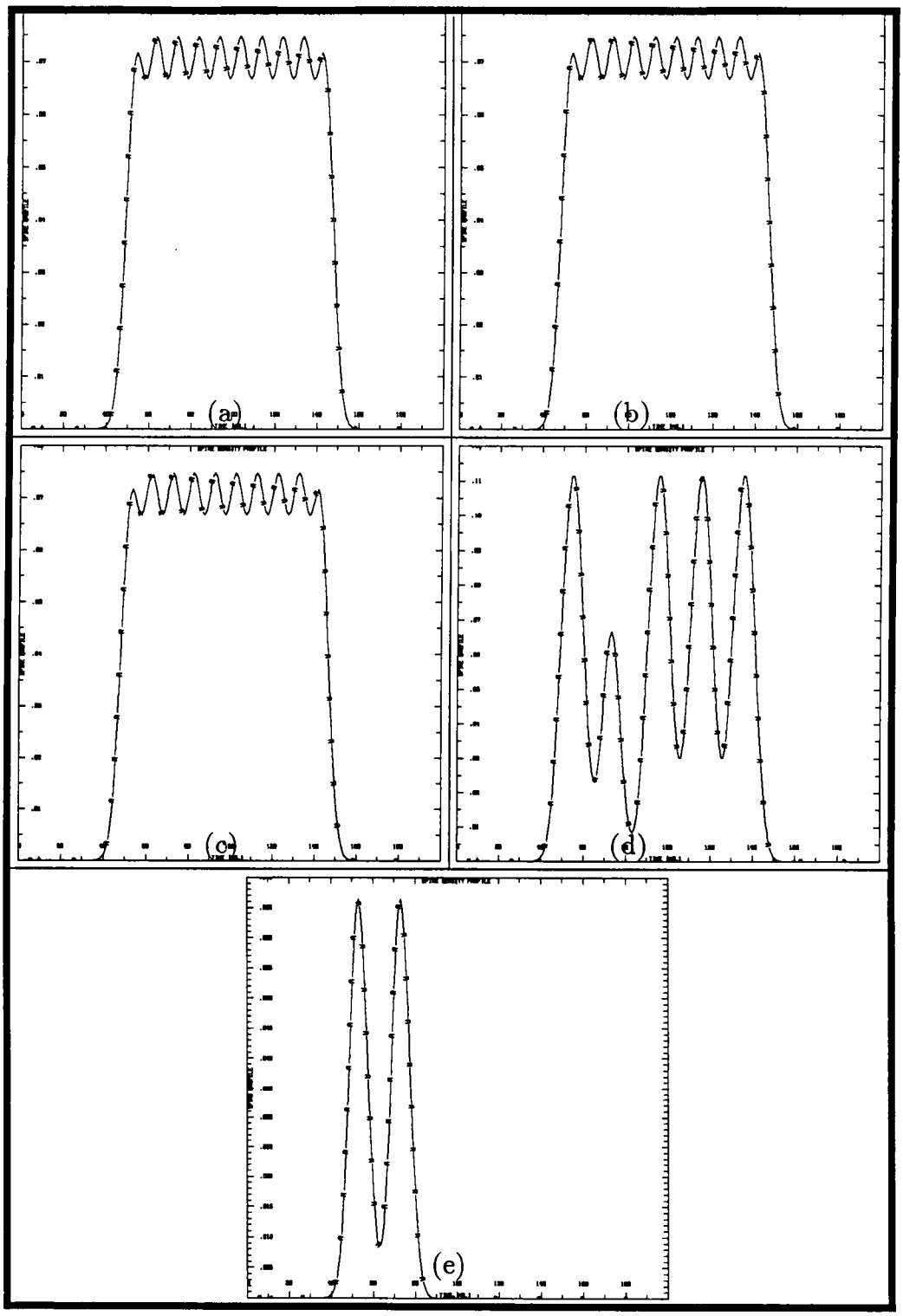


Figure 4.17: Response Profiles of E_c (a): Case (e); (b): Case (f); (c): Case (g); (d): Case (b) middle; (e) Case (d) edge

case of full excitatory coverage and partial inhibitory coverage, respectively; the profiles can be used to group the 5 cases into 2 groups. Further differentiation is not possible since, while the additional inputs in cases (e), (f), and (g) had a substantial effect on the spatial firing patterns, they did not, because of their location, affect E_c. The most obvious feature, the firing frequency, is not the differentiating characteristic in the waveform. There is a one time step difference in the latency to firing betweeen cases (a) and (e) and cases (c), (f), and (g). The shorter latency in (c), (f), and (g) is a result of a larger area of the excitatory region of E_c being involved. This further emphasizes the highly local information contained in the tuned receptive fields. The profile in cases (b), E_c positioned at the edge of the half excitatory and inhibitory field coverage input, and (d), E_c positioned at the center of a full excitatory and inhibitory field coverage input, show a single initial firing and then the neuron remains quiescent throughout the remaining peristimulus interval. The response of the neuron positioned at the center of the input in case (b) is shown in Fig. 4.17. This neuron does not have as much activity as E_c because of the intralayer excitatory and inhibitory synapses. It does reflect, because of it's position relative to the input, more global information processing than E_c. The response of the neuron positioned at the edge of the input in case (d) is shown in Fig. 4.17. This neuron does not remain quiescent after the initial firing, but has a second spike a short time later. This is repeated, though not shown for this short of a peristimulus interval, after a long period of stimulation. It does remain substantially less

active than the other neurons.

In the preceding, the behavior of the tuned receptive fields used in this work was pictorially demonstrated. Two of the three pertinent waveform characteristics have been discussed, latency to firing and firing frequency. A single time step difference in firing can make a substantial difference over a peristimulus interval as the signals propagate to subsequent layers of neurons. Furthermore, the firing frequencies are often not as pertinent as inter-spike distances. Each of the three characteristics are discussed in the following.

The output of a single neuron can reflect the encoding of the globally pertinent stimulus features seen by the entire ensemble of neurons. That is to say, not only can the time-varying spatial response of an ensemble of neurons uniquely encode and transmit the pertinent stimulus parameters, but a single neuron can uniquely encode and transmit the pertinent stimulus parameters. This is the topic of the next section.

CHAPTER 5

Development of a Layered System

In Chapter 4, the dynamics of individual neurons, their receptive fields, and the dynamics of an ensemble of neurons have been developed in terms of encoding and transmitting features from an input stimulus. Stimulus features were shown to be encoded and transmitted by the dynamics of individual neurons within an ensemble by the time-varying spatial firing patterns of a layer of neurons and the response profiles of individual neurons within the ensemble. At this level, the main neuron parameter responsible for the time-varying responses is the time delay discussed in the development of the receptive fields. The processing was shown to be highly localized at individual neurons; while the processing of the ensemble reflected the global processing. In this section, the architecture and embedded time delays are adjusted so that the signal processing of individual neurons encode and transmit global features, transmitted by $E1$, through the time-varying firing patterns of a second layer of neurons, $E2$. The coarseness of global processing, defined as the sensitivity to detail in the input signal, is controlled by the size and weighting of the inter- and intralayer receptive fields and Δt_{ji}. Global processing is shown in both a coarse and a fine encoding of the input parameters. Layer $E2$ receives a feedforward signal from the $E1$. The

pertinent parameter values for coarse and fine encoding are given in Table 5.1.

5.1 Coarse Encoding

The objective of the following is to develop an ensemble, $E2(m,n)$, whose E_c response profile reflects the encoding of the global stimulus parameters, transmitted from $E1$, in a coarse sense. The layer receives a feedforward signal from $E1$, described in Section (4.3). The time-varying spatial firing patterns and the response profile of E_c are discussed to explain the signal processing.

5.1.1 Architecture of the Second Layer

The architecture of $E2$ is similar to $E1$. The nomenclature is defined in the following. Layer $E2$ is an $NE2 \times NE2$ array of neurons with receptive fields defined as follows. For each neuron, i, in $E2(m,n)$, there is an $SE1_i \times SE1_i$ neighborhood in $E1(k,l)$ that composes the first feedforward receptive field of i. Likewise, for each neuron, i, in $E2(m,n)$, there is an $SE2_i \times SE2_i$ neighborhood in $E2(m,n)$ that composes the intralayer receptive field of i. The two receptive field components, together, define the receptive field of the neuron. The interlayer receptive fields are defined by: a point (k,l) in $E1$ is an element of the receptive field of neuron i in $E2$ if $|D_{ji}| \leq int(SE1_i/2)$, where $D_{ji} = max(k-k_j, l-l_j)$. The terms k_j and l_j designate the position in the array of points in $E1$. Points outside of this neighborhood have no direct synaptic links to neuron i. The mapping may or may not provide a complete mapping of each point in $E1$ to a receptive field

Table 5.1: Tuning Parameters: Receptive Field Sizes and Weighting.

Simulation	*coarse*	*fine*	*localize*	*learn*
SI	13	13	13	13
CI	5	5	5	5
ω_{SI}	-0.068	-0.068	0.04	-0.068
ω_{CI}	0.19	0.19	0.04	0.19
SE	13	13	13	13
CE	5	5	5	5
ω_{SE}	-0.55	-0.55	-0.55	-0.55
ω_{CE}	0.21	0.21	0.01	0.21
$\Delta t_{layer}(inter)$	4	4	3	4
$\Delta t_{layer}(intra)$	3	3	2	3
θ_i *E1*	0.5	0.5	0.5	0.5
SE1	15	15	15	15
CE1	7	7	7	7
ω_{SE1}	-0.045	-0.045	0.061	-0.045
ω_{CE1}	0.091	0.091	0.061	0.091
SE2	15	15	15	15
CE2	7	7	7	7
ω_{SE2}	-0.55	0.55	-0.55	0.55
ω_{CE2}	0.33	-0.33	0.13	-0.33
τ	4.3	4.3	4.3	4.3
$\Delta t_{layer}(inter)$	2	2	2	2
$\Delta t_{layer}(intra)$	4	4	4	4
θ_i *E2*	0.5	0.5	0.58	0.5
Δt_{ref}	5	5	5	5
Inp_{delay}	10	1	10	
Δt_{float}			30	
B_{rest}			0.1	
Δt_{learn}				50
C_{learn}				0.09
Δt_{set}				14

center in $E2$. In the incomplete case, sampling is very coarse. The mapping in this section is complete; the coarse encoding is provided by other mechanisms, as explained in the Section (5.1.2). The intralayer receptive fields are defined by: a point (m,n) in $E2$ is an element of the receptive field of neuron i in $E2$ if $|D_{ji}| \leq int(SE2_i/2)$, where $D_{ji} = max(k - k_j, l - l_j)$. The terms k_j and l_j designate the position in the array of points in $E2$. Points outside of this neighborhood have no direct synaptic links to neuron i.

Each neighborhood has a structure composed of a center-surround (**C-S**) architecture. The C-S connections from $E1$ are defined first. The surround is an $SE1_i \times SE1_i$ annulus with strength w_{is} and the center is a $CE1_i \times CE1_i$ neighborhood with strength w_{ic}. The C-S connections within $E2$ are defined similarly. The surround is an $SE2_i \times SE2_i$ annulus with strength w_{es} and the center is a $CE2_i \times CE2_i$ neighborhood with strength w_{ec}. All connections are assumed to be unchangeable in strength and linkage in this section. The dimensions of each region are given in Table (5.1).

5.1.2 Time-varying Characteristics of the Second Layer

The receptive fields of the neurons in $E2$ are tuned to respond to larger inputs, or lower spatial frequencies, than $E1$. This is done by increasing the spatial extent of both the center and surround mechanisms of $E2$ with respect to $E1$. The tuning of neurons in an ensemble above the first layer can not be done on the basis of the spatial extent of the input signal to the layer. The time-

varying characteristics of the signal impose a unique set of problems in the tuning process. For the ensemble discussed in this section, the receptive fields have been tuned in the same manner as $E1$ but are then adjusted to perform with the desired coarseness by adjusting Δt_{ji}. This section focuses on the analysis of $E2$ in response to various shapes introduced to $E1$ by I and is not concerned with analyzing the $E2$ response to variations in texture (spatial frequency). The objective is to *tune* the receptive fields of $E2$ such that the response profile of E_c in $E2$ reflects global features of $E1$, and thus of I.

The receptive fields are tuned in two steps. First, the spatial extent of the receptive fields in $E2$ is larger than that used in $E1$. They are tuned as if they receive a direct input from I. The larger spatial extent means that a larger input stimulus is necessary to elicit a response from the neurons in $E2$ because each synapse is effectively weighted by a weaker link. A further difference is that each neuron integrates excitatory synapses over a longer time period than those in $E1$. Thus, there is a trade-off between the increased spatial input seen by each neuron, which potentially would make each neuron more sensitive, and the combined effect of weaker links and increased decay of each signal (due to larger D_{ji}), which makes each neuron less sensitive to smaller inputs. Similar arguements apply to the inhibitory surround. The second step in the tuning process is an adjustment of Δt_{layer} to increase the sensitivity of $E2$ to specific features, characterized by mass activity in $E1$ and transmitted from $E1$.

The net result is that neurons in $E2$ will not fire unless they receive a large

number of excitatory synapses from $E1$ over a relatively short time interval. While a given static signal may elicit a response in $E2$; the same signal presented in full through piecewise presentations over a period of time may not elicit a response in $E2$. This is exploited to make $E2$ less sensitive to small features transmitted from $E1$. Once $E2$ does respond to $E1$, each neuron is in a heightened state of excitement, which is increased by the intralayer synapses. Neurons in this state may respond to smaller inputs. Overall, $E2$ responds to large amounts of activity in $E1$.

The response profiles of E_c in $E2$ reflect this behavior as shown in Fig. 5.1 and 5.2; corresponding to case (a), half excitatory field coverage; case (b), half excitatory and inhibitory field coverage; case (c), full excitatory field coverage; case (d), full excitatory and inhibitory field coverage; case (e), half excitatory and partial inhibitory field coverage; and cases (f) and (g), full excitatory and partial inhibitory field coverage. The response profiles in cases (a) and (e) show no activity from E_c. In both cases, the same input signal will elicit a response in $E2$ if $E2$ is directly stimulated from I instead of from $E1$. This exemplifies the significance of including time in the tuning process of layers above the initial $E1$ layer and suggests a tuning strategy for textured inputs, in which multiple layers of neurons tuned for different resolutions could be used to encode textural properties. The response of E_c in cases (c), (f), and (g) is similar in each case, indicating the coarseness of the encoding. In cases (b) and (d), the firing frequency and the latency to firing are equal but the interspike time differences

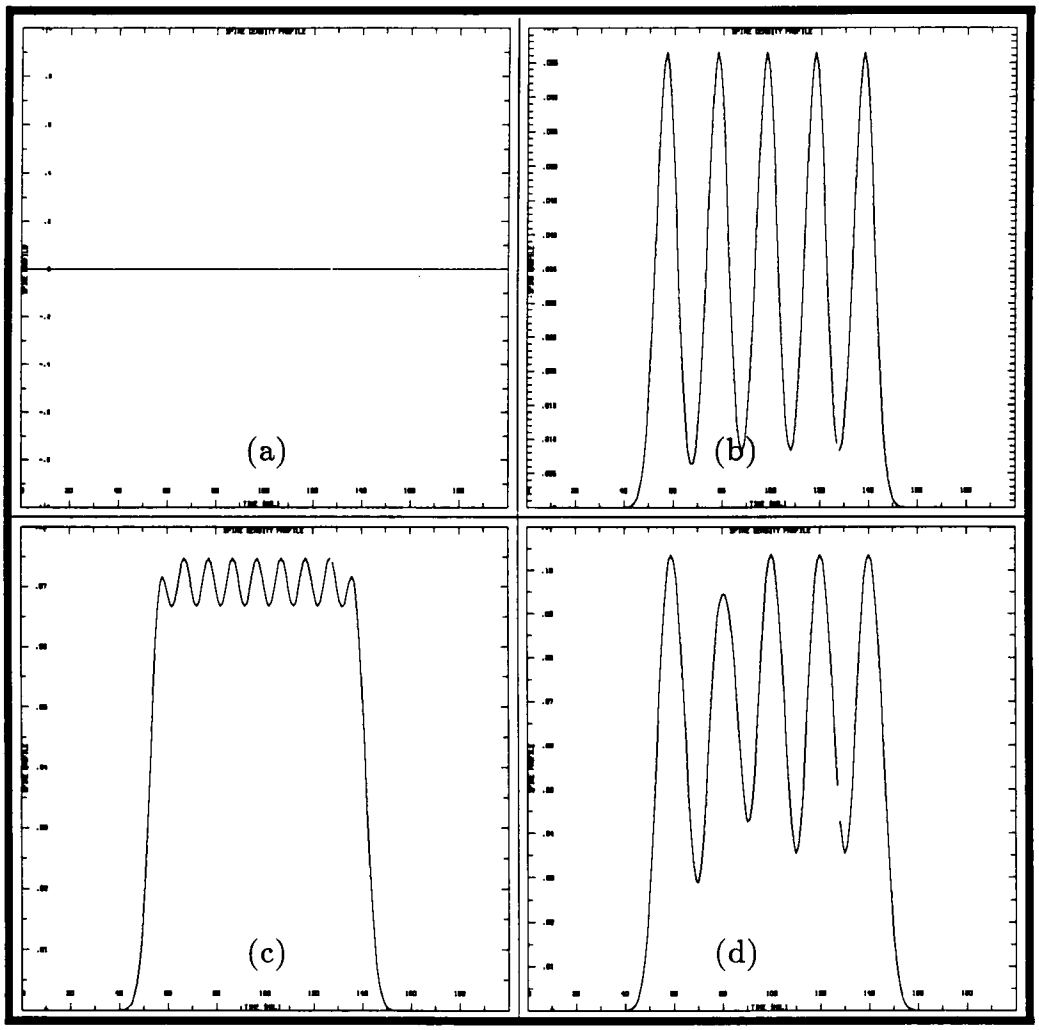


Figure 5.1: Response Profiles of E_C in $E2$ (a): case a: Half excitatory field coverage; (b): case b: Half excitatory and inhibitory field coverage; (c): case c: Full excitatory field coverage; (d): case d: Full excitatory and inhibitory field coverage

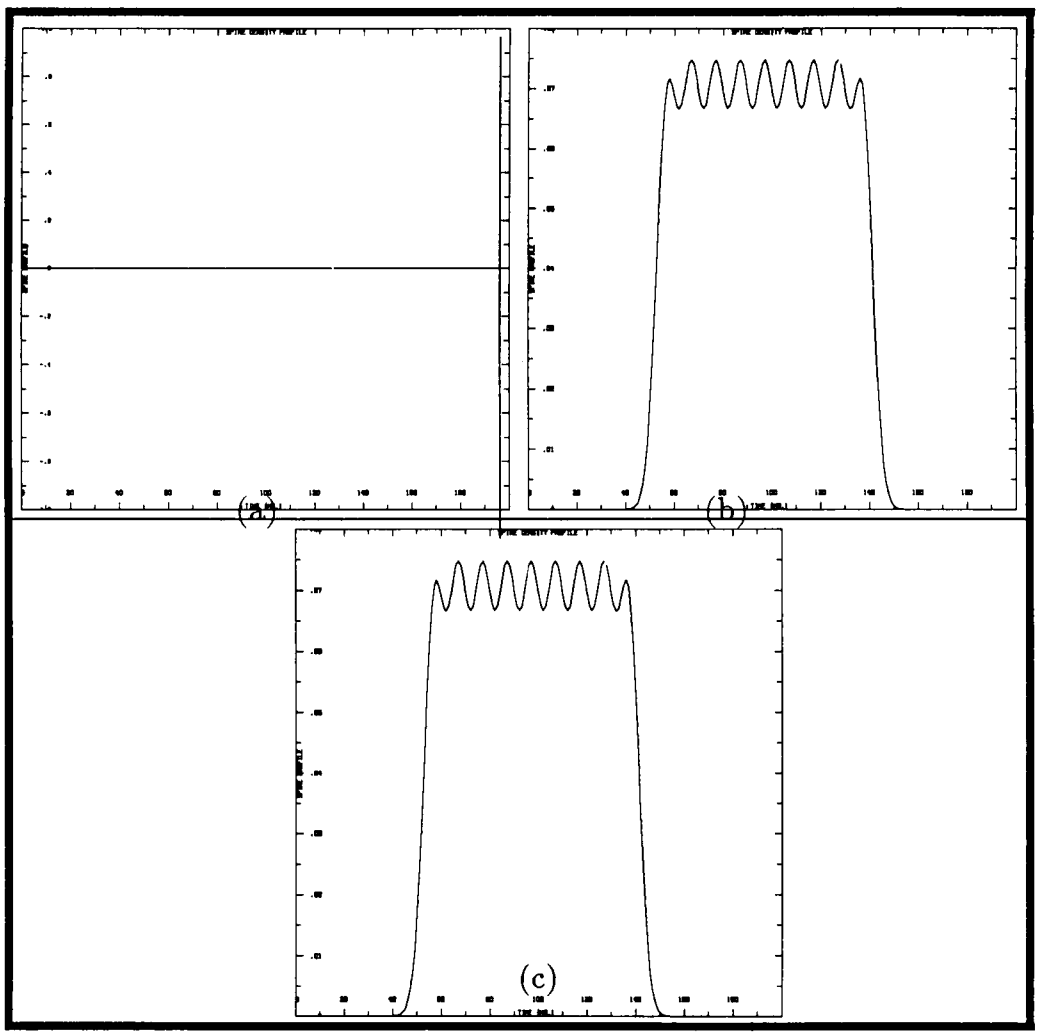


Figure 5.2: Response Profiles of E_c in $E2$: (a): case e: Half excitatory and partial inhibitory field coverage; (b): case f: Full excitatory and partial inhibitory field coverage; (c): case g: Full excitatory and partial inhibitory field coverage

result in differring waveform shapes. The interspike time differences provide another dimension for information encoding and transmission in addition to spike frequency and latency to firing.

In Figs. 5.3 to 5.12, the time-varying spatial patterns of $E2$ are shown for each of the seven cases, excluding cases (a) and (e), for which no response was elicited in $E2$. Only cases (b) and (f) are discussed as they are representative of the behavior of $E2$. The others figures are included for completeness. In case (b), the amount of activity in $E2$ is initially larger than that of $E1$, reflecting the coarseness of the processing done by $E2$. The response at $T = 14$ is the result of a relatively small input from $E1$ in conjunction with the intralayer synapses. The response at $T = 19$ is fairly small in comparison to the input from $E1$, $T = 16$. At $T = 29$ and 30 a great deal of activity results from the large input from $T = 26$. The intralayer synapses from this period are strong enough that the relatively small input at $T = 31$ from $E1$ elicits a response at $T = 35$ in $E2$. Neither of the inputs at $T = 36$ and 45 are seen by $E2$. Finally, a large input from $T = 46$ elicits spikes in $E2$ during two of the four excitatory input intervals, $T = 49$ and 50. In summary, large inputs take $E2$ into a highly excited state that results in a great deal of activity, which may keep $E2$ excited enough to respond to a relatively small input. If $E2$ is not in an excited state, it does not respond to smaller input stimuli.

In case (f), the response in $E2$ is less than that of $E1$ in each time step. This is predictable from the responses as discussed in case (b) since the input is

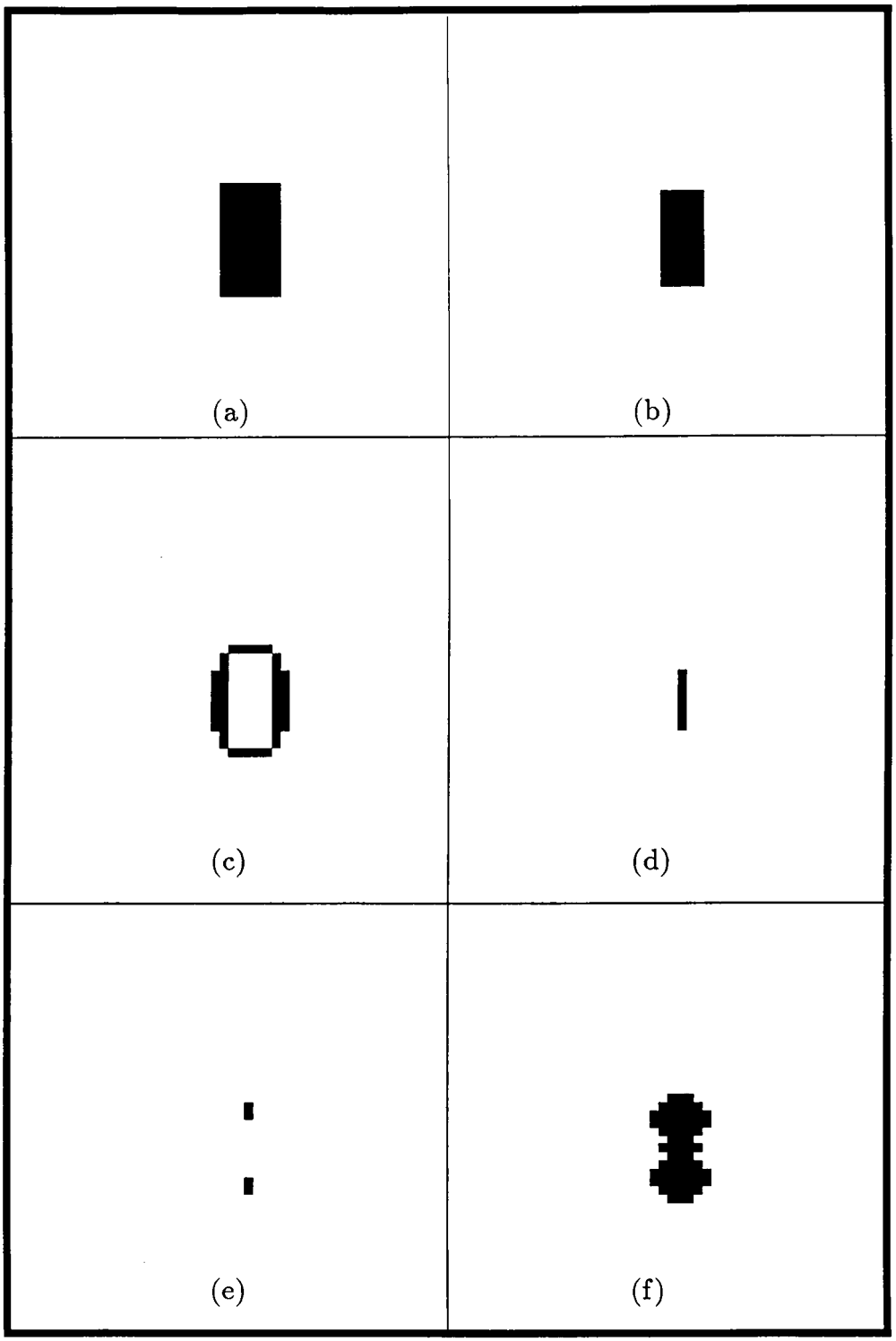


Figure 5.3: (a): Input: Half excitatory and inhibitory field coverage; (b): T = 8; (c): T = 9; (d): T = 14; (e): T = 19; (f): T = 29

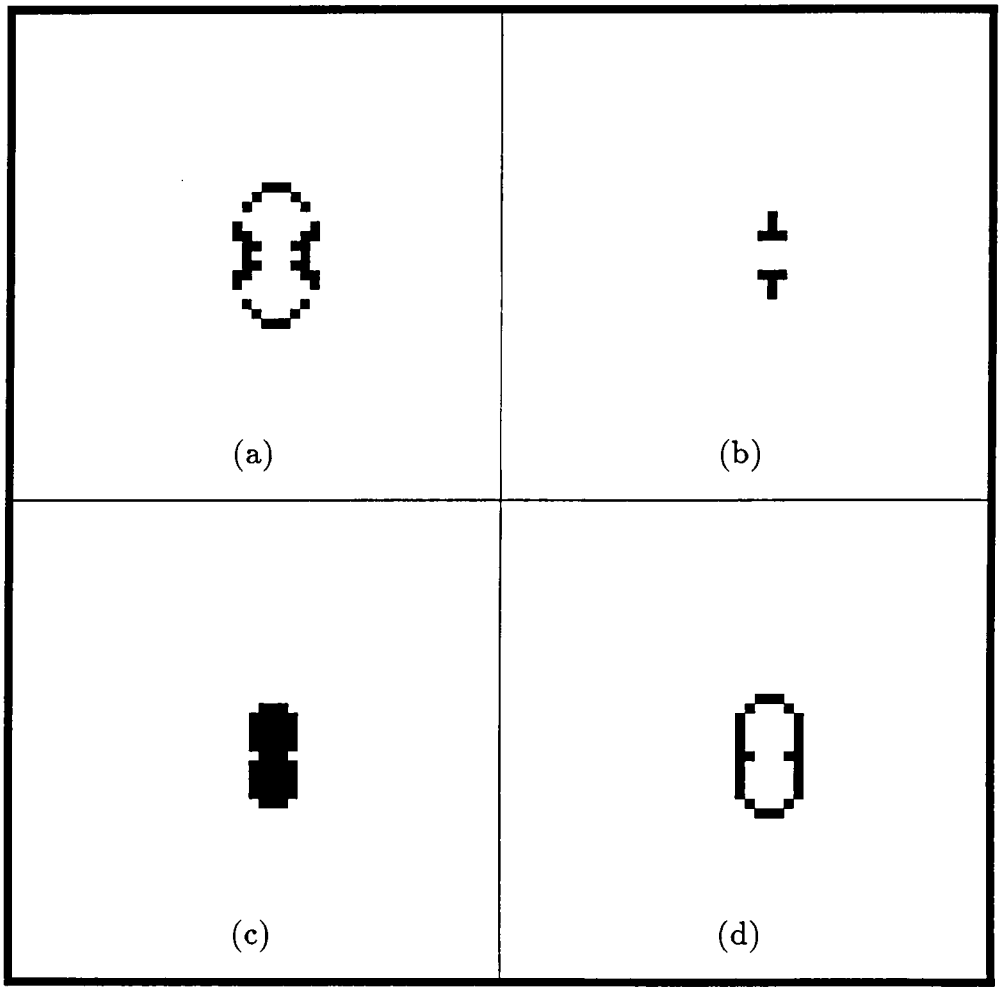


Figure 5.4: (a): T = 30; (b): T = 35; (c): T = 49; (d): T = 50

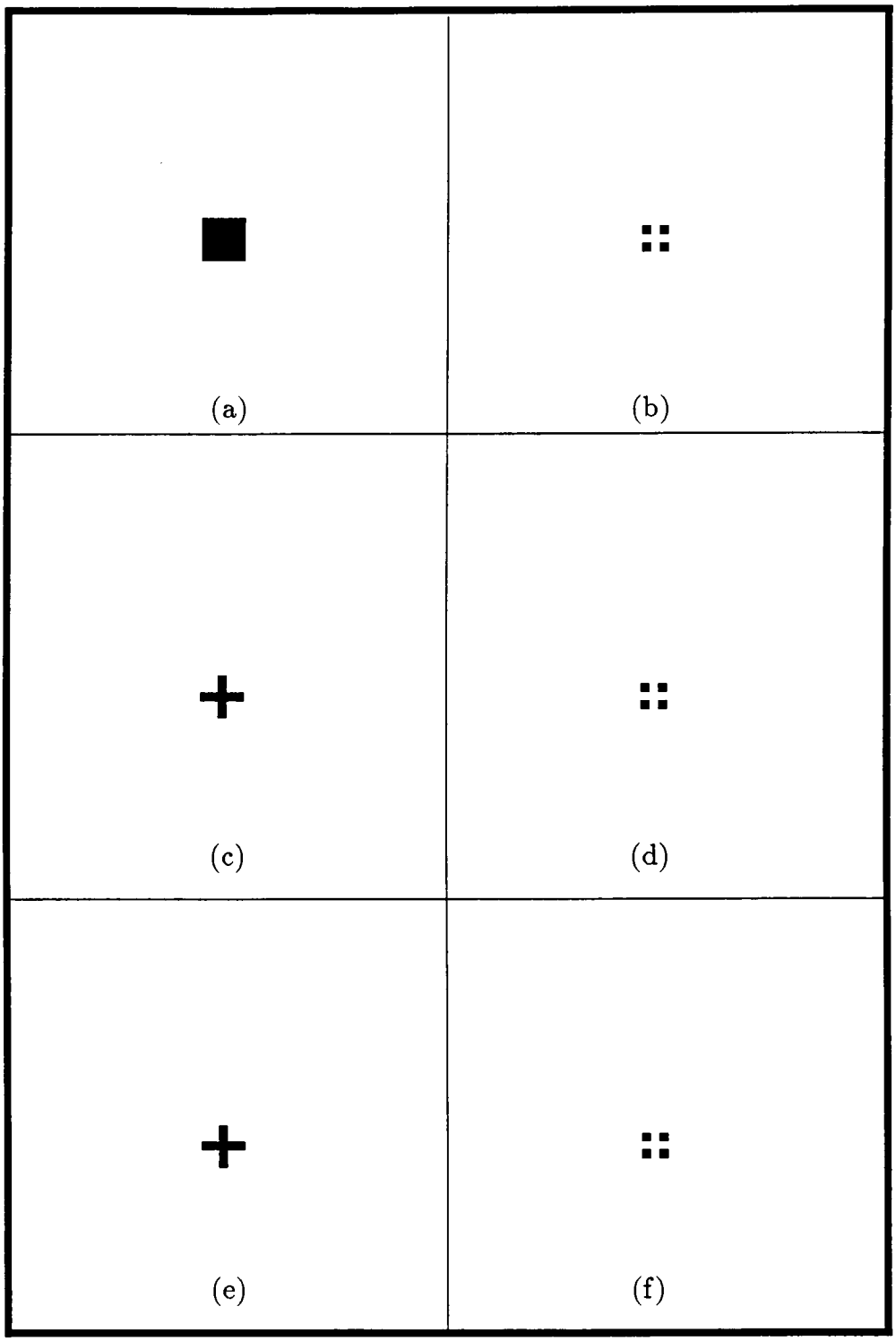


Figure 5.5: (a): Input: Full excitatory field coverage; (b): T = 8; (c): T = 9; (d): T = 18; (e): T = 19; (f): T = 28

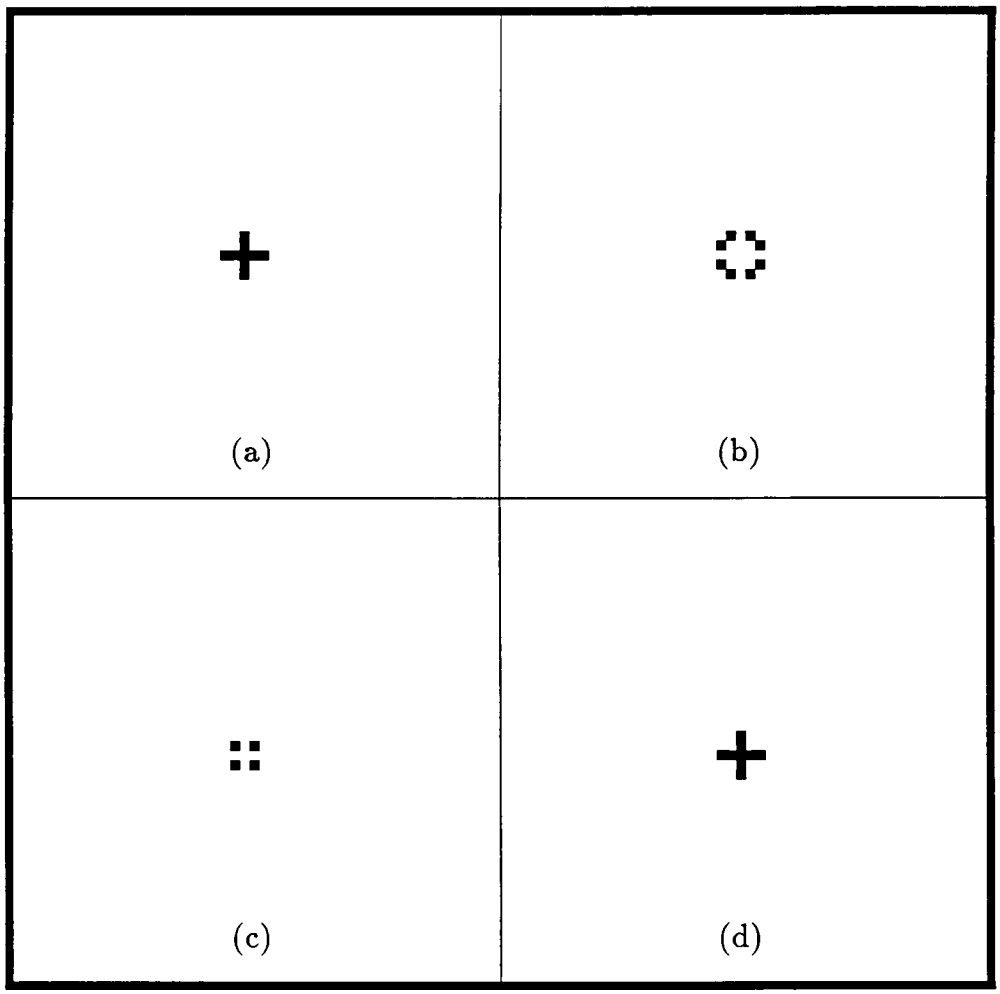


Figure 5.6: (a): T = 29; (b): T = 30; (c): T = 38; (d): T = 39

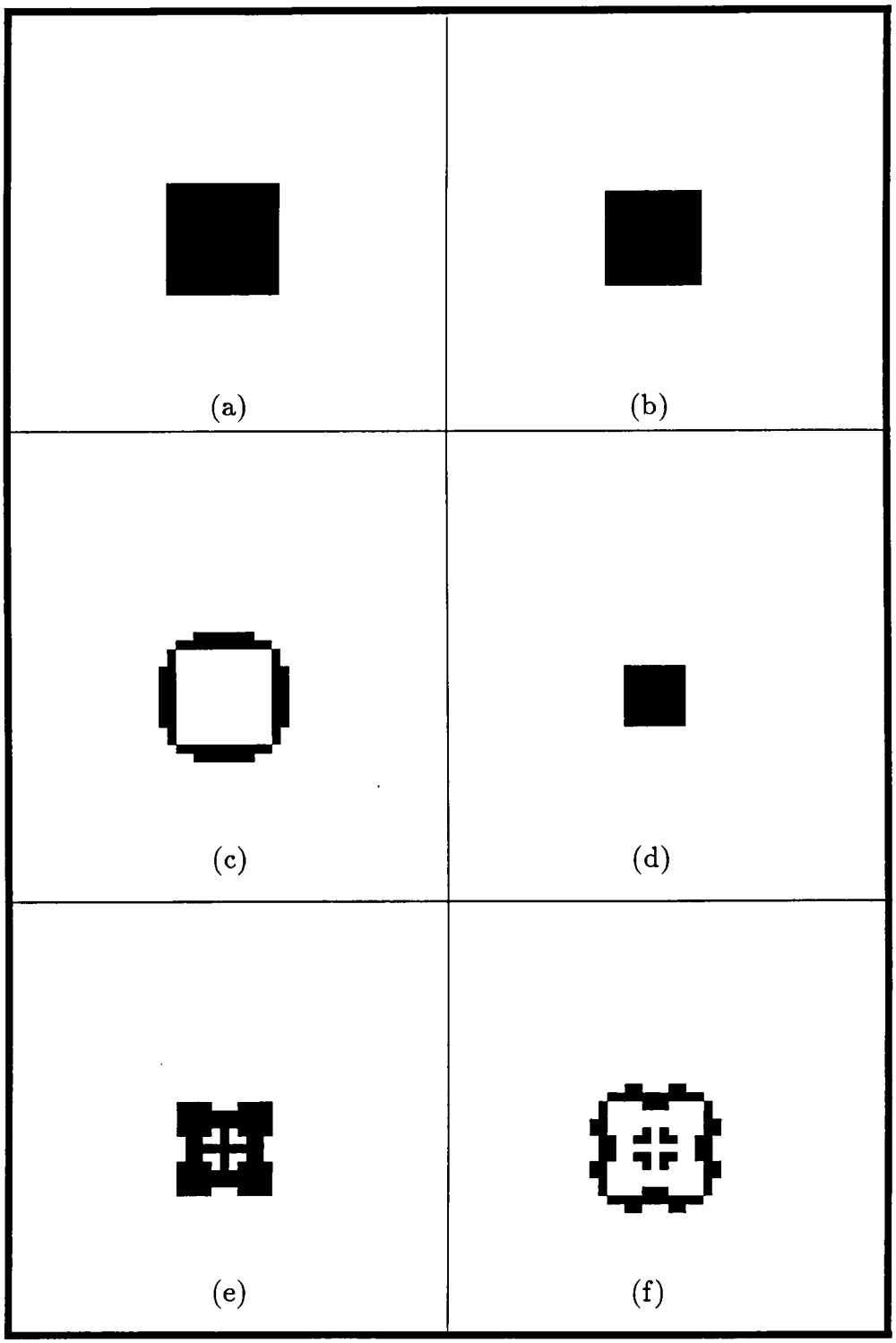


Figure 5.7: (a): Input: Full excitatory and inhibitory field coverage; (b): T = 8; (c): T = 9; (d): T = 14; (e): T = 29; (f): T = 30

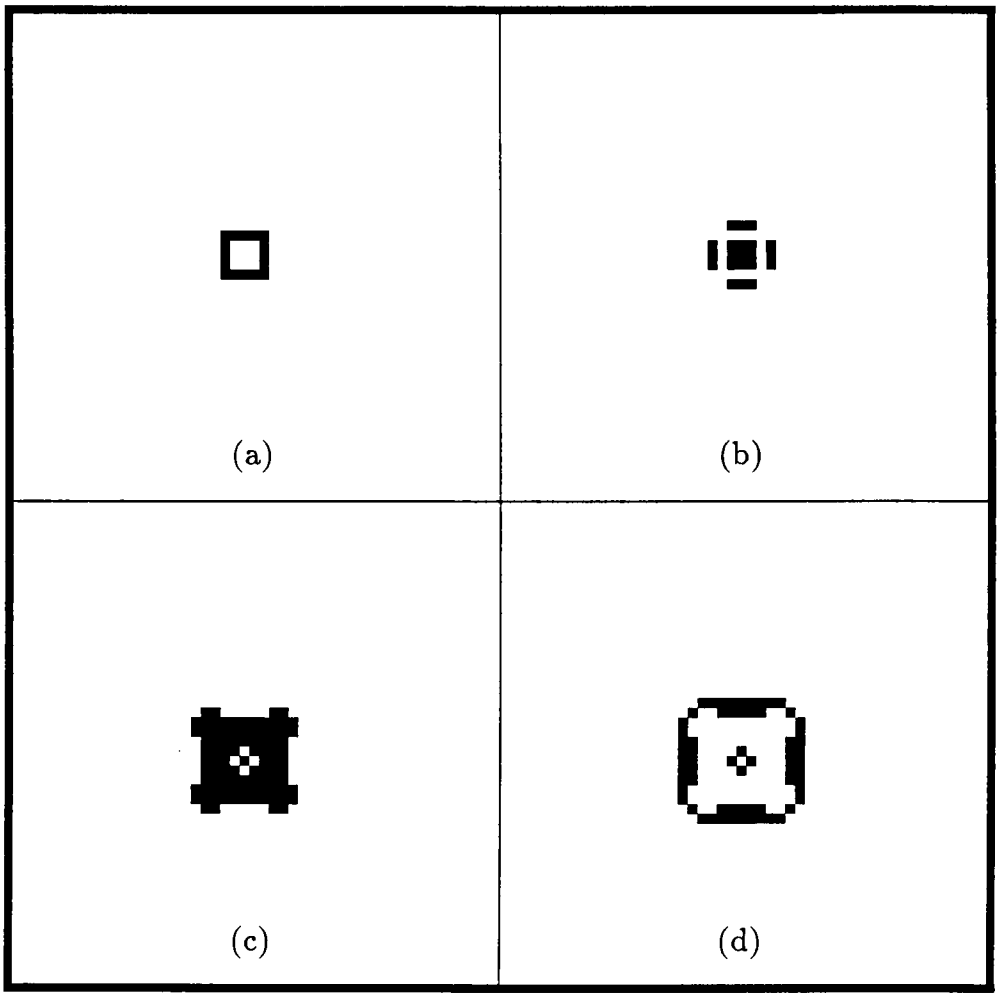


Figure 5.8: (a): T = 35; (b): T = 36; (c): T = 49; (d): T = 50

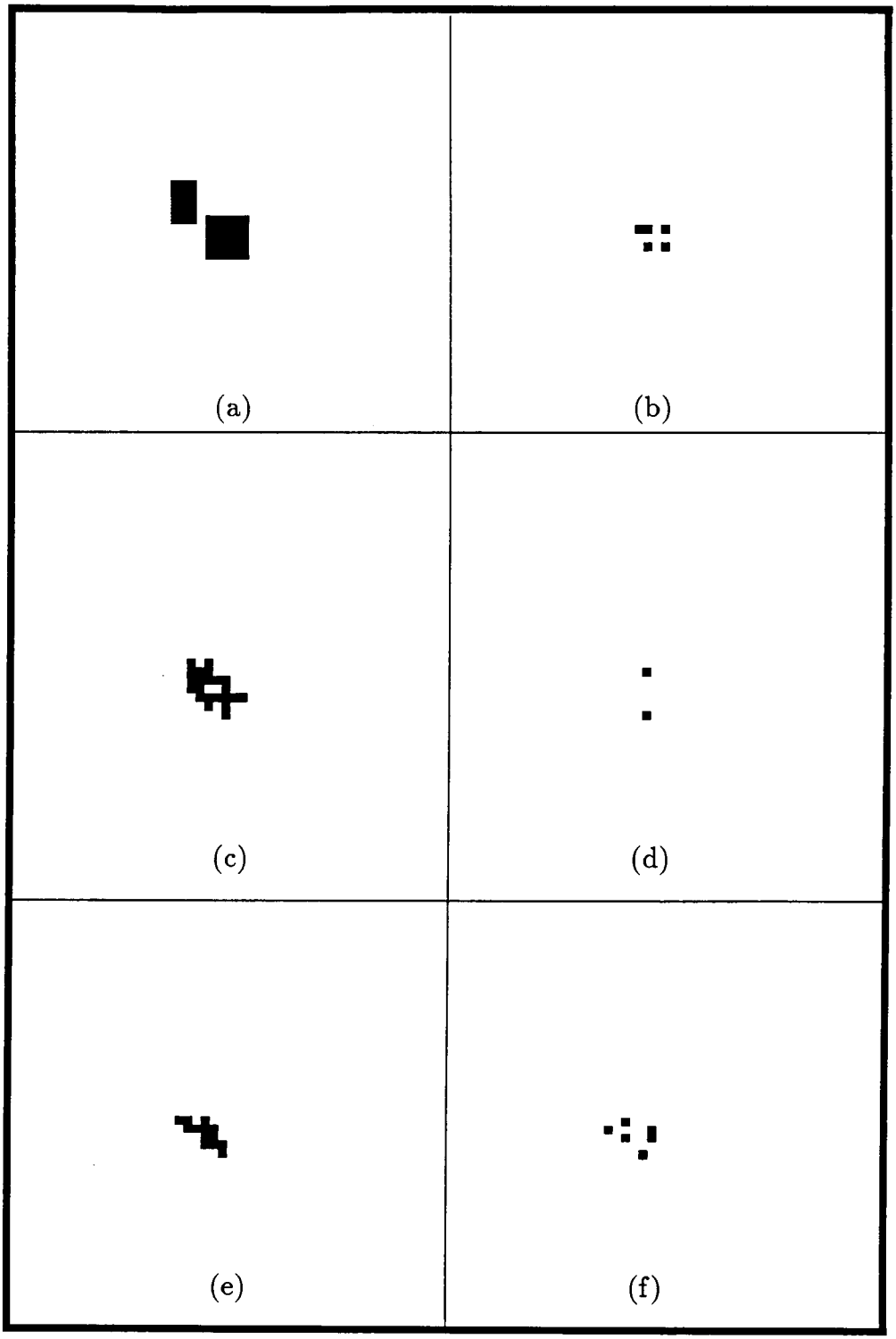


Figure 5.9: (a): Input: Full excitatory and partial inhibitory field coverage; (b): T = 8; (c): T = 9; (d): T = 10; (e): T = 19; (f): T = 20

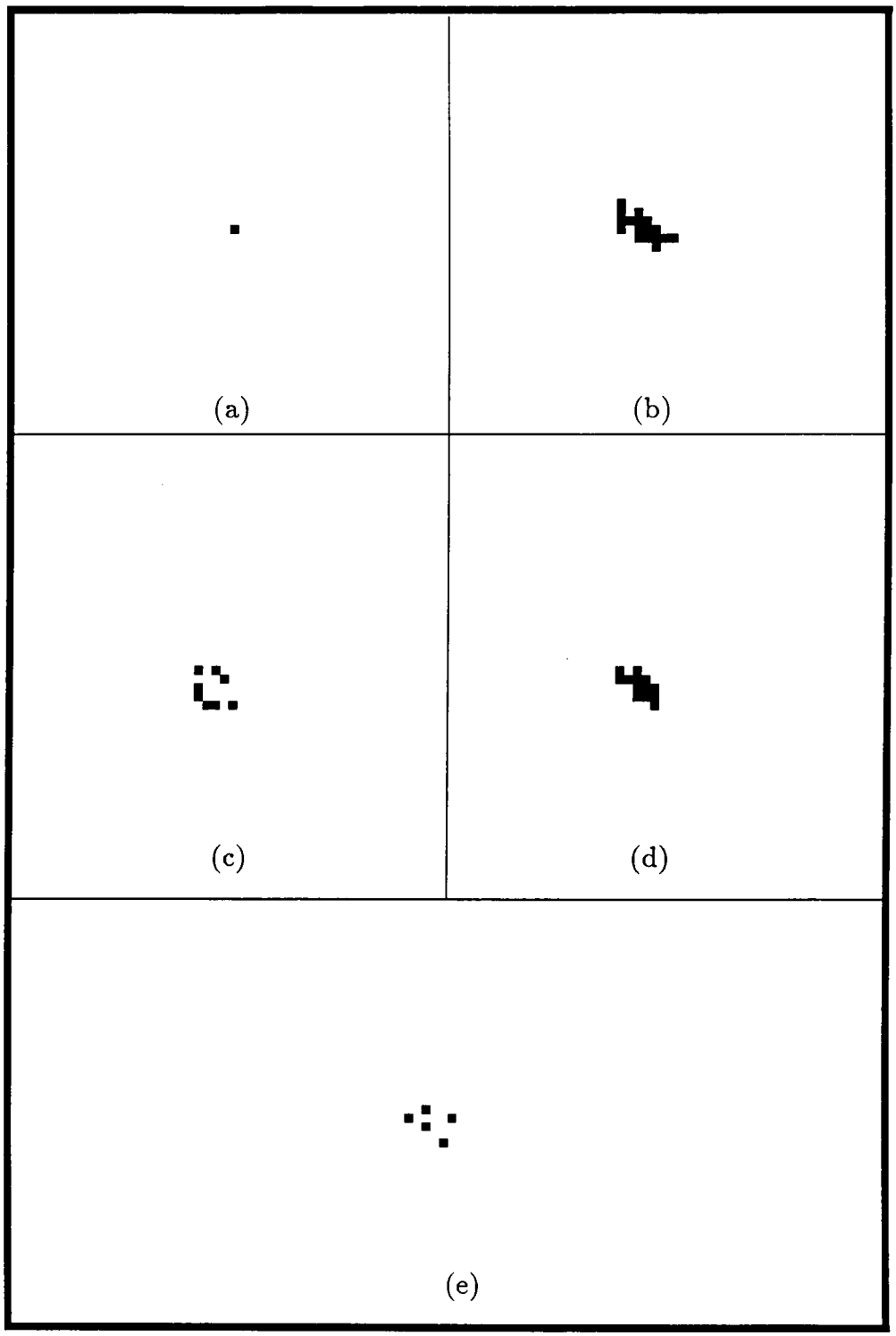


Figure 5.10: (a): T = 28; (b): T = 29; (c): T = 30; (d): T = 39; (e): T = 40

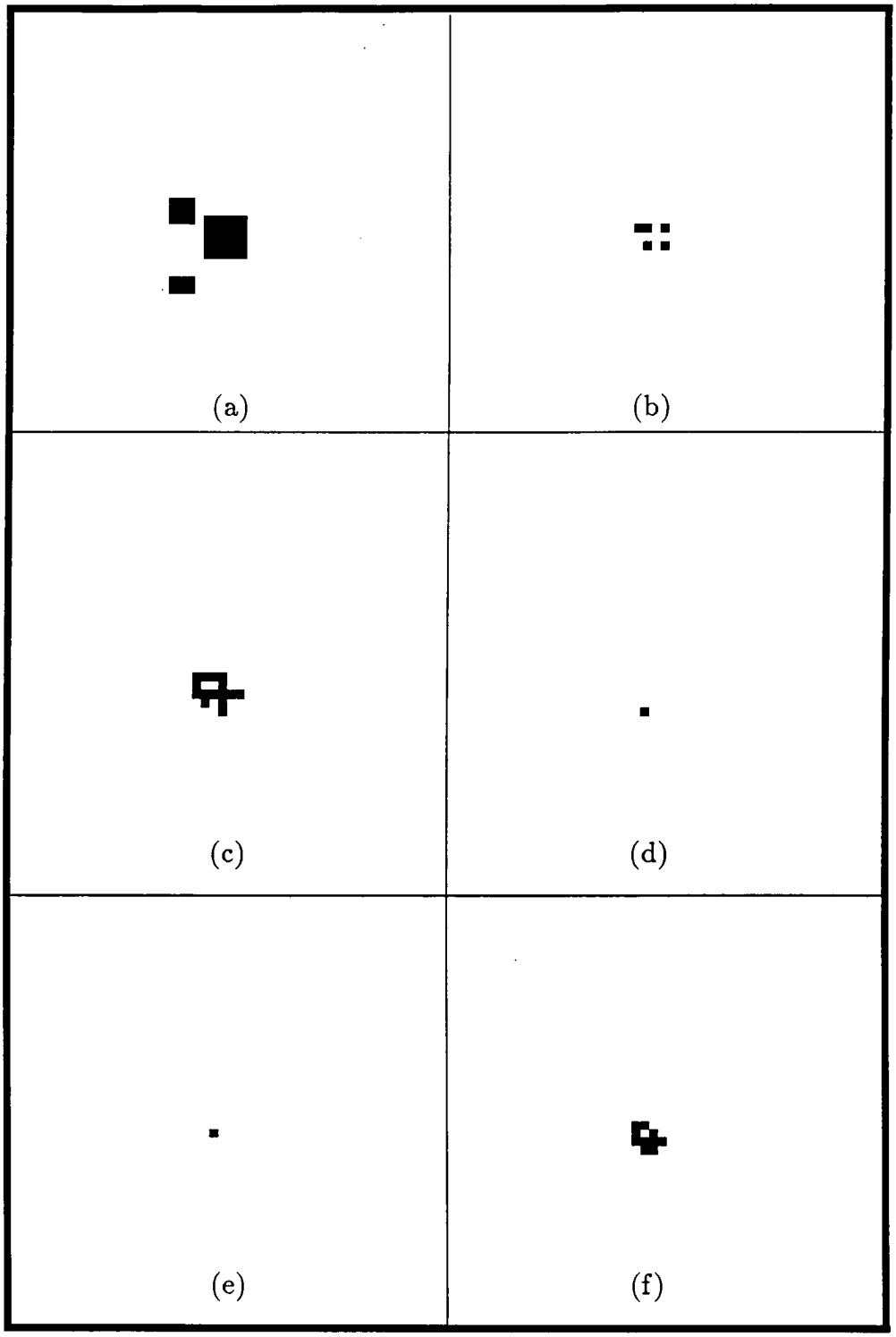


Figure 5.11: (a): Input: Full excitatory and partial inhibitory field coverage; (b): T = 8; (c): T = 9; (d): T = 10; (e): T = 18; (f): T = 19

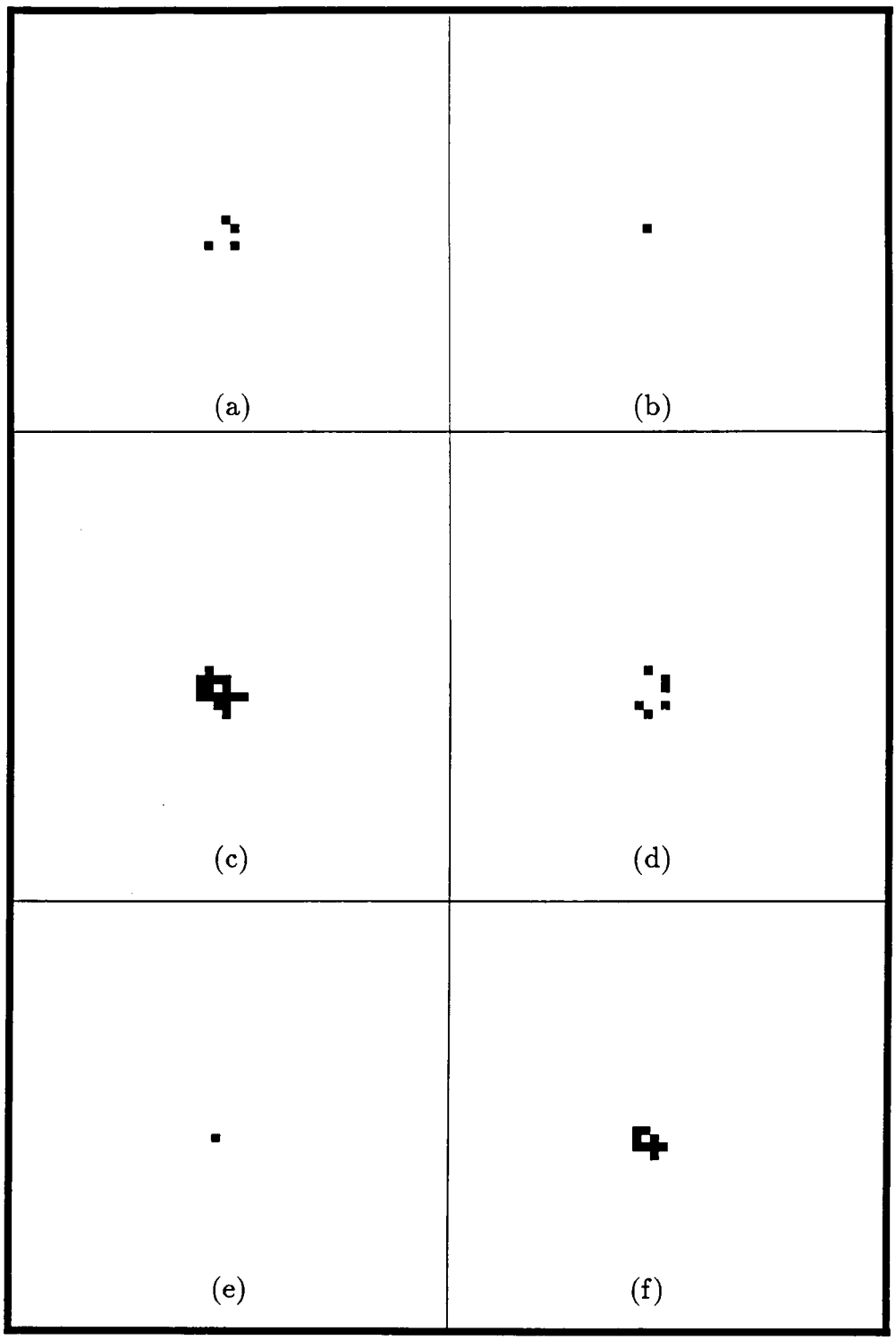


Figure 5.12: (a): T = 20; (b): T = 28; (c): T = 29; (d): T = 30; (e): T = 38; (f): T = 39

small at each time step. Unless the input is relatively large, the activity in $E2$ will be minimal. At the same time, the amount of inhibition is small because of the limited spatial extent of the firing in $E1$. As a result, $E2$ responds to every input from $E1$.

As before, the firing patterns within this configuration change spatially over time. The response waveforms of E_c reflect only coarse encoding of the input signal from $E1$. The time delays in this stage have been adjusted to obtain a large amount of activity within $E2$ only in the case of large input from $E1$.

5.1.3 Shape Analysis

Shape analysis introduces another problem in the design of the ensemble architecture. The problem is one of size invariance. From the preceeding, it is obvious that a given *tuned* receptive field responds in a specific manner to an optimal input stimulus – optimal in the sense of size and shape. The encoding of the shape parameters for a given shape will be unique for a specific tuned receptive field. However, the same basic shape, differing in size only, will not necessarily elicit the same response either in the time-varying spatial pattern or the response profile of E_c. In addition, two ensembles of neurons, each tuned to a different size stimulus, will have different response profiles to the same shape of the optimal size for the specific tuning. Two different sizes of circles, one with a diameter of 13 units (Fig. 5.13.a) and one with a diameter of 15 units (Fig. 5.13.b), are used to demonstrate this behavior. The distortions in the im-

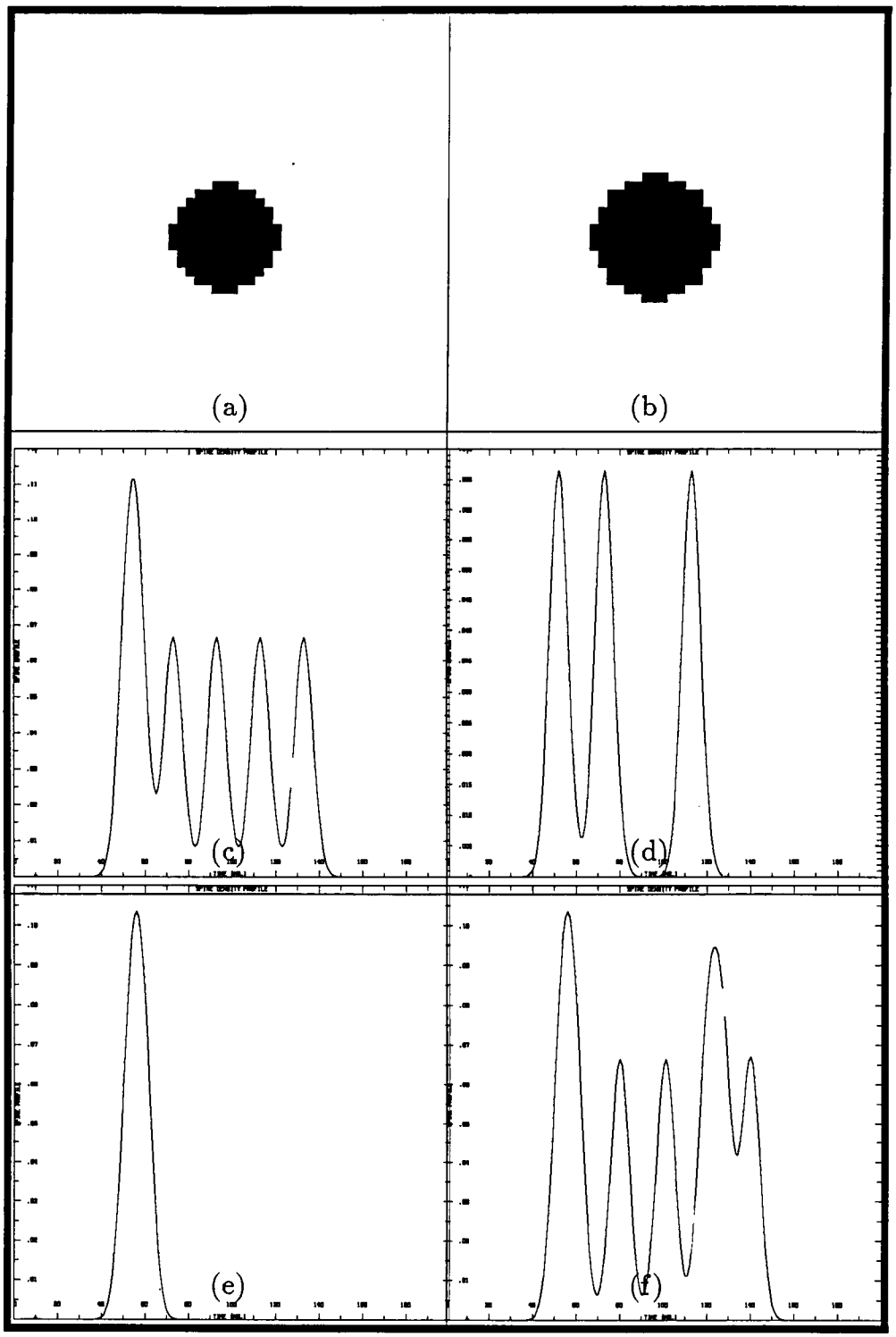


Figure 5.13: Response profiles(a): Input: Diameter=13; (b): Input: Diameter=15; (c): Response SI=SE=13, CI=CE=5 to (a); (d): Response SI=SE=13, CI=CE=5 to (b); (e): Response SI=SE=15, CI=CE=7 to (a); (f): Response SI=SE=15, CI=CE=7 to (b)

ages are two to quantization errors that are further exaggerated by enlarging for display purposes. In Fig. 5.13.c, the response profile of E_c in $E1$, with receptive field dimensions $SI = 13$, $CI = 5$, $SE = 13$, and $CE = 5$ in response to a circle with diameter of 13 units in I is shown. The response to a circle with diameter of 15 units is shown in Fig. 5.13.d. The response profile of E_c in $E1$ to the same input stimuli with receptive field dimensions $SI = 15$, $CI = 7$, $SE = 15$, and $CE = 7$, is shown in Figs. 5.13.e and 5.13.f. The response profiles in each case are unique. While this information is usefull to discriminate between different sizes of objects, it is an obstacle to size-invariant shape analysis.

For the remainder of this section, the problem of size-invariance is not addressed. Instead, shape analysis of basic geometric shapes that are considered to be optimal in size for the receptive field tunings of $E1$ is investigated. Four shapes have been chosen for this analysis: a circle, a square, a cross, and a rectangle. Again, the distortions in the images are to exaggeration of the quantization distortion by enlarging the images for display. The discussion begins with the response profiles of E_c in $E2$.

The response profiles of E_c in $E2$ are shown in Fig. 5.14. The response profile for the circle, square, cross, and rectangle are all very similar. The firing frequencies of each are the same, as is the latency time. In addition, each of the waveforms are characterized by a high degree of periodicity or regularity. The difference is in the shape of the waveform, the result of the interspike distances.

The time-varying spatial firing patterns provide an explanation to the re-

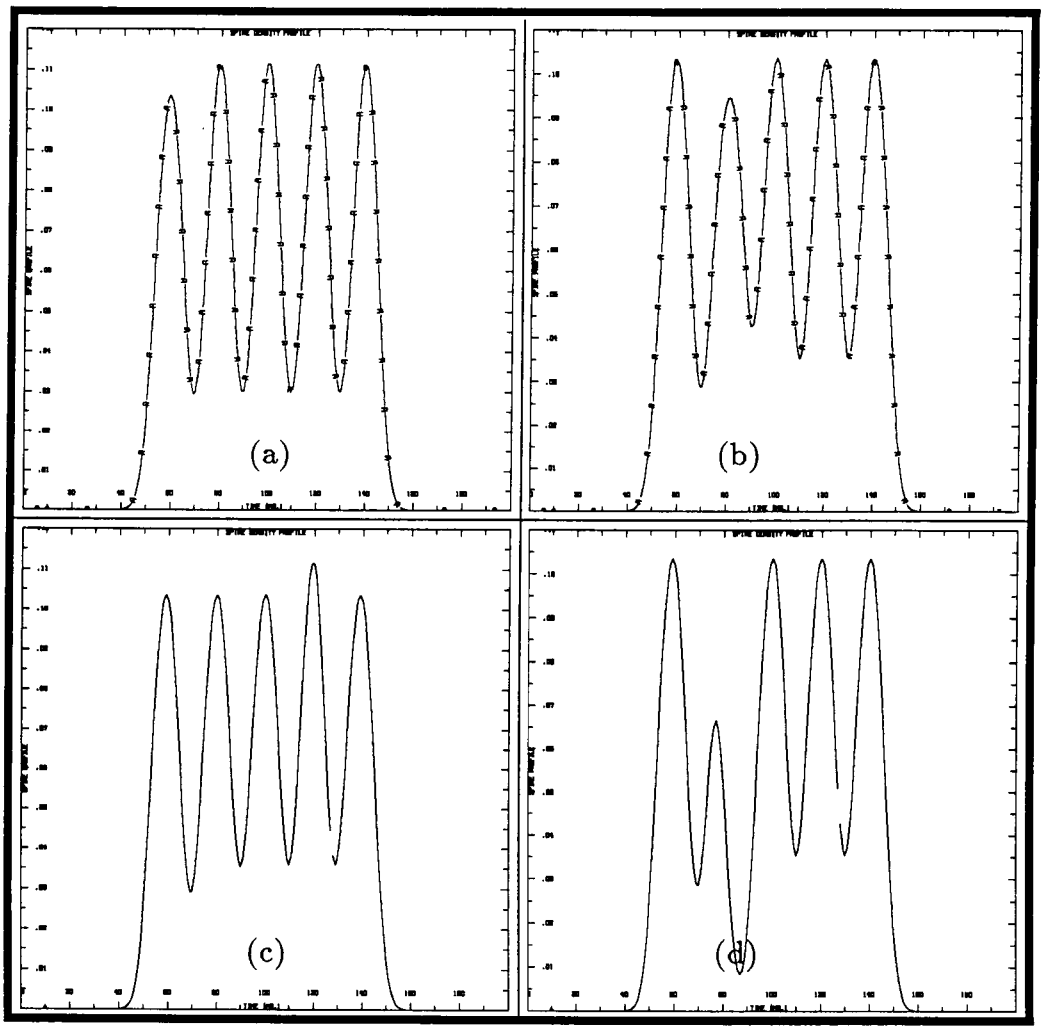


Figure 5.14: Response profiles of E_c to (a): Circle; (b): Square; (c): Cross; (d): Rectangle

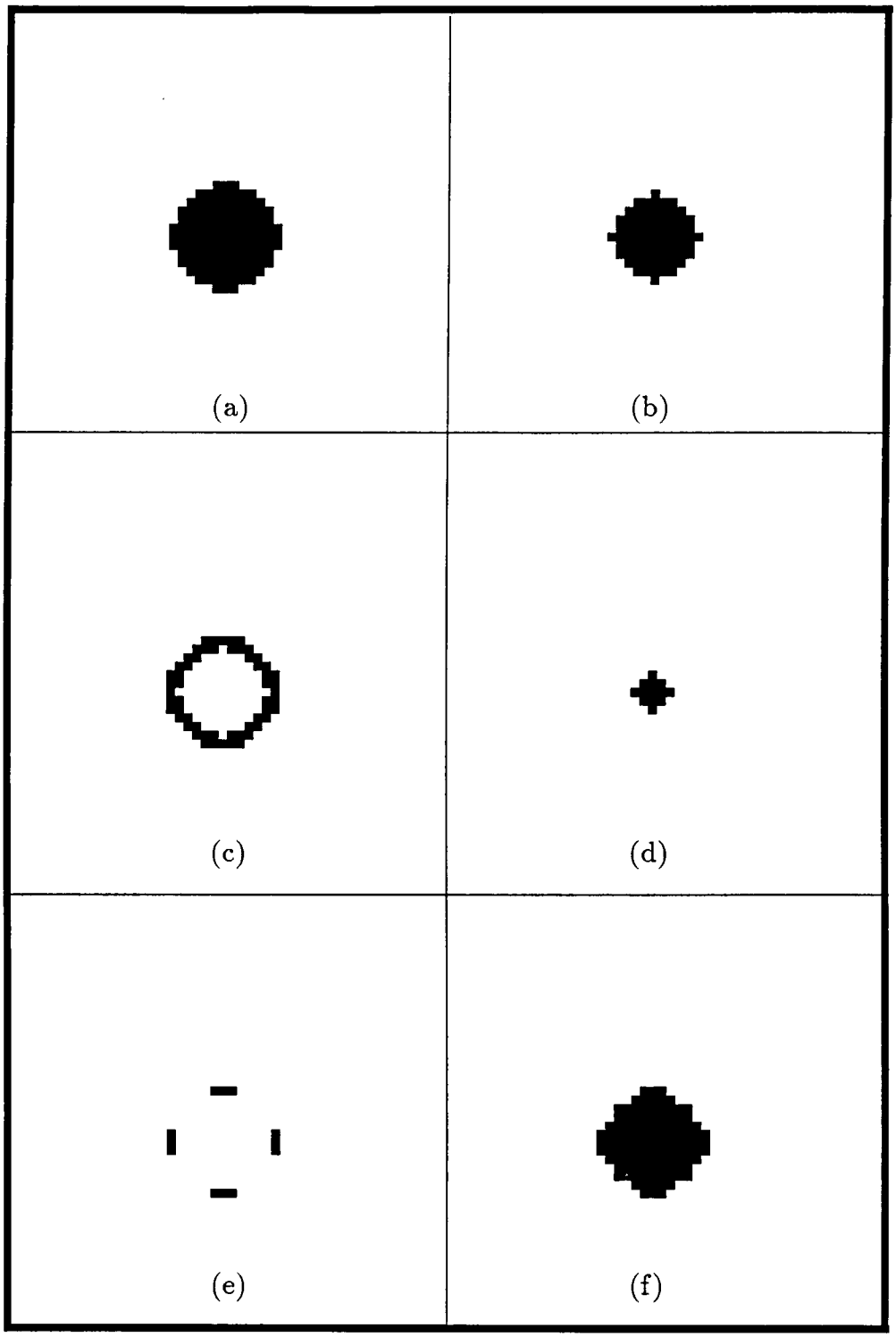


Figure 5.15: Layer $E1$(a): Input: D=13; (b): T=5; (c): T=6; (d): T=10; (e): T=16; (f): T=26

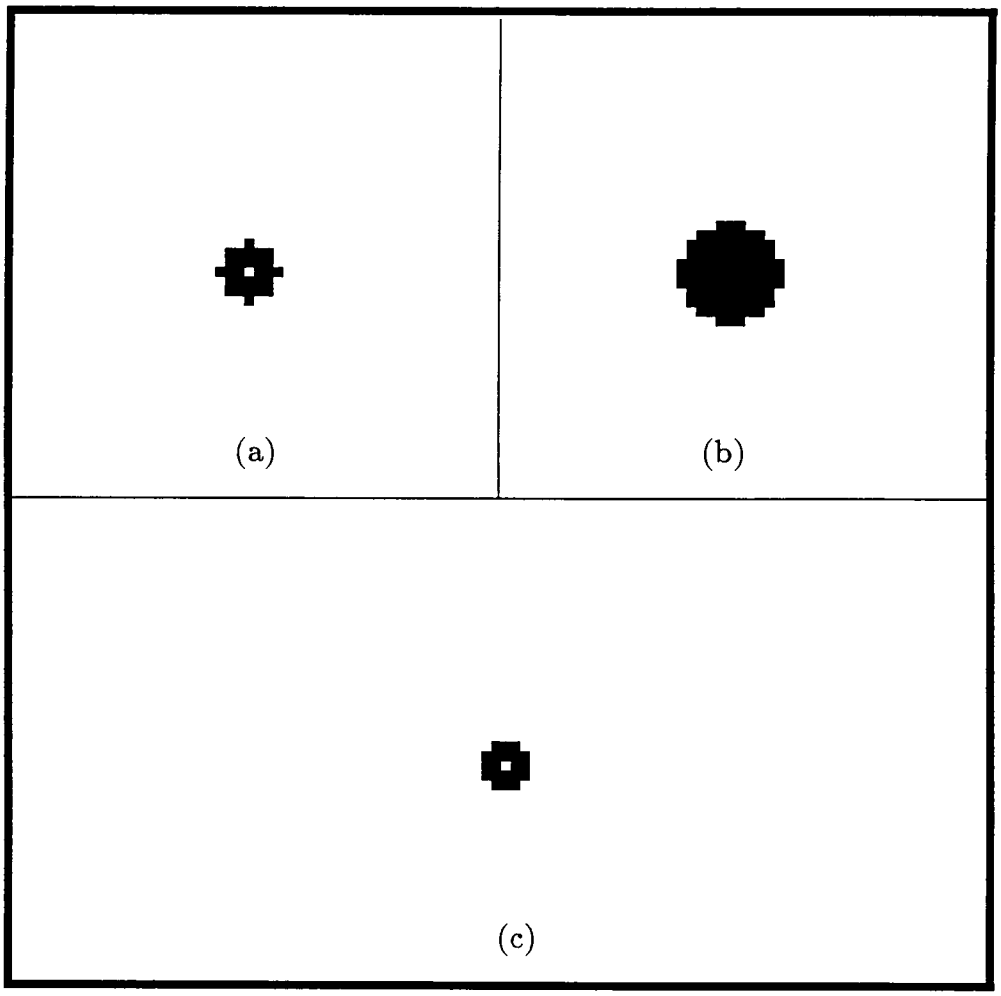


Figure 5.16: (a): T=31; (b): T=46; (c): T=51

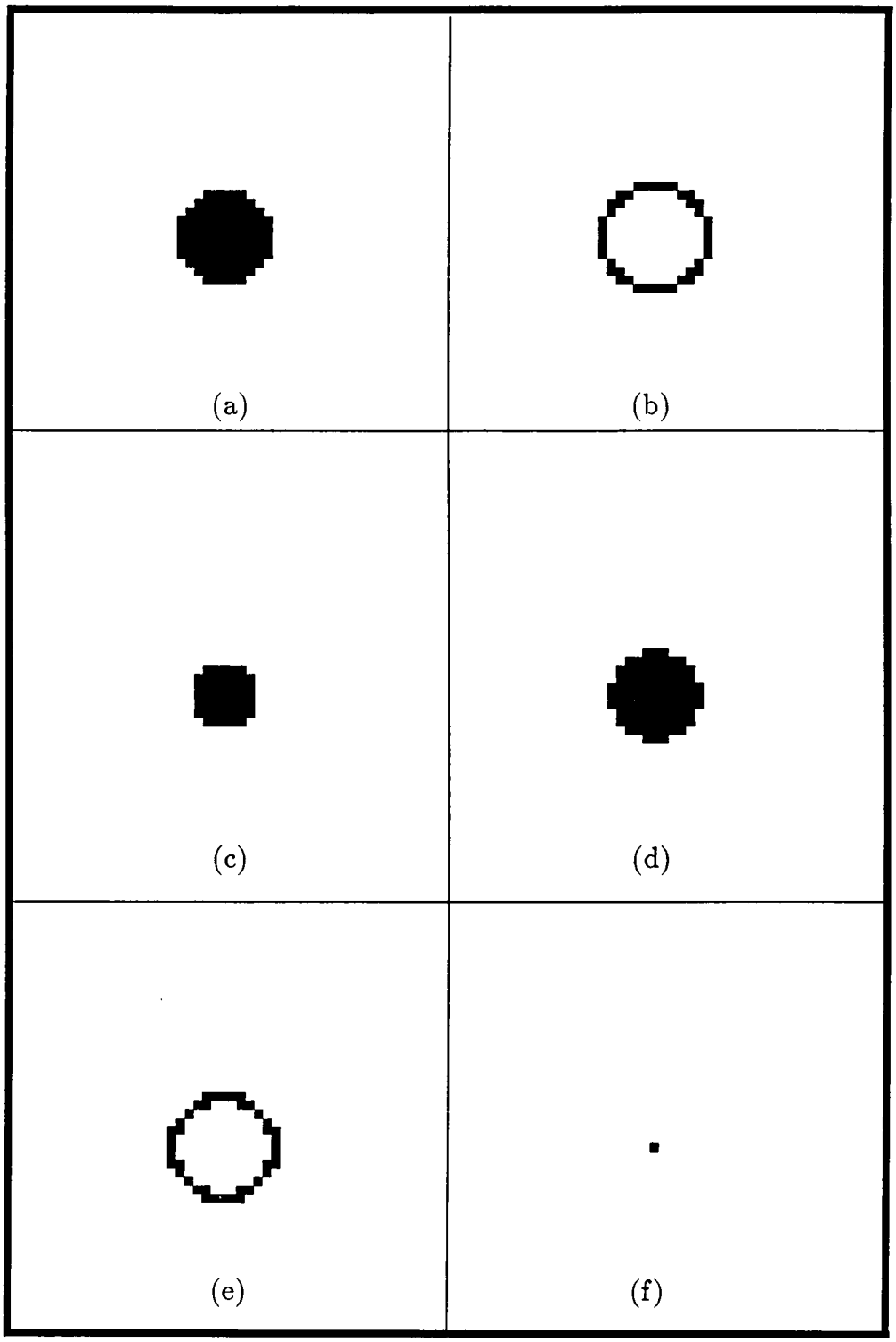


Figure 5.17: Layer $E2$ (a): T=8; (b): T=9; (c): T=14; (d): T=29; (e): T=30; (f): T=34

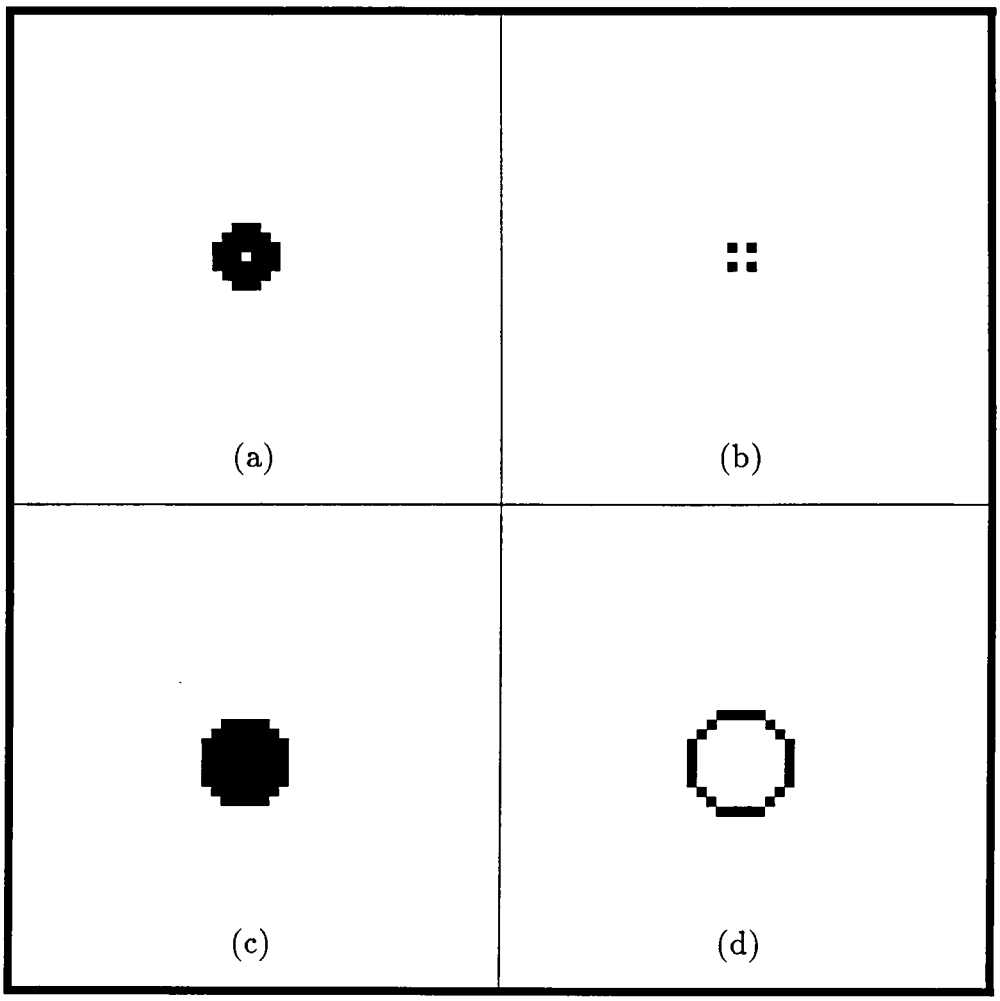


Figure 5.18: (a): T=35; (b): T=41; (c): T=49; (d): T=50

sponse profiles (Figs. 5.15 to 5.30). The firing patterns in each case reflect concentrated activity due to large spatial regions of stimulation. This large activity is reflected in the frequency of firing in the response profiles of E_c in $E2$. The shape of the input is encoded in the shape of the waveform due to the electrotonic distances embedded in Δt_{ji}. This, in addition to Inp_{delay}, imposes the high degree of periodicity seen in the response profiles.

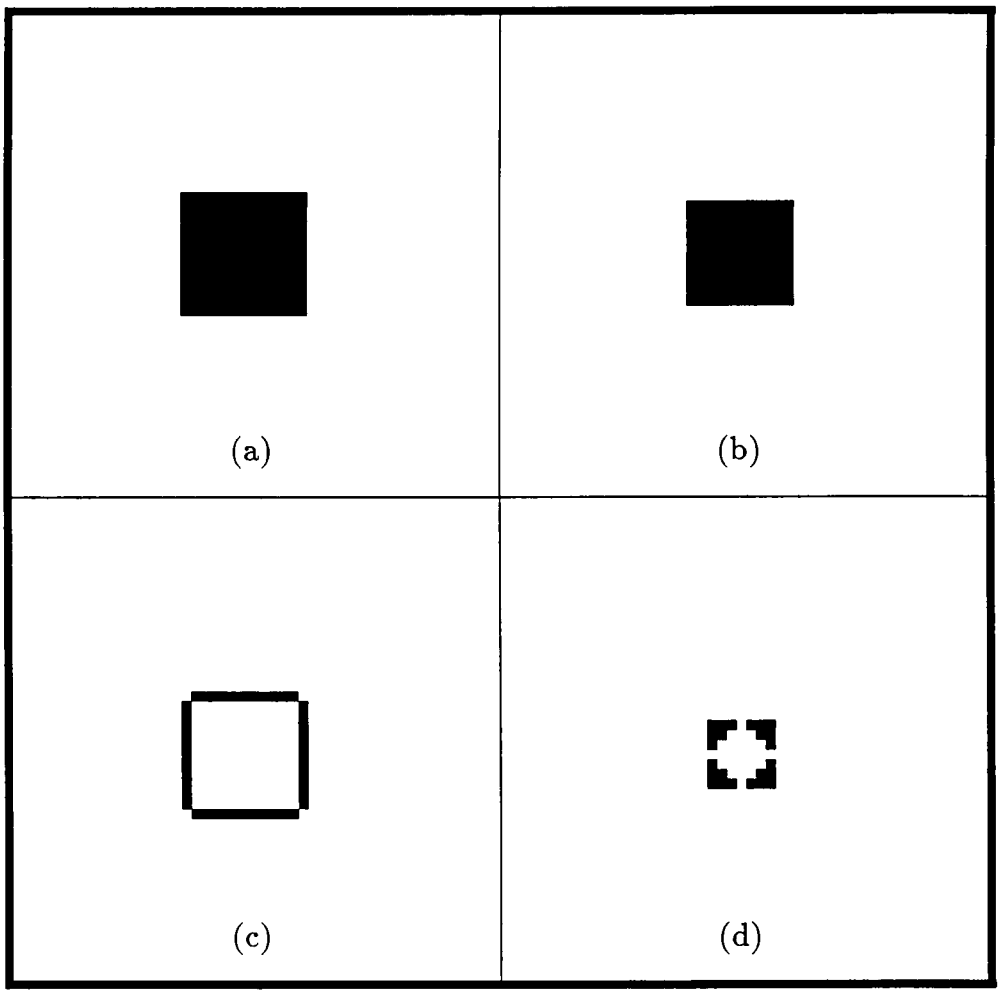


Figure 5.19: Layer $E1$ (a): Input: square; (b): T=5; (c): T=6; (d): T=10

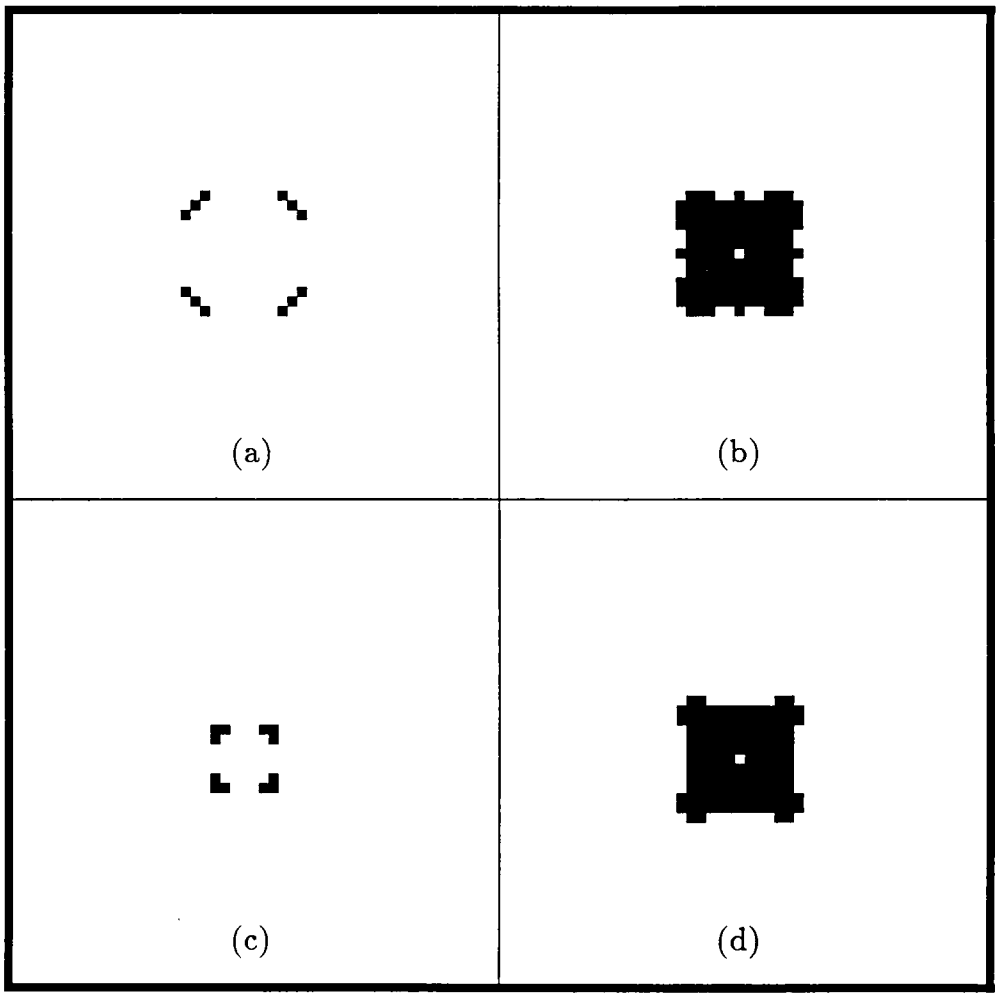


Figure 5.20: (a): T=16; (b): T=26; (c): T=31; (d): T=46

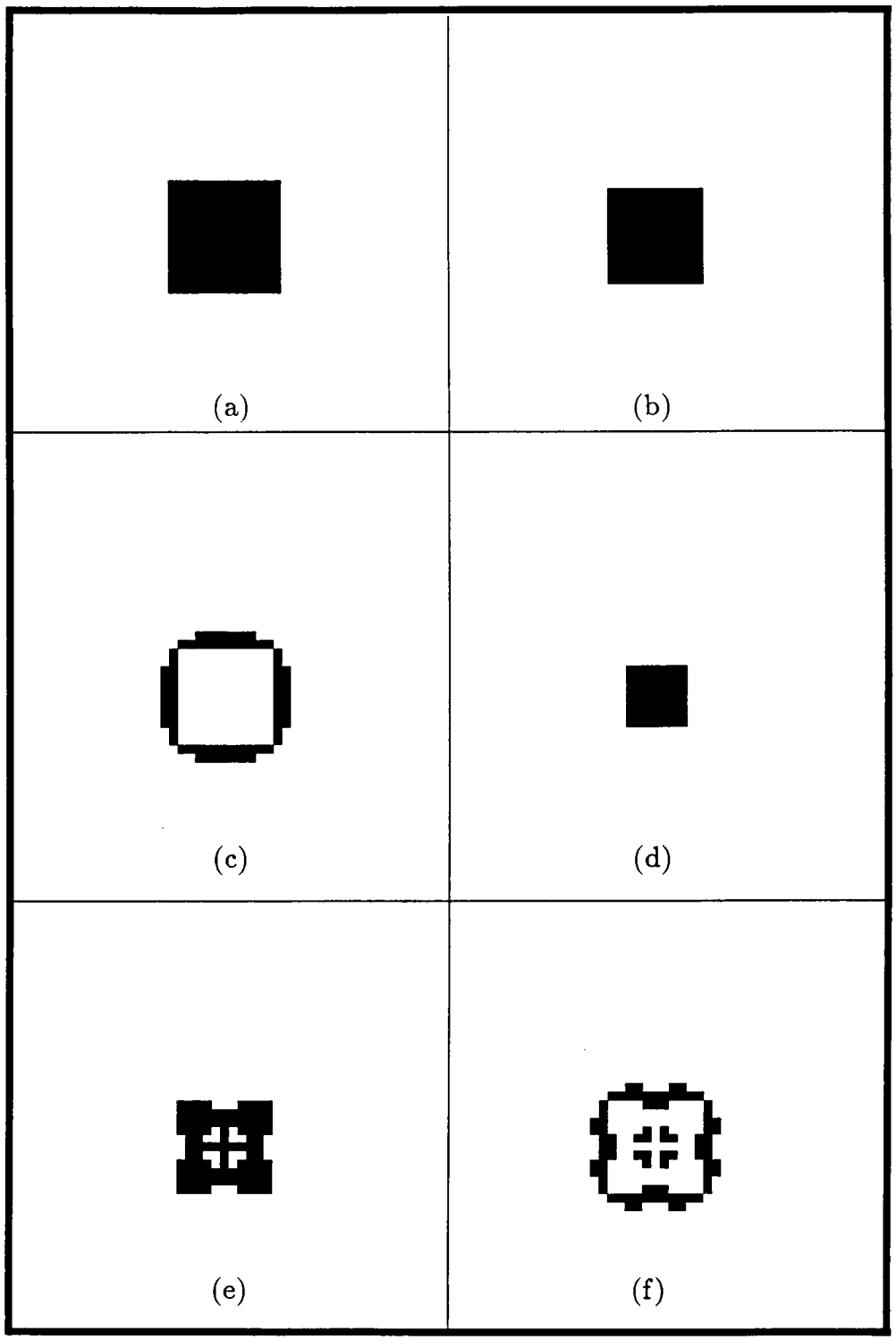


Figure 5.21: Layer $E2$ (a): Input: square; (b): T=8; (c): T=9; (d): T=14; (e): T=29; (f): T=30

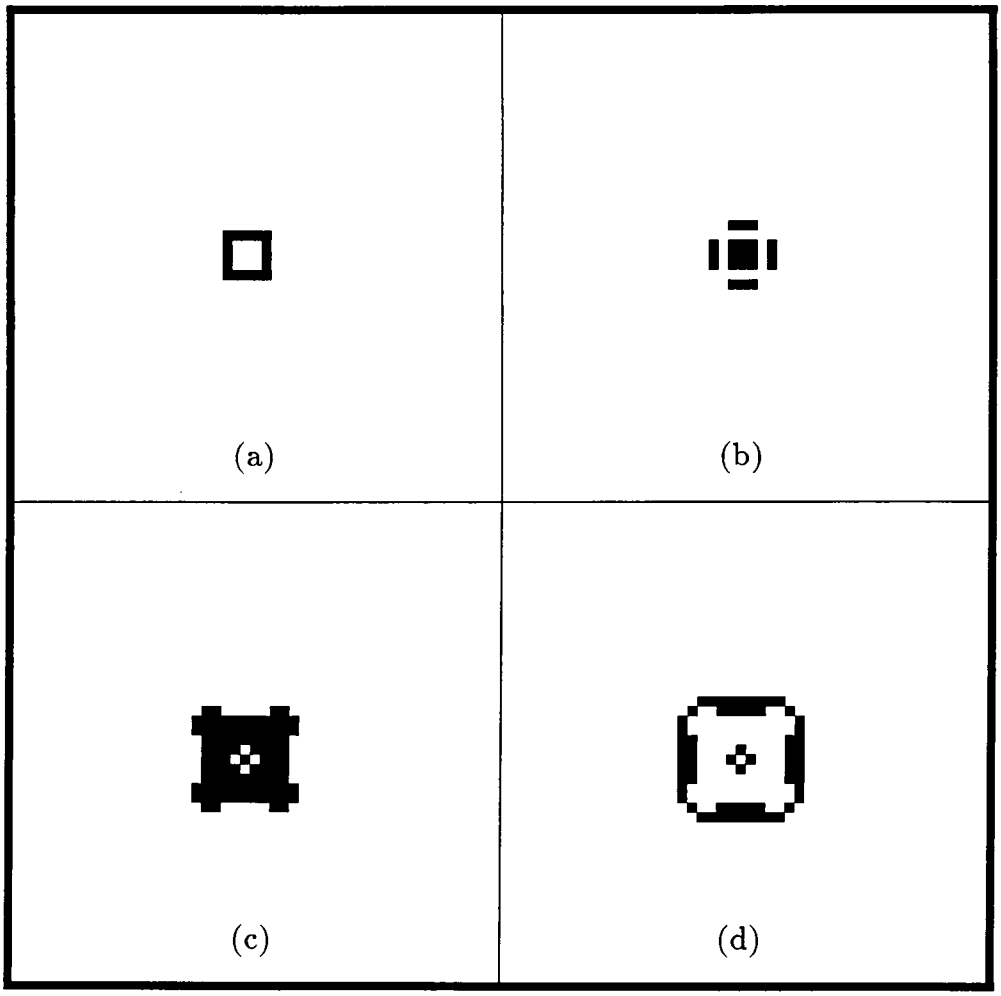


Figure 5.22: (a): T=35; (b): T=36; (c): T=49; (d): T=50

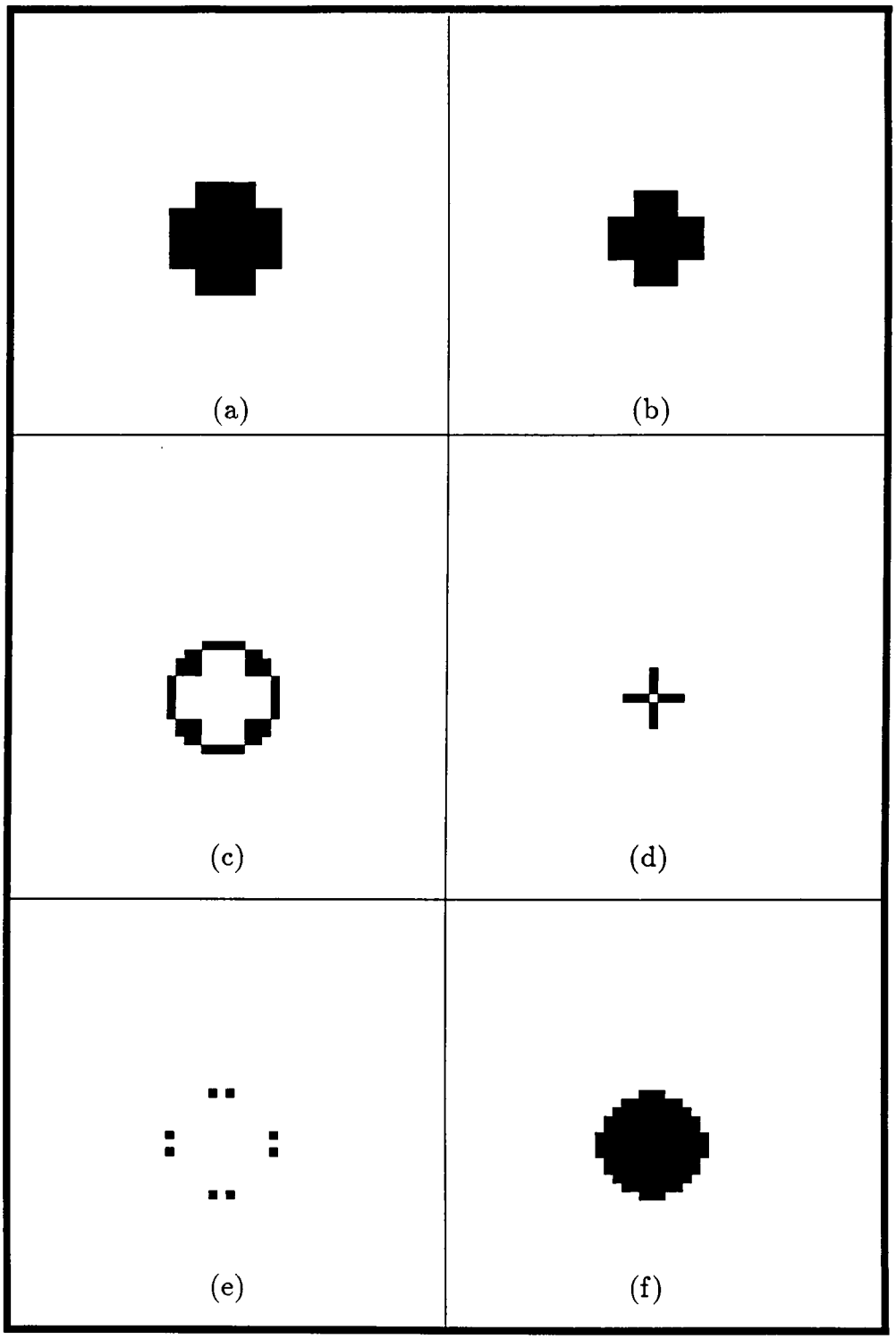


Figure 5.23: Layer $E1$ (a): Input: cross; (b): T=5; (c): T=6; (d): T=10; (e): T=16; (f): T=26

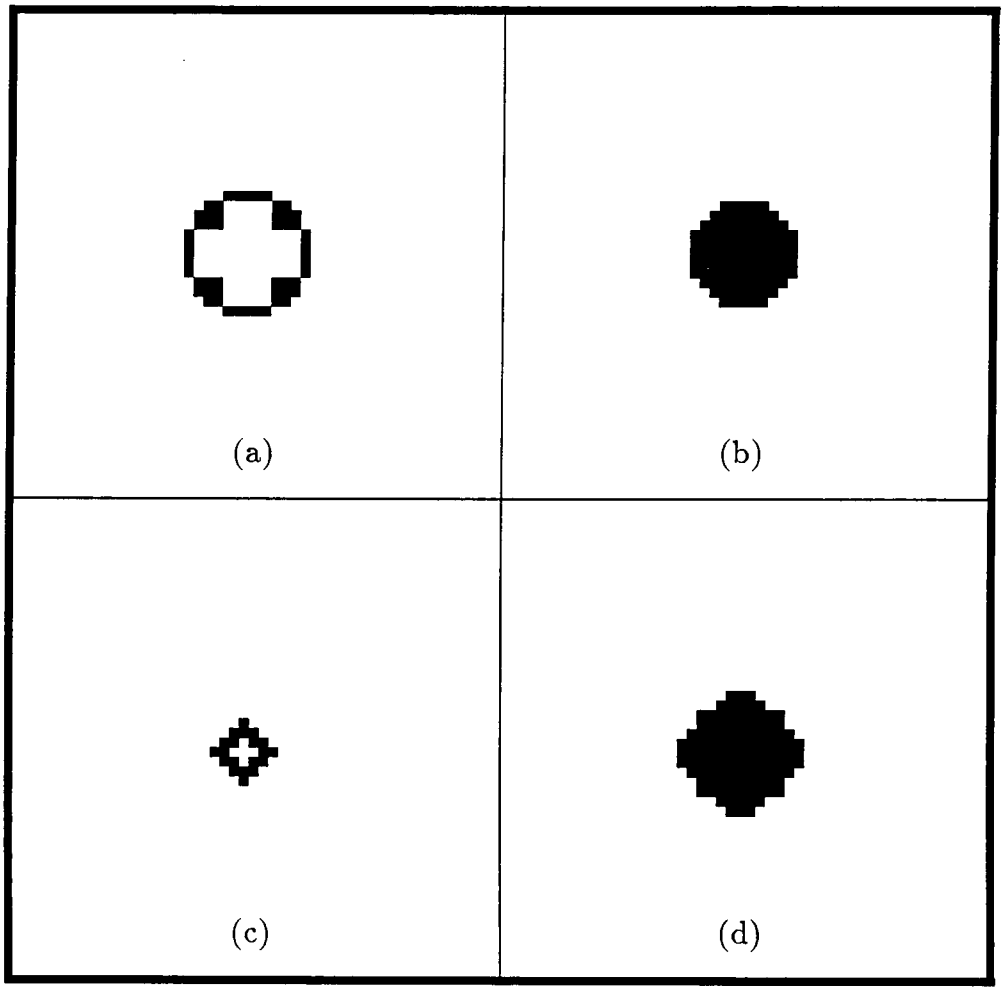


Figure 5.24: (a): T=31; (b): T=46; (c): T=51; (d): T=66

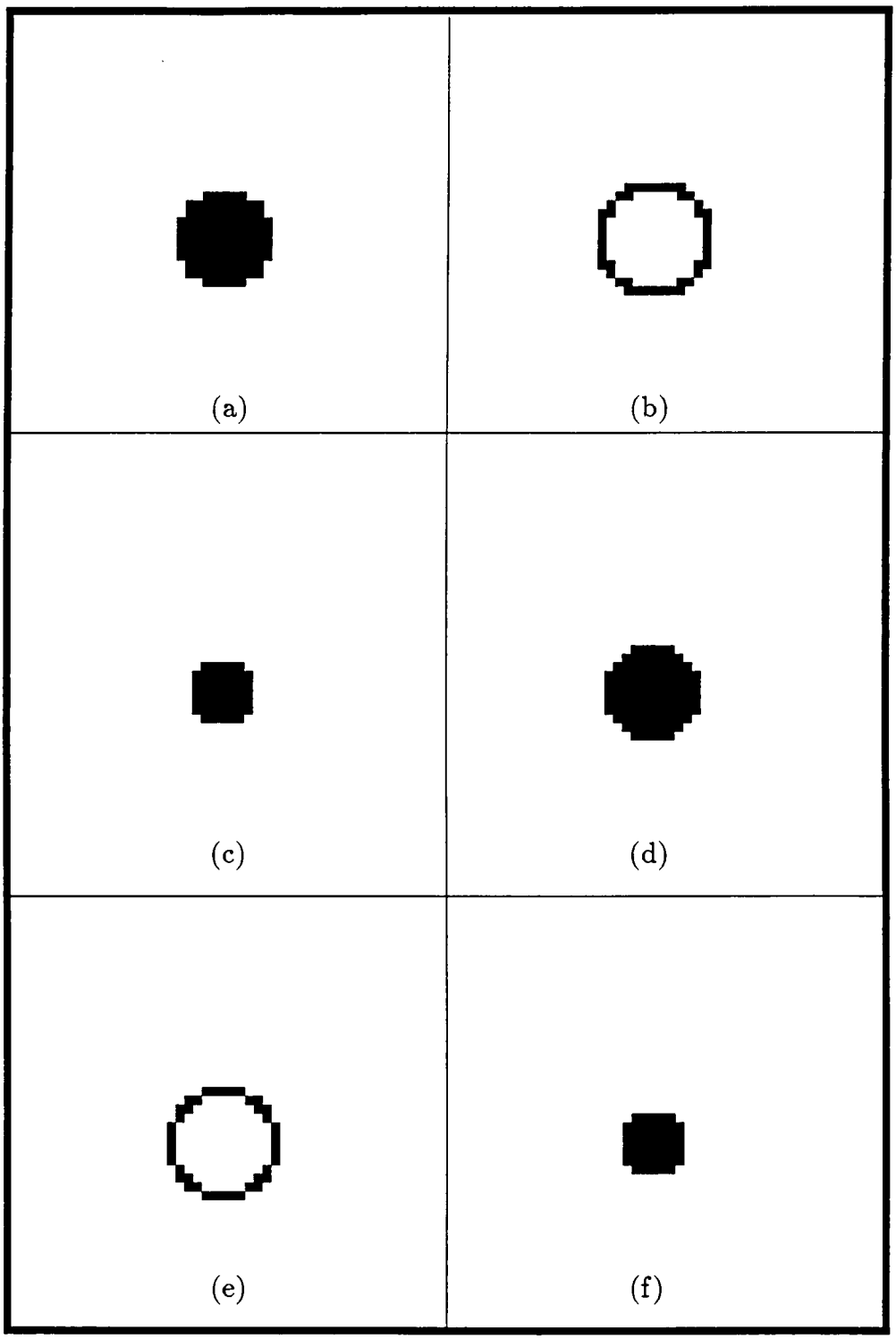


Figure 5.25: Layer $E2$ (a): T=8; (b): T=9; (c): T=14; (d): T=29; (e): T=30; (f): T=35

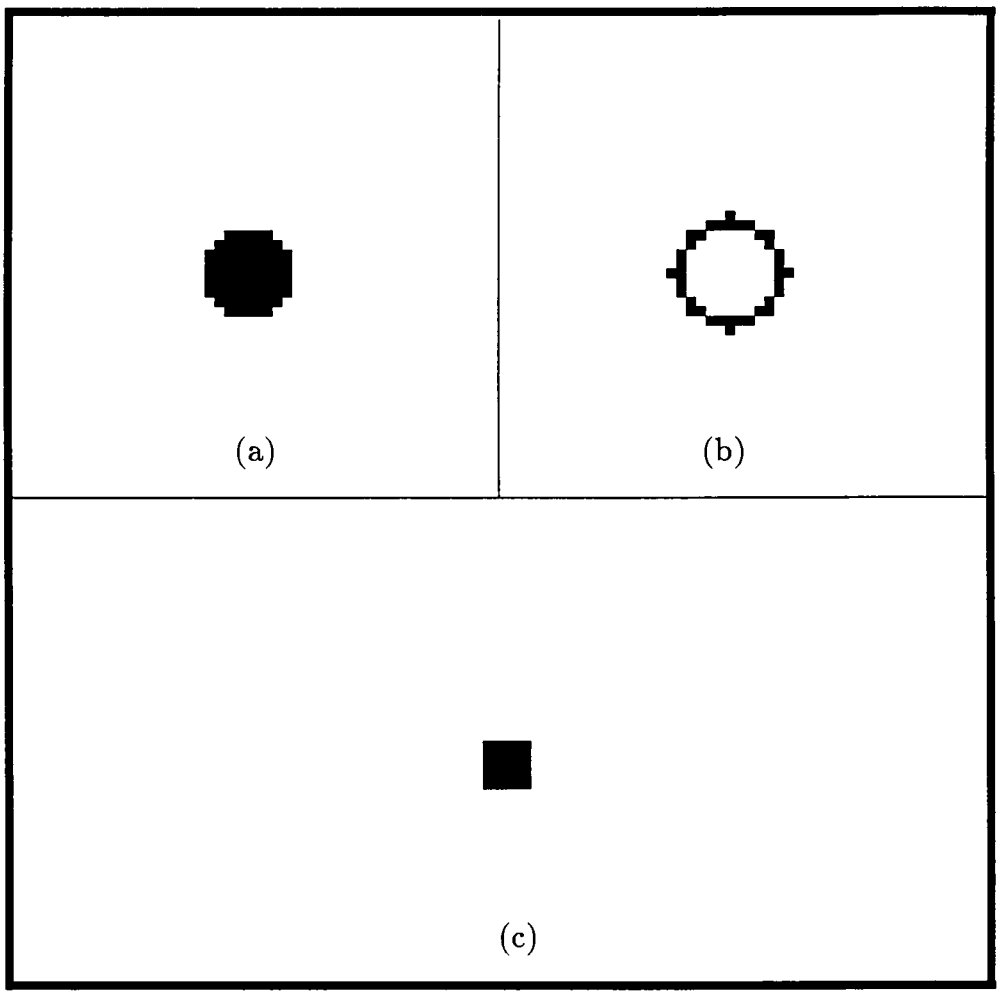


Figure 5.26: (a): T=49; (b): T=50; (c): T=55

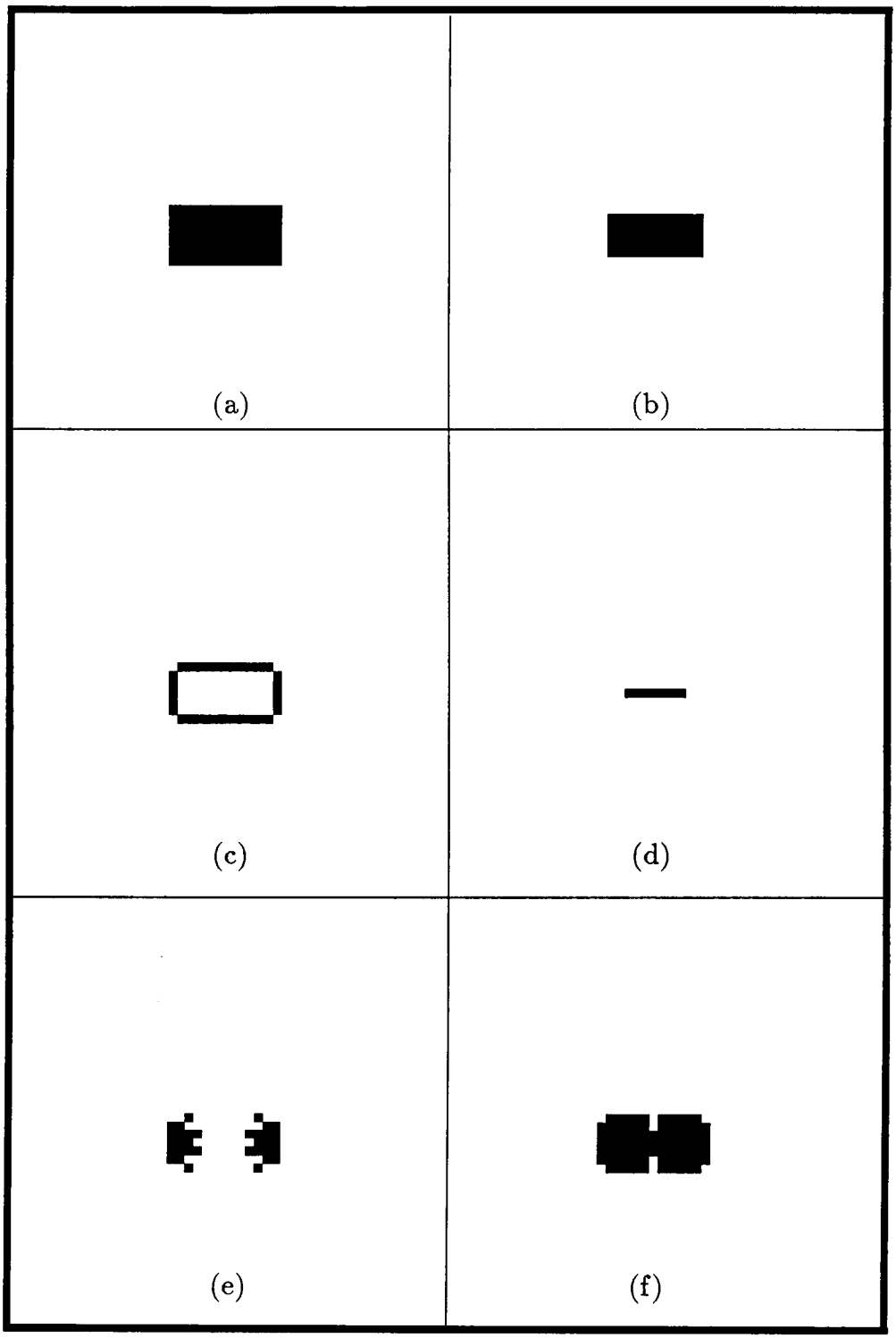


Figure 5.27: Layer $E1$ (a): Input: rectangle; (b): T=5; (c): T=6; (d): T=10; (e): T=16; (f): T=26

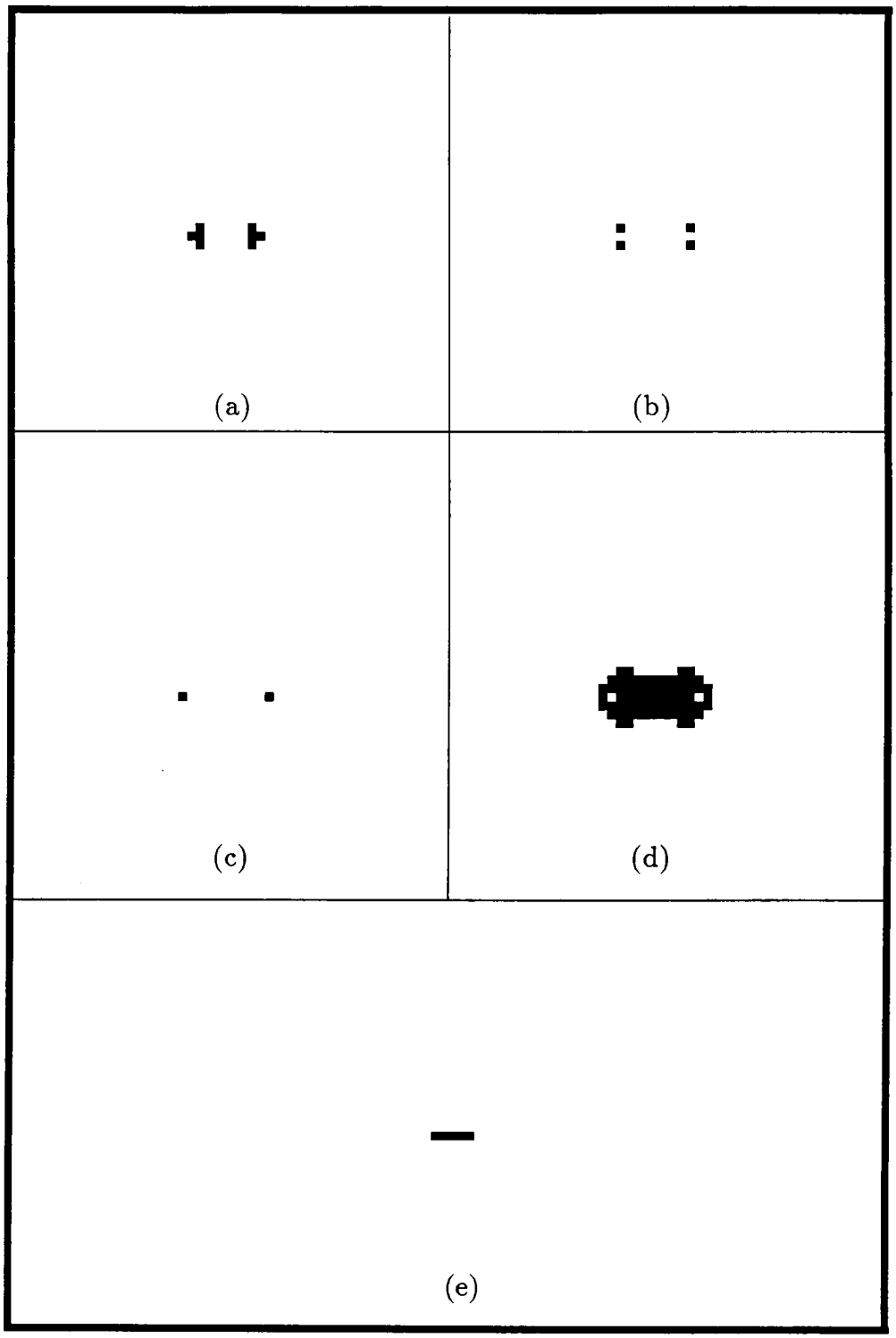


Figure 5.28: (a): T=31; (b): T=36; (c): T=45; (d): T=46; (e): T=51

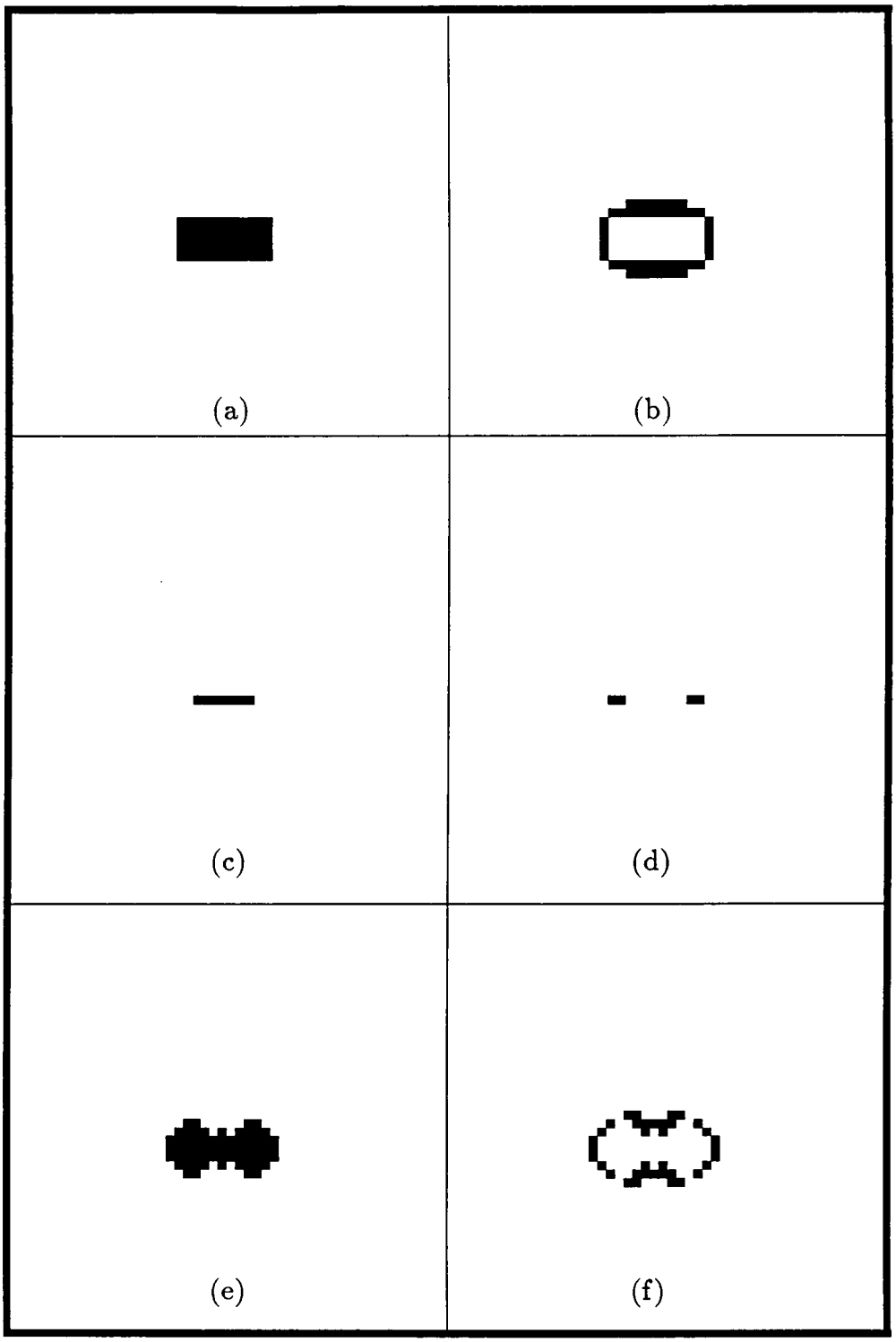


Figure 5.29: Layer $E2$ (a): T=8; (b): T=9; (c): T=14; (d): T=19; (e): T=29; (f): T=30

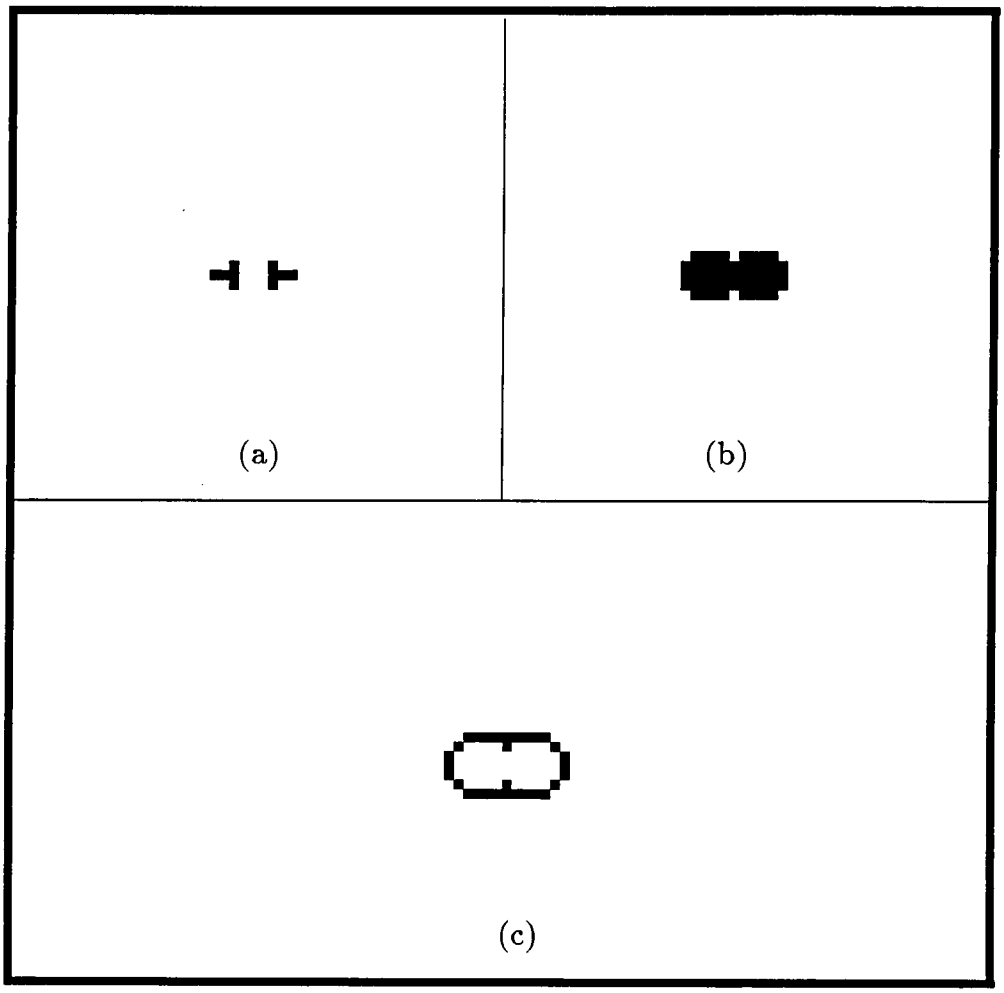


Figure 5.30: (a): T=35; (b): T=49; (c): T=50

5.2 Fine Encoding

In this section, two changes are made in the design of $E2$ which result in fine spatial resolution encoding. First, a single parameter that is shown to have a substantial affect on the time-varying characteristics of the response profile is changed so as to increase the amount of time-varying activity within each layer. The parameter is Inp_{delay}, which controls the time-sampling frequency of each neuron in $E1$. The architecture of the layers is the same, in the initial investigation, as before and the values for each parameter is given in Table (5.1). The spatial-sampling frequency is complete, as before. The behavioral changes of the layers are discussed by examining the activity in response to the same stimuli used with $Inp_{delay} = 10$: the $E1$ response to circles with diameters of 13 and 15 units; the $E2$ response to a circle, a square, a cross, and a rectangle. The $E1$ response to the circles demonstrates the increased activity. This leads to the parameters chosen for the two layer architecture used for shape analysis and to the second change in the design of $E2$: a change in the receptive field weighting to transfer the increased activity to the response profile of E_c.

5.2.1 Time-Varying Responses in E1

Two different sizes of circles, one with a diameter of 13 units (Fig. 5.31.a) and one with a diameter of 15 units (Fig. 5.31.b), are used to investigate the increased activity resulting from the change in Inp_{delay}. In Fig. 5.31.c, the response profile

of E_c in $E1$, with receptive field dimensions $SI = 13$, $CI = 5$, $SE = 13$, and $CE = 5$ in response to a circle with diameter = 13 in I is shown. The response to a circle with diameter = 15 is shown in Fig. 5.31.d. The profile is the same in each case; however, the amount of information encoded is very limited. Only, the mass activity at the onset is transferred to E_c. After the initial bursts, there is no activity transferred to E_c. The time-varying spatial patterns, Fig. 5.32 and Fig. 5.33, reveal a large number of time steps in which there are neurons firing in layer $E1$, indicating encoding of shape information. There is a long delay, $T = 10$ to 20, in which there is no activity in $E1$. After this interval the activity remains high. The response profile of E_c in $E1$ to the same input stimuli with receptive field dimensions $SI = 15$, $CI = 7$, $SE = 15$, and $CE = 7$, is shown in Figs. 5.31 e and f. The firing frequencies and interspike distances are different in the profiles for each stimulus. In addition, the time-varying spatial patterns, Fig. 5.34 and Fig. 5.35, show a great deal of activity in terms of the number of time steps in which neurons are firing in $E1$. The larger summation period for a given stimulus is responsible for this.

The very different behaviors of the two receptive field sizes are used to design a two layer system for shape analysis. First, the signs of the weighting of the intralayer receptive fields are reversed, *i.e.*, $SE2$ is excitatory and $CE2$ is inhibitory, to transfer the shape information encoded in $E1$ and $E2$ to E_c. The values of the parameters are given in Table (5.2).

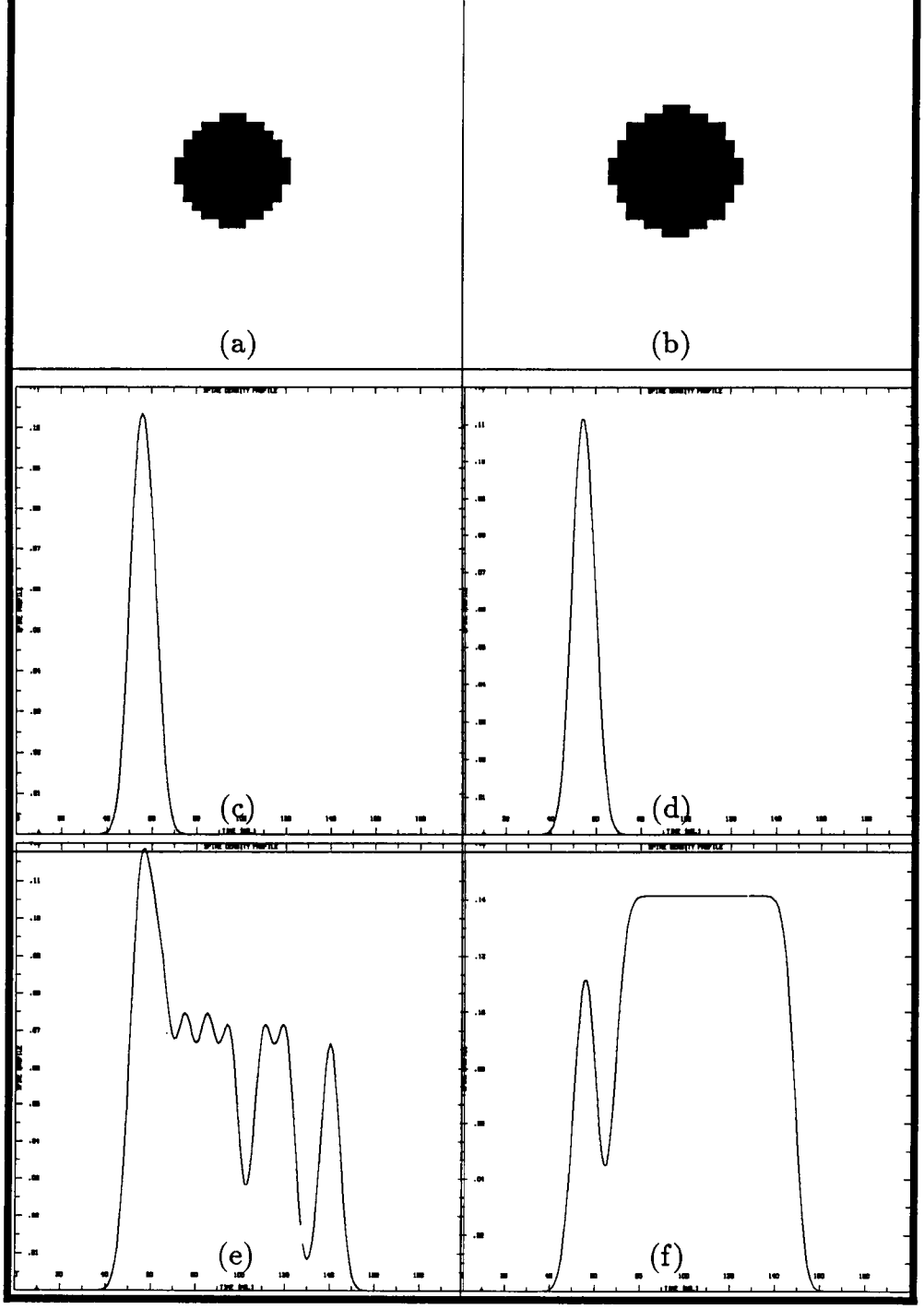


Figure 5.31: Response profiles of E_c in layer $E1$, Inp delay =1: (a): Input: Diameter=13; (b): Input: Diameter=15; (c): Response SI=SE=13, CI=CE=5 to (a); (d): Response SI=SE=13, CI=CE=5 to (b); (e): Response SI=SE=15, CI=CE=7 to (a); (f): Response SI=SE=15, CI=CE=7 to (b)

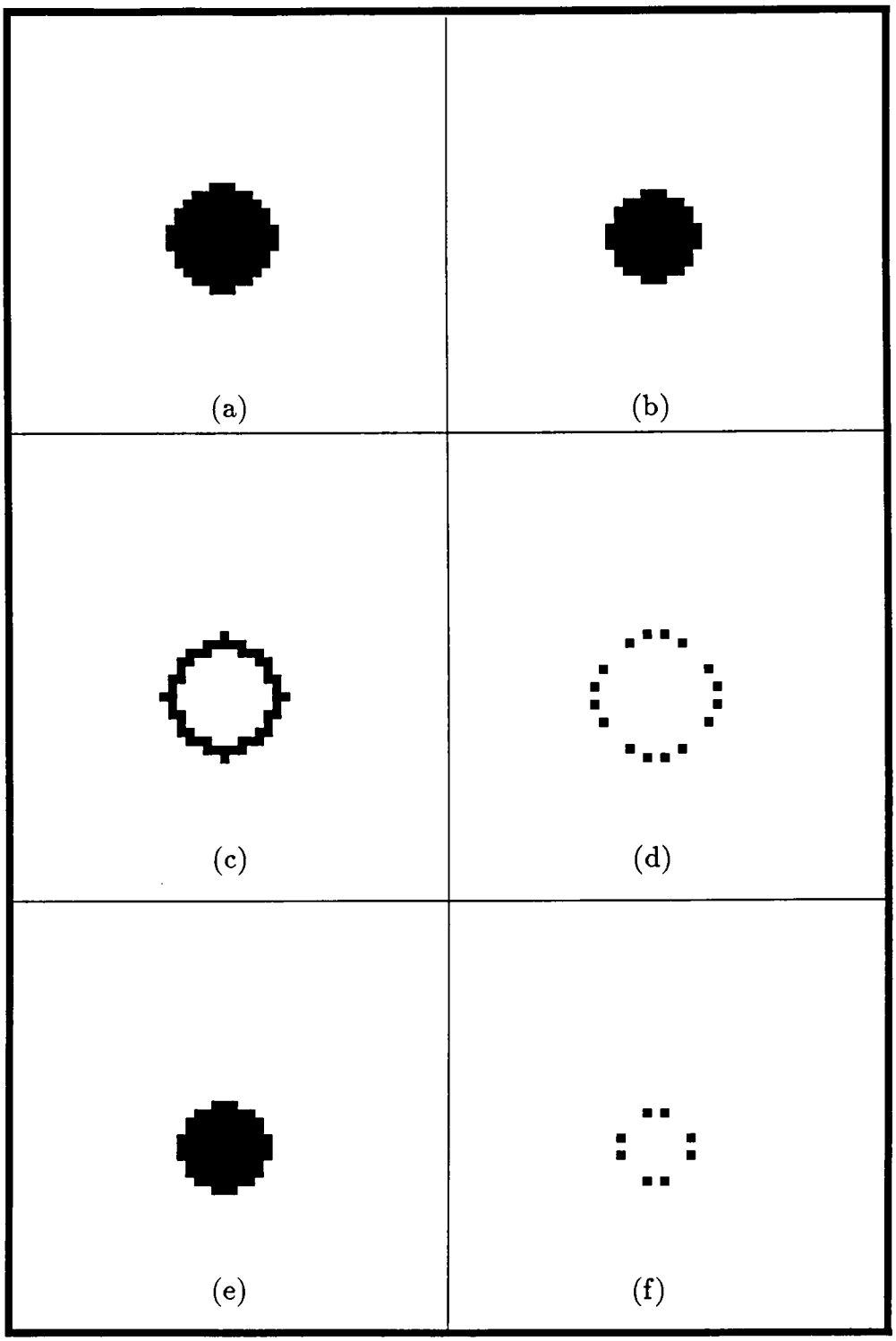


Figure 5.32: Layer $E1$ activity, Input delay=1, SI=SE=13: (a): Input; (b): T=5; (c): T=6; (d): T=7; (e): T=10; (f): T=20

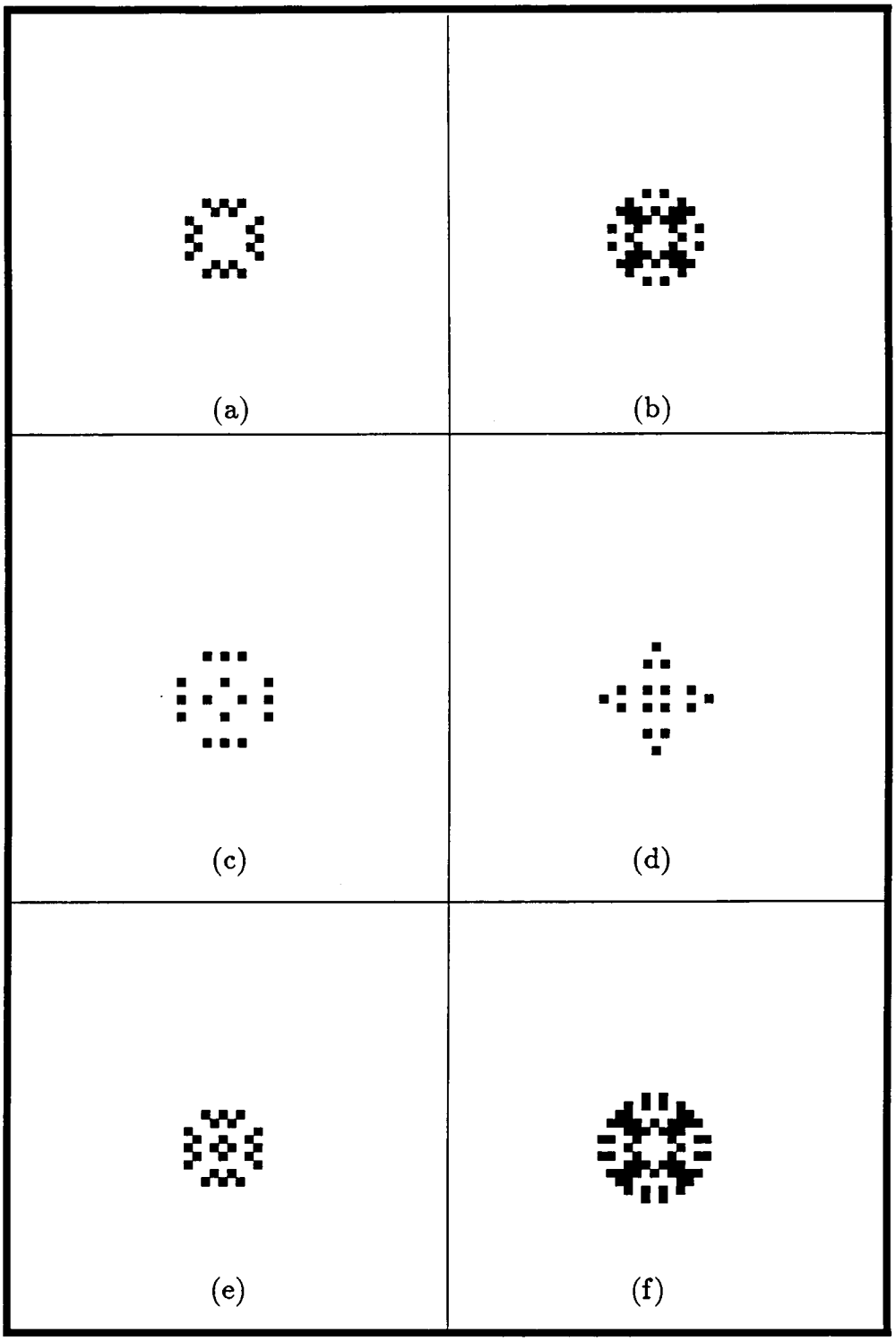


Figure 5.33: Layer $E1$ activity, Input delay=1, SI=SE=13: (a): T=21 ; (b): T=22; (c): T=23; (d): T=25; (e): T=26; (f): T=27

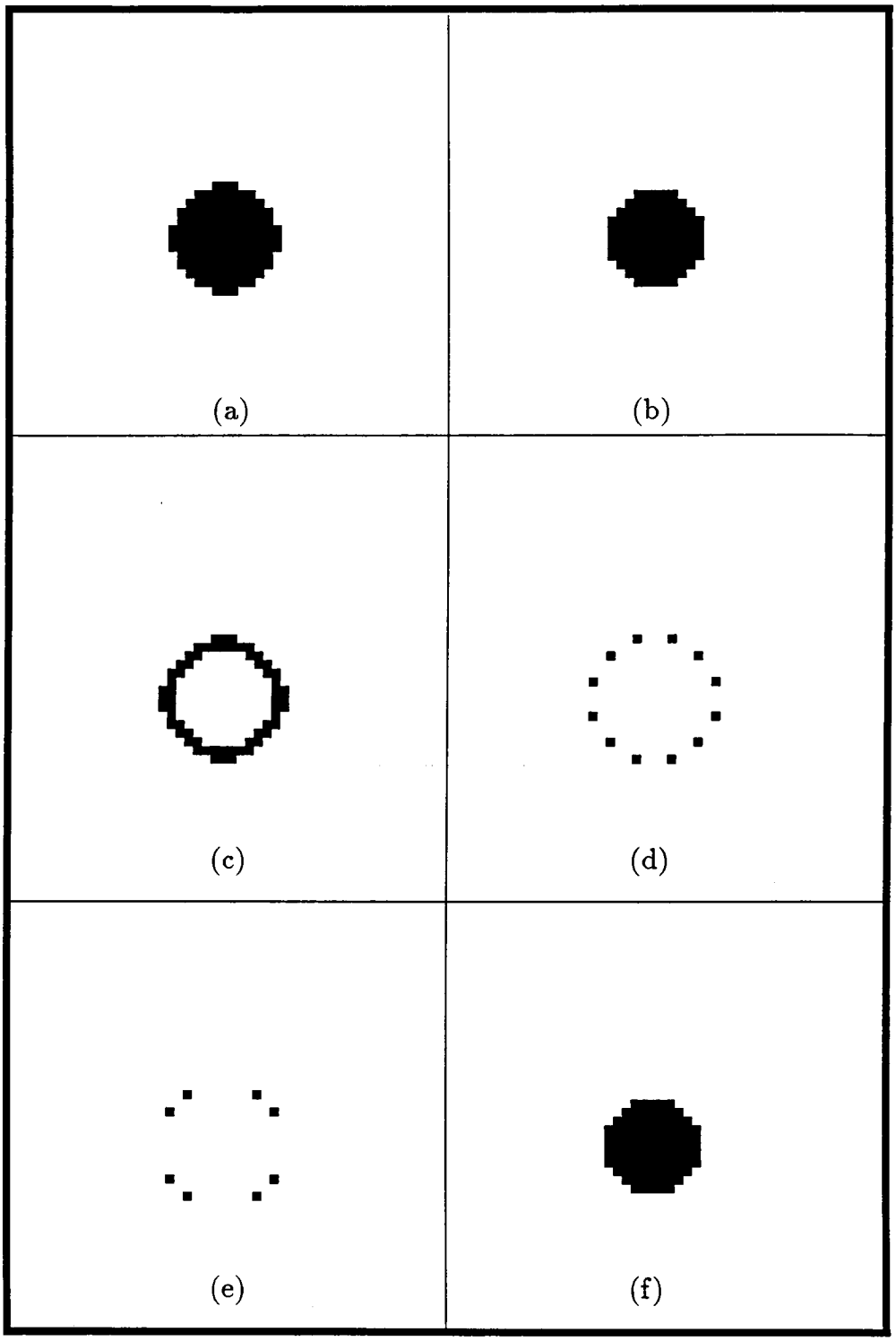


Figure 5.34: Layer $E1$, Input delay=1, SI=SE=15 :(a): Input; (b): T=6; (c): T=7; (d): T=8; (e): T=9; (f): T=11

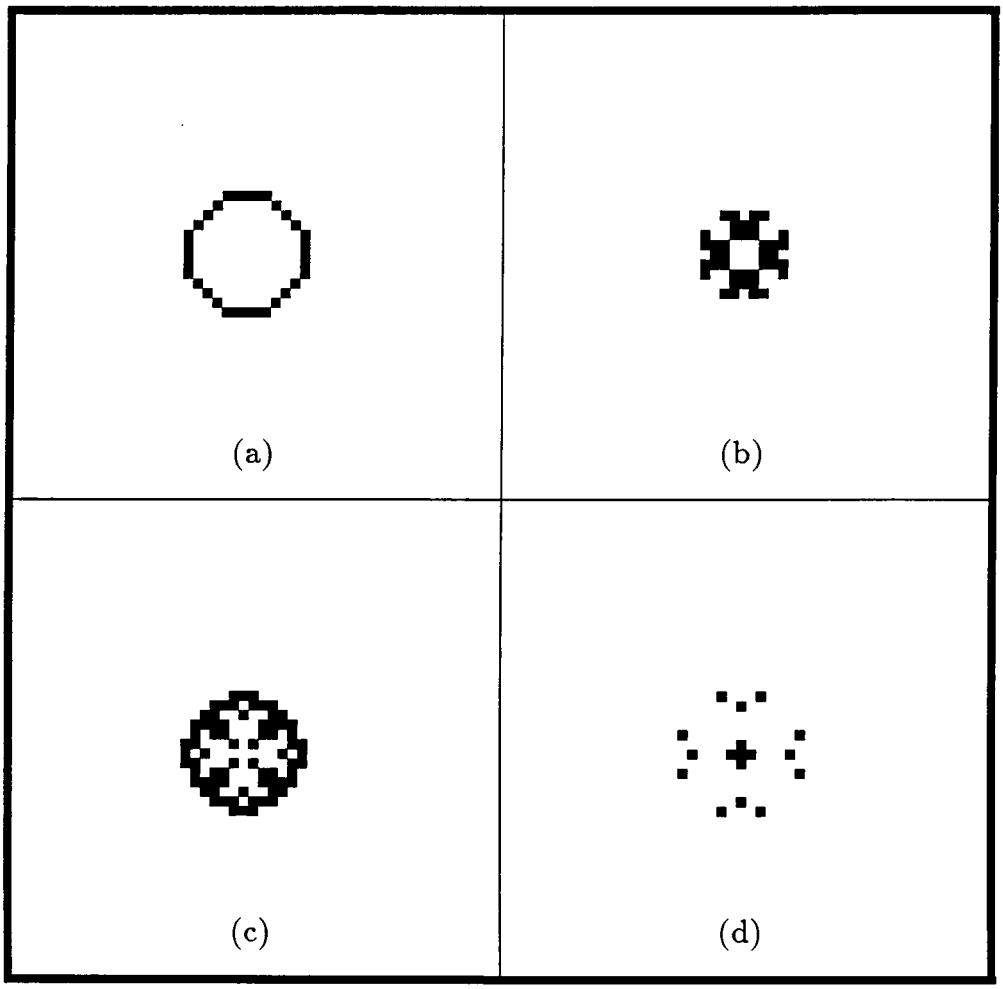


Figure 5.35: Layer $E1$, Input delay=1, SI=SE=15: (a): T=12; (b): T=16; (c): T=17; (d): T=18

Table 5.2: Shape Analysis and Learning and Memory parameters, receptive field sizes, and weighting. Signs in the heading refer to the sign of the center mechanism in the receptive field.

R F Configuration	*small/+*	*small/−*	*medium/+*	*medium/−*	*large/+*	*large/−*
SI	13	13	13	13	13	13
CI	5	5	5	5	5	5
ω_{SI}	-0.068	-0.068	-0.068	-0.068	-0.068	-0.068
ω_{CI}	0.19	0.19	0.19	0.19	0.19	0.19
SE	13	13	13	13	13	13
CE	5	5	5	5	5	5
ω_{SE}	-0.55	-0.55	-0.55	-0.55	-0.55	-0.55
ω_{CE}	0.21	0.21	0.21	0.21	0.21	0.21
$\Delta t_{layer}(inter)$	4	4	3	4	4	4
$\Delta t_{layer}(intra)$	3	3	2	3	3	3
θ_i $E1$	0.5	0.5	0.5	0.5	0.5	0.5
$SE1$	9	9	13	13	15	15
$CE1$	5	5	7	7	9	9
ω_{SE1}	-0.0007	0.053	-0.023	0.042	-0.036	0.055
ω_{CE1}	0.057	-0.0083	0.038	-0.0026	0.026	-0.0013
$SE2$	9	9	13	13	15	15
$CE2$	5	5	7	7	9	9
ω_{SE2}	-1.1	-1.1	-1.1	-1.1	-1.1	-1.1
ω_{CE2}	0.9	0.9	0.9	0.9	0.9	0.9
τ	4.3	4.3	4.3	4.3	4.3	4.3
$\Delta t_{layer}(inter)$	2	2	2	2	2	2
$\Delta t_{layer}(intra)$	4	4	4	4	4	4
θ_i $E2$	0.55	0.55	0.55	0.55	0.55	0.55
Δt_{ref}	5	5	5	5	5	5
Inp_{delay}	1	1	1	1	1	1
Δt_{learn}	40	40	40	40	40	40
INC	2	2	2	2	2	2
L	4	4	4	4	4	4
O_{learn}	12	12	12	12	12	12
LS	4	4	4	4	4	4
LM	0.5	0.5	0.5	0.5	0.5	0.5
Δt_{sat}	14	14	14	14	14	14
Δt_{per}	160	160	160	160	160	160
Δt_{add}	70	70	70	70	70	70
T_{spikes}	120	120	120	120	120	120

Following this, the Inp_{delay} time is changed to increase the number of time steps that neurons are firing in both layers. This allows each layer to settle into states of excitement that makes each sensitive to less global, or mass, input stimuli.

5.2.2 Shape Analysis With Fine Resolution

In this section, changes are made to the architecture of $E2$ so that the information encoded and transmitted by the time-varying spatial patterns are transfered to E_c. From the preceding, larger receptive fields result in more activity (again, in terms of the number of time steps that neurons are firing) within a layer. The response profiles reflect this increased activity. The smaller receptive fields potentially encode input parameters on a finer spatial scale; although the information is not seen in the response profile of E_c. The following combines these two features in a two layer system. The first system is constructed from the smaller receptive fields in $E1$ which provide a feedforward input to $E2$, with larger receptive fields. The signs of the intralayer weightings in $E2$ are reversed, as stated in the preceding. It is shown that, while the response profile of E_c in this configuration is unique to each of the four shapes previously used, the amount of information encoded in the response still reflects predominately mass action from $E1$. In the second system, the value of Inp_{delay} is changed and the activity within each layer is greatly increased, in terms of the number of time steps in which neurons are firing.

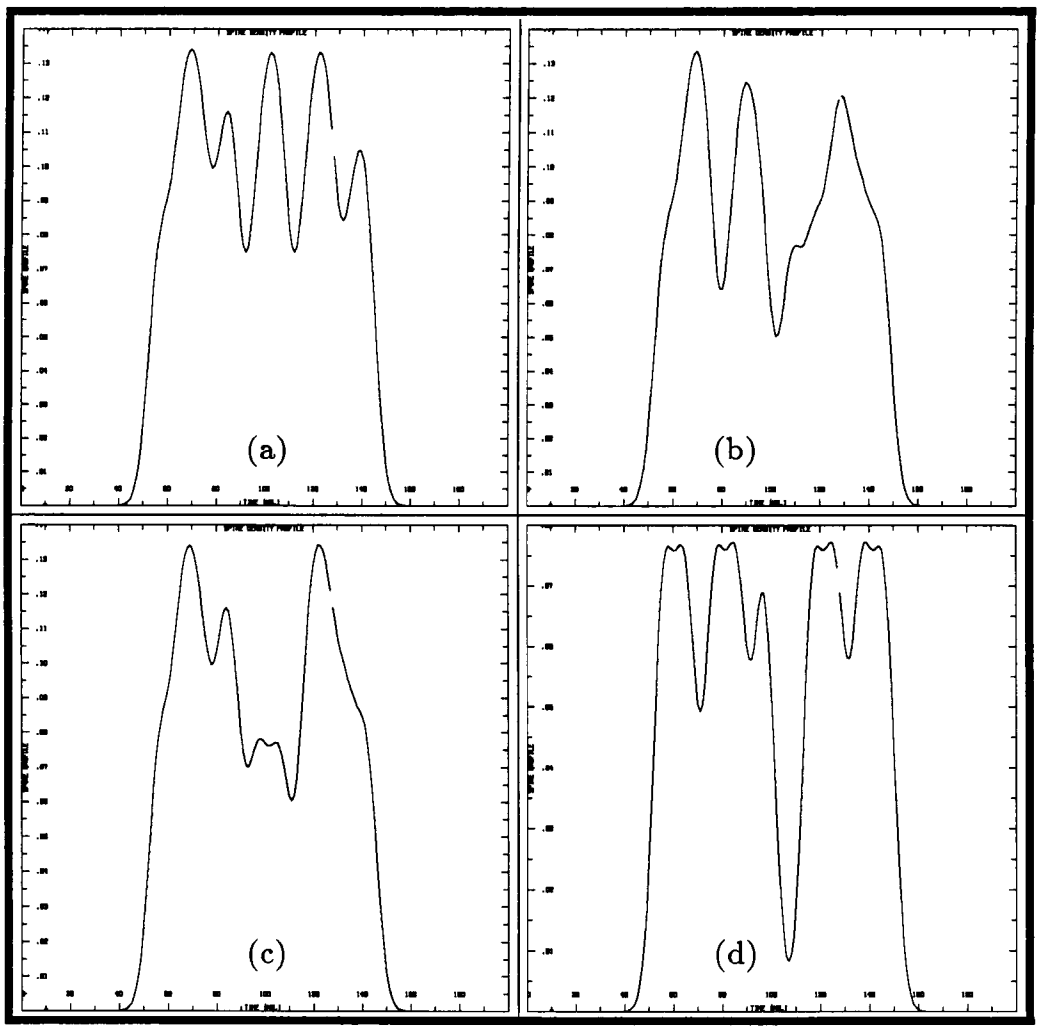


Figure 5.36: Response profiles of E_c in layer $E2$, Input delay=10, E2 Reversed fields: (a): Circle; (b): Square; (c): Cross; (d): Rectangle

The increased activity results in a waveform of E_c that reflects both global and finer encodings. The response profiles of the first system are shown in Fig. 5.36. The input signals to $E1$ are a circle, a square, a cross, and a rectangle. The change in the architecture results in a response profile that reflects a great deal more information encoding. The physiological basis for the change is the following. It is known that ganglion cells can be classified as either on-centered or off-centered (Chapter 2). By combining the two types of cells in a single layer, *i.e.*, on-centered interlayer and off-centered intralayer, the activity in the peripheral neurons is transmitted to the central E_c location in an excitatory manner and the excitatory coarser central information from $E1$ are both encoded in the response of E_c in $E2$. The parameter values are shown in Table (5.2). The peaks seen in the profiles are the result of mass firings in the central location of $E1$ and also the result of numerous time steps of firings in more peripheral neurons. The periodicity of Inp_{delay} still dominates much of the response profile of E_c, as seen in the strong peaks reflecting the mass firings in $E1$.

The response profiles of E_c for the second system are shown in Fig. 5.37. In this system, $Inp_{delay} = 1$. The firings in $E1$ during the onset of the stimulus are generally quite large, spatially. This is seen in the initial peaks in each of the profiles. There are other periods of mass spatial activity in $E1$ that are also reflected in the profiles, although these are often interrupted or have firings from more peripheral neurons superimposed on the peaks. This is readily seen by comparing these profiles with the response profiles of the system with

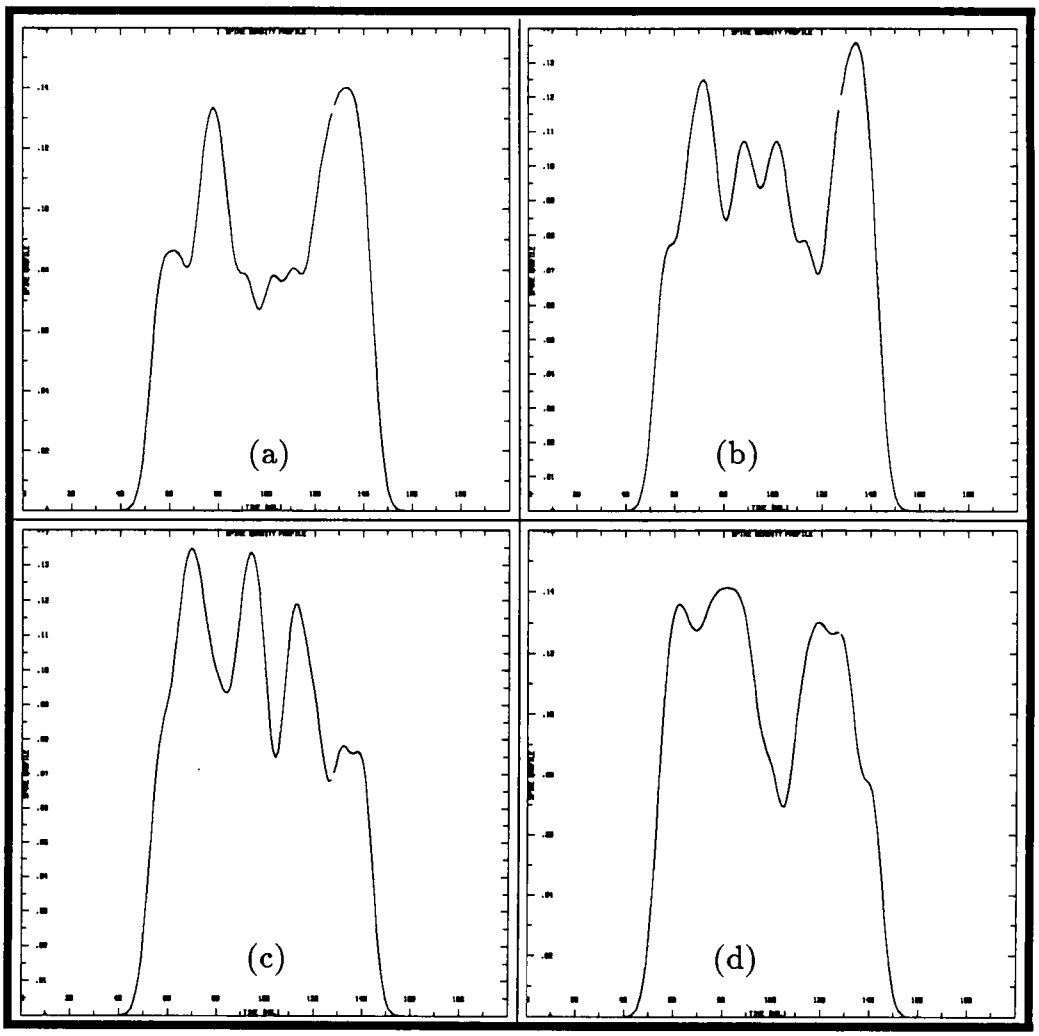


Figure 5.37: Response profiles of E_c in $E2$, Input delay=1, E2 Reversed Fields: (a): Circle; (b): Square; (c): Cross; (d): Rectangle

$Inp_{delay} = 1$ and the signs of the intralayer weightings not reversed, Fig. 5.38. The latter profiles show very little finer encoding. In addition, the profiles in Fig. 5.37 lack the coarse domination of the waveform imposed by the periodic sampling, Fig. 5.36.

5.3 Rotation and Shift Invariance

The spatial sampling frequency and the dynamics of the individual neurons used in this work result in highly localized processing. As a result, the encoding of information from the input is invariant to shift and rotation of the input signal. Since the sampling strategy employed in this simulation is the basis of the rotation and shift invariance characteristics, a few physiological mechanisms pertaining to sampling are briefly reviewed.

As discussed in Section (2.1), the sampling frequency in the physiological retina is not constant across the retina. Thus, the encoding of stimulus parameters in the physiological system is not constant in terms of spatial resolution across the retinal grid. For example, the more peripheral a signal is on the retinal grid, the more difficult it is for a human being to identify an object. In addition, the magnification factor of various retinal representations in striate cortex complicates any efforts to simulate the sampling of the physiological system. Modeling the actual receptor cell distribution is impractical and the data is insufficient for anything but a gross approximation. Even if the spatial dis-

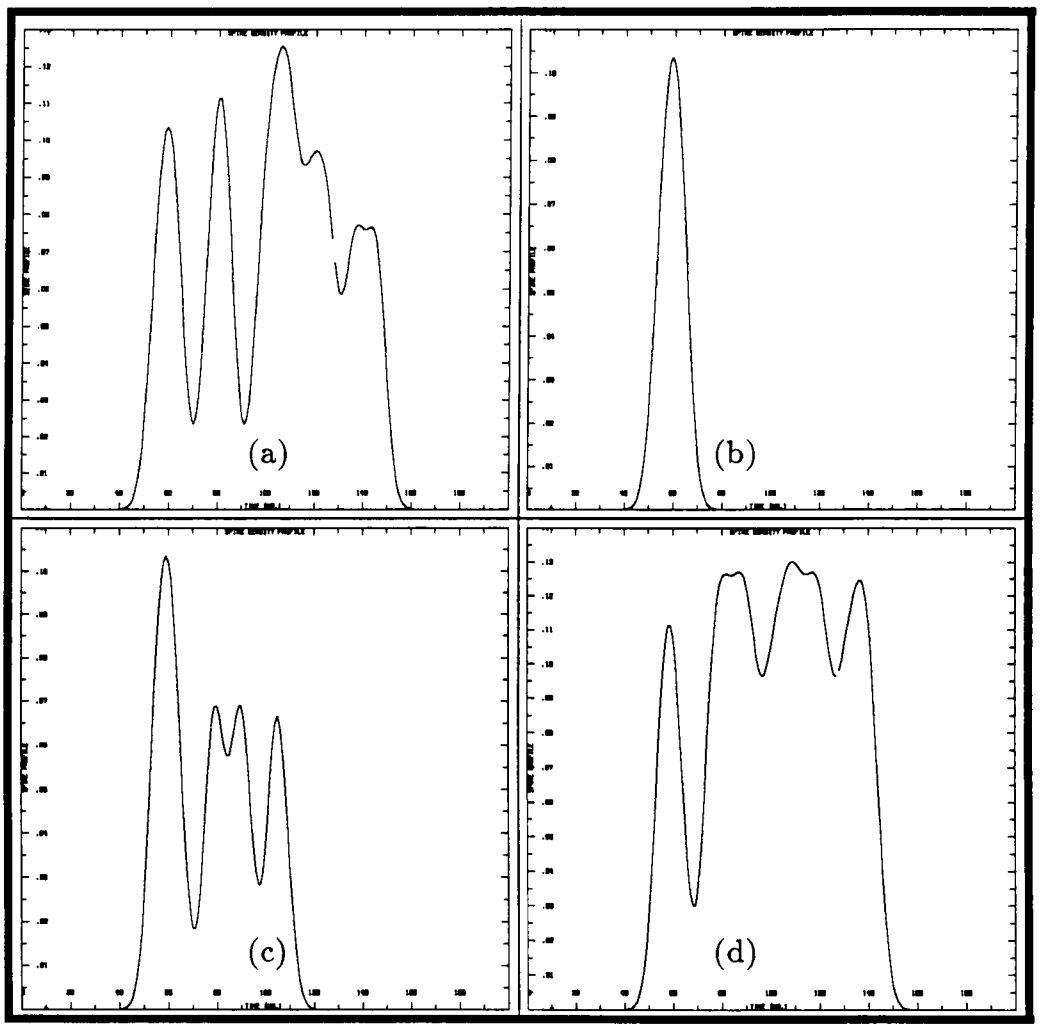


Figure 5.38: Response profiles of E_c in layer $E2$, Input delay=1, E2 Non-reversed fields: (a): Circle; (b): Square; (c): Cross; (d): Rectangle

tribution and function of the various cells in the retina could be approximated in hopes of investigating the sampling frequency, modeling would be further confounded by insufficient data on eye movement mechanisms. As previously stated, these issues are not directly addressed in this thesis, although the ommission is not intended to belittle the significance of either. In fact, inclusion of these dynamics may lead to some very useful features in a simulated visual system.

Orientation specific cells are not modeled in this work. However, orientation information can be extracted in this simulation by including layers of orientaion specific cells, designed from striate cortex data. The orientation columns founds in striate cortex have been the subject of intensive physiological research, inspired by the seminal work of Hubbel and Weissel. The center-surround structure presented here is a possible mechanism for encoding from striate cortex to obtain a signal for object recognition independent of orientation.

5.3.1 Rotation Invariance

The system's rotation-invariant characteristic is developed in two steps. First, since each neuron is processing locally in a radially symmetric receptive field and every point in the input is sampled, any point in the input stimulus is guaranteed to be processed in exactly the same manner independent of it's position or rotation. The time-varying spatial patterns of a given input change only in there position in $E1$ relative to the rotation of the input. Second, the system

described in Section (5.2) is designed to transfer information in the peripheral receptive field to the center of $E2$ and, hence, is encoded by E_c, as shown in the response profiles of E_c. Thus, assuming compatability of the size of the input stimulus and the size of the receptive fields in $E1$, encoded in the response profile of E_c are the parameters of the input signal, independent of the rotation of the input. The response profile of E_c has been used throughout this work as a means of representing the recognition of objects in layer I. At this point the relevance of transferring the encoded stimulus parameters to E_c becomes apparent.

The time-varying spatial patterns of layers $E1$ and $E2$ are shown in Figs. 5.39 through 5.42 for a vertical and a horizontal bar. The time-varying spatial patterns are identical in each time step, except for the rotation of 90°. The response profiles are identical, Fig. 5.43. Problems occur with quantization errors for angles other than 0°, 45°, and 90°.

5.3.2 Position Invariance

Position-invariance is inherent in the design of the system since the stimulus parameters are encoded in the same manner across the first layer of the model independent of the position in $E1$, as stated above. Thus, if the time-varying spatial patterns are defined as the method of object recognition, the same discussion given in Section (5.3.1) is applicable here. However, the concepts of pre-attentive behavior and foveating can be modeled and incorporated in the

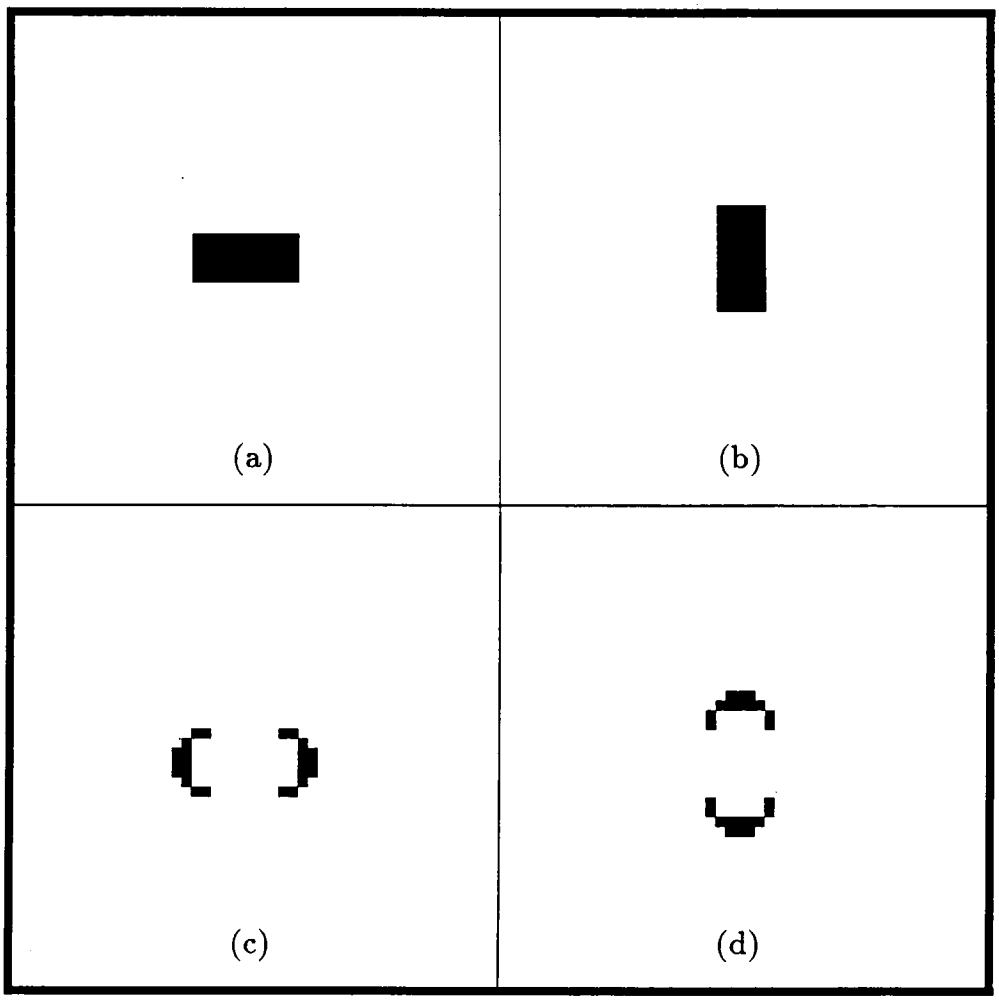


Figure 5.39: Position invariance, Layer $E1$, Input delay=1: (a): T=10; (b): T=10; (c): T=11; (d): T=11

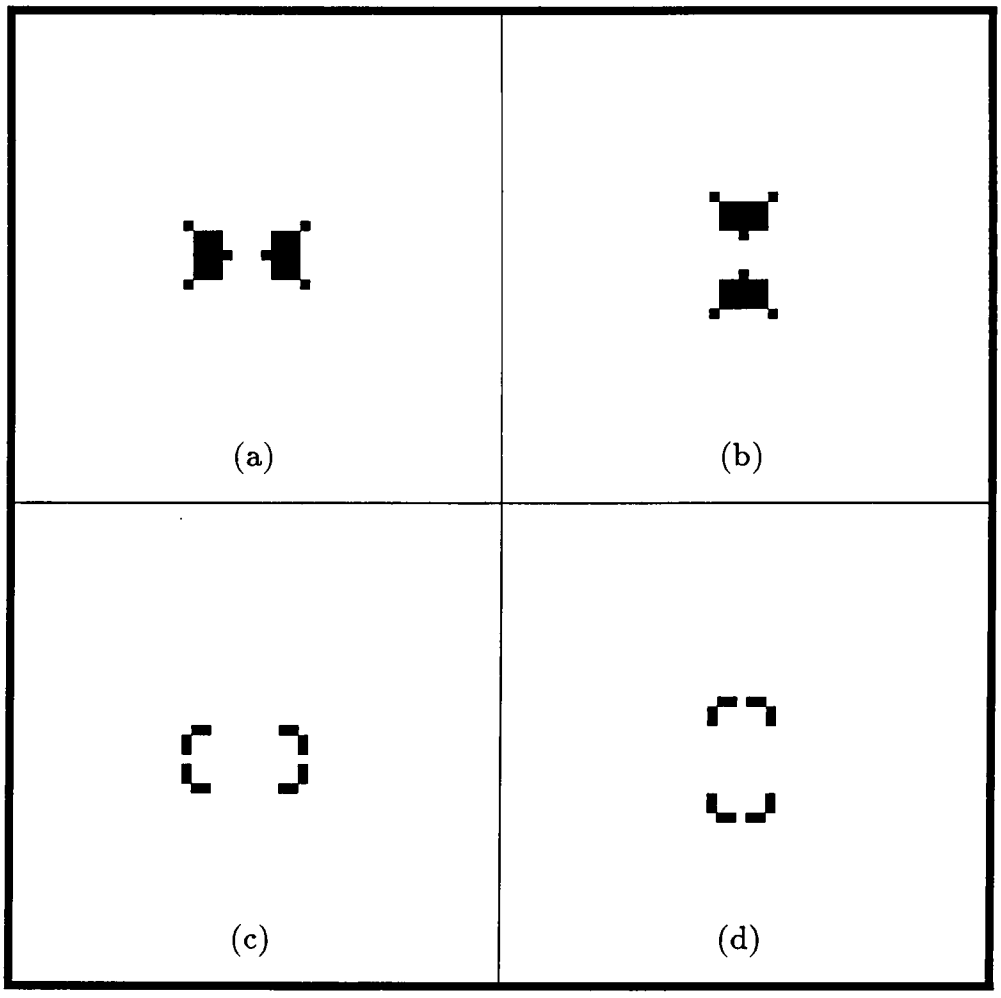


Figure 5.40: Position invariance, Layer $E1$, Input delay=1 (a): T=15; (b): T=15; (c): T=16; (d): T=16

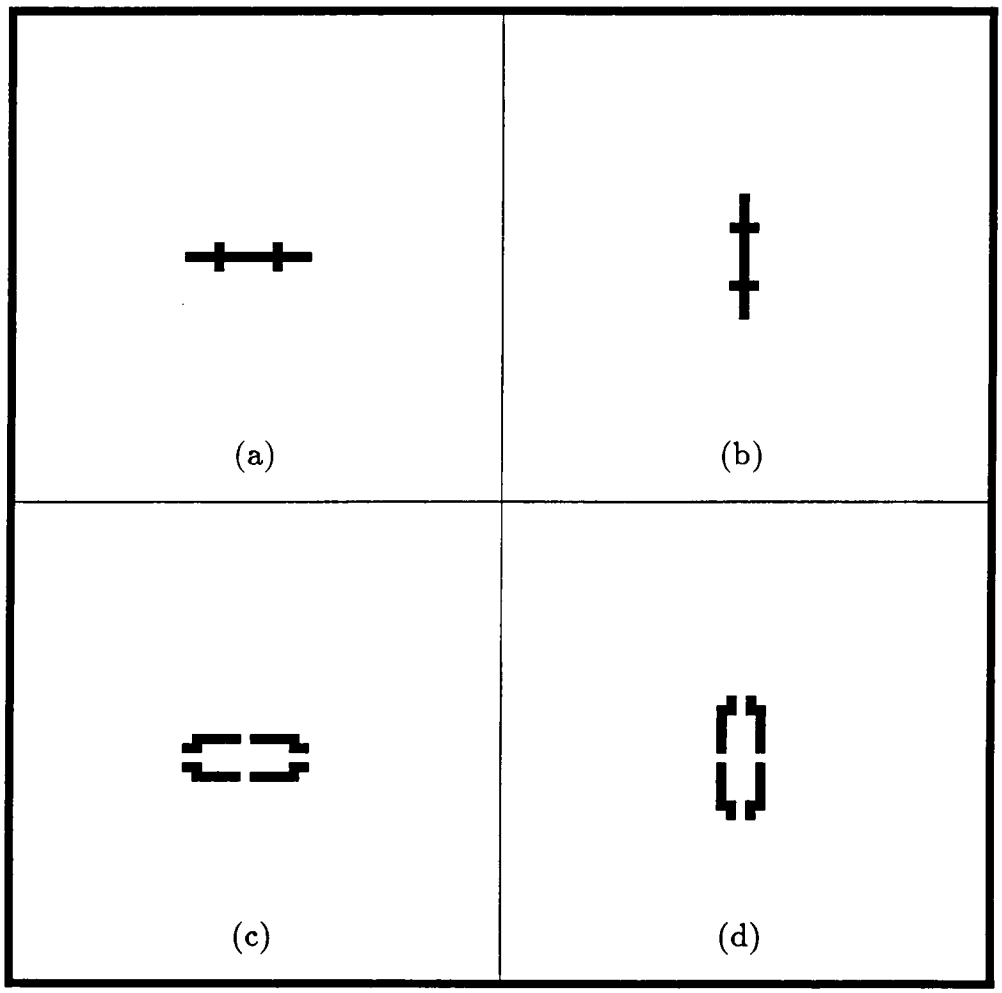


Figure 5.41: Position invariance, Layer $E2$, Input delay=1: (a): T=13; (b): T=13; (c): T=14; (d): T=14

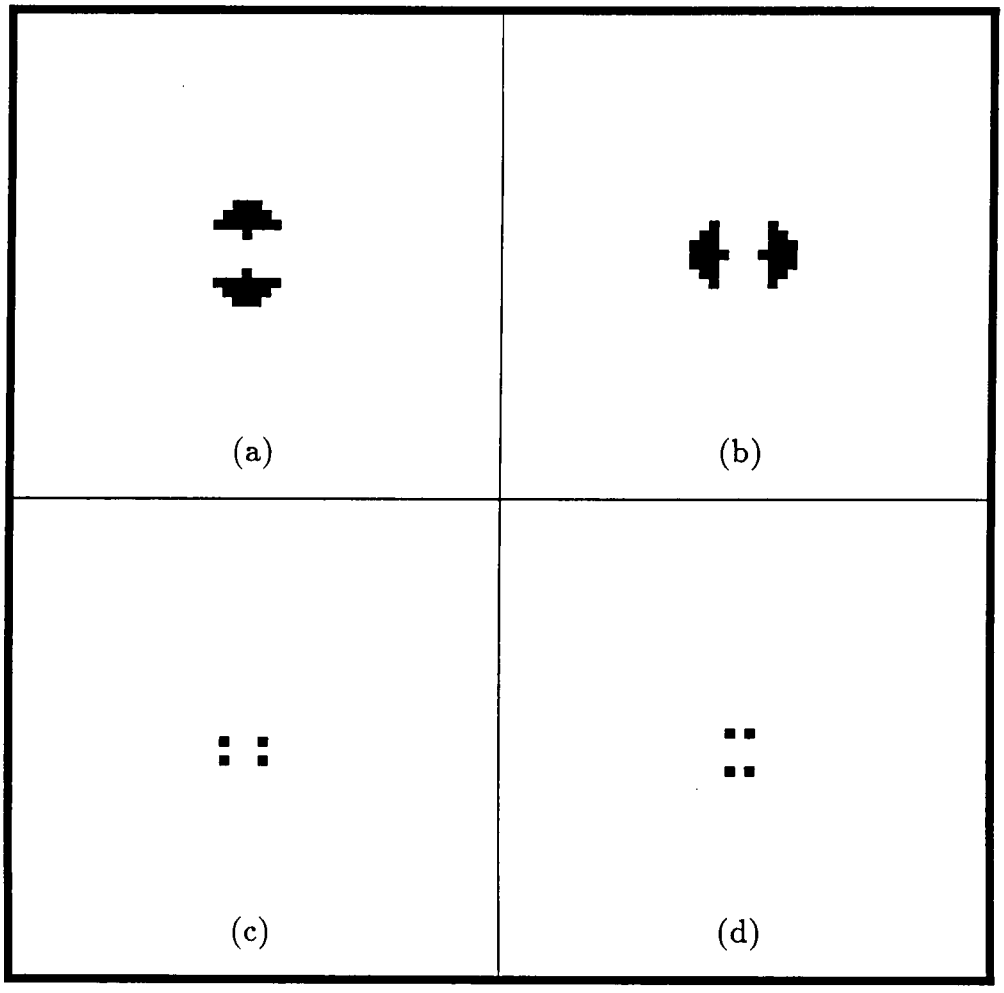


Figure 5.42: Position invariance, Layer $E2$, Input delay=1 (a): T=16; (b): T=16; (c): T=17; (d): T=17

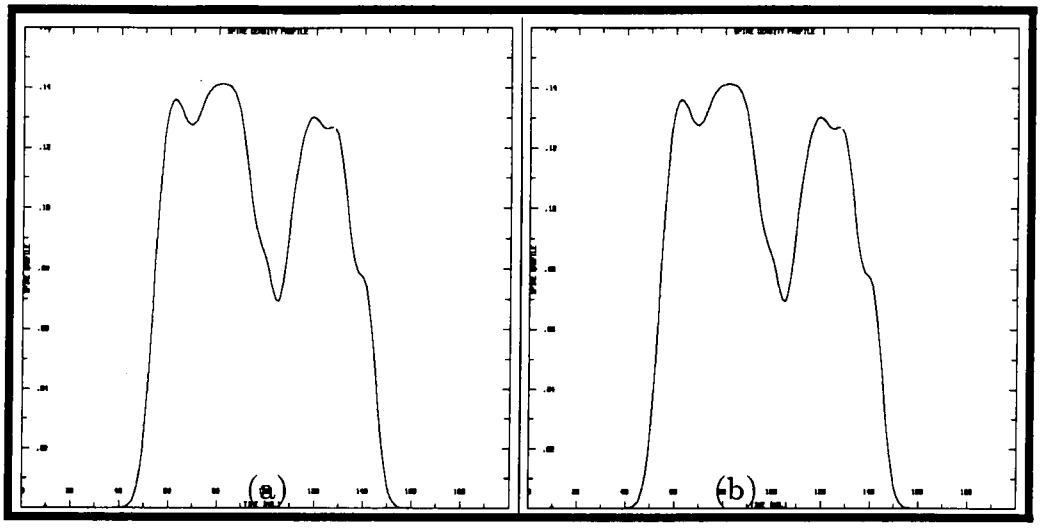


Figure 5.43: Response Profiles for Rotation Invariance: (a): Vertical; (b): Horizontal

simulation to bring an ensemble into alignment with the input stimulus. This allows for a response profile from E_c to be used in the recognition process.

As discussed in Chapter 1, the human visual system analyses the information in the visual field at various resolutions. One such division is the X-cell and Y-cell pathways. The center-surround dynamics of the Y-cell behaviour, which may be associated with coarse processing, may provide a mechanism for pre-attentive behaviors and foveating. The surround mechanism of the Y-cell receptive field is delayed with respect to the center mechanism. This suggests that a blurred representation of the visual field may be utilized by the visual system at an early stage in the processing.

In this thesis, a two layer system characterized predominately by center mechanisms is used to establish the location of an object in the visual field.

Information from this subsystem could then be used as a feedforward signal to a second system that foveates the input and activates the system described in Section (4.3).

The architecture and the signal flow is as before. The difference lies in the weighting of the inter-layer synapes. In this simulation, all inter-layer synapses are positive and of equal weighting, spatially. This weighting insures that only very coarse information is encoded in each layer. The resting membrane potentials of the neurons in $E1$ are set to a very low initial value with respect to the firing threshold level. This minimizes the activity within layer $E1$ so that the coarseness of the processing is increased beyond that provided by the choice of weighting. In addition, $Inp_{delay} = 10$ as in the case of coarse processing, Section (5.1). The reason for this is it is assumed that as the eye initially scans the visual field it adapts to the level of light brightness and the predominate features in the visual field impinge on any given region of the retina only as often as the scanning mechanisms permit.

The spatial firing patterns reflect very coarse processing in $E1$. The only activity is found in those neurons with large amounts of their receptive fields stimulated by I. The inhibitory surround intralayer synapses, along with the constant decay of the membrane potential at the hillock, restrain the lateral propagation within $E1$. For each of the four shapes used as input, only a few neurons in $E1$ respond.

Since there is no inhibitory signal from $E1$ to $E2$, the membrane potentials

within $E2$ continue to increase over time. Initially there is no activity within layer $E2$. If no neuron fires within a a time interval Δt_{float}, chosen so that the neurons in layer $E2$ have summed across the entire extent of their receptive fields, the membrane potential of the neurons in $E2$ are allowed to float with afferent activity. The membrane potentials of those neurons having the highest average potential over the time interval Δt_{float} are changed with respect to the firing threshold. This membrane potential provides a baseline resting potential, B_{rest}, which is not involved in the decay of Eq. (4.3). Thus the effective membrane potential, MP_{Eff}, is

$$MP_{Eff} = MP_i + B_{rest}. \tag{5.1}$$

The resting potential continues to increase for neurons having the highest potentials over each interval in time Δt_{float} until a neuron, or small neighborhood of neurons, fires in layer $E2$. A feedforward signal from this layer could then provide a signal, or a gate, to the system described in Sections (5.1) and (5.2).

The weighting of the receptive fields, Table (5.1), results in a single neuron firing in layer $E2$ after a time delay of 10 ms for the circle and the cross. A 3×3 neighborhood of neurons in $E2$ fired after a time delay of 10 ms in the case of the square. Only in the case of the rectangle was it necessary to float the membrane potential of the active neuron in layer $E2$. In which case, a single neuron fired after 61 ms. In each case, the activity in layer $E2$ is minimized so that the region in I corresponding to the highest concentration of intensity is localized.

5.4 Incorporating Parameters for Learning and Memory

Learning, and subsequently memory, are defined on a local level in terms of physiological mechanisms. To recapitulate the main physiological mechanisms for learning and memory: The basic learning mechanism is based on Hebbian rules of synapse modification. The general rule is when both the pre-synaptic and post-synaptic neurons are active, the link between the two is strengthened. Various modifications have been made to this general concept. In the work cited in Section (3.7), the mechanism for permanent membrane changes associated with memory is the movement of calcium ions across the membrane into the pre- and post-synaptic intracellular fluids. The calcium ions are a catalyst for the increased link strength that results in both learning and memory. The changes may be dependent on a floating threshold value that fluctuates with local firing activity and are a result of the membrane permeability changes to sodium and potassium ions. A more detailed description of the physiological mechanisms is given in Chapter 3. The system developed for localization is an example of learning by floating the membrane potential of the post-synaptic neurons. The membrane potential of neurons with the most active afferents is allowed to float until until there is firing in $E2$. This learning mechanism is modified and extended to active layers, those in which there is firing present.

In the first simulation presented in this section, the learning mechanism allows for changes in the synaptic efficacy by increasing the value of ω. The

changes are short term changes that do not result in a permanent weight change. In the model, changes are made to excitatory synapses within $E2$. In this way, layer $E1$ continues to encode stimulus parameters according to the tuning imposed on them [Section(4.3.3)]. The changes in $E2$ either accentuate or depress specific features that have been transmitted from $E1$. The signal does not propagate to layer $E2$ until a time period of Δt_{set}. This allows layer $E1$ to settle into a characteristic activity level prior to the signal propagating to $E2$. Changes are made according to the following. The region of highest activity during a time interval Δt_{learn} in an $N \times N$ neighborhood and all regions with an activity level of 90% of the maximum activity are targeted for learning. The neuron, i, with the highest spike count in each region is the neuron chosen for learning. The intralayer excitatory weights from this neuron to all neurons, j, within the $N \times N$ region are changed according to the following

$$\omega_{ji}(t+1) = \omega_{ji}(t) + C_{learn} * \frac{SP_j}{SP_i}, \tag{5.2}$$

where C_{learn} is a constant, SP_i is the number of spikes from neuron i and SP_j is the number of spikes from neuron j during Δt_{learn}.

The assumptions implicit in this learning rule are discussed in the following. First, it is assumed that ion flow in the intercellular fluid is toward the region of greatest activity due to the changing membrane potentials. Second, it is assumed that the dendritic modifications associated with learning are in response to high levels of stimulation. For this reason, modifications are made, not to the most active neuron, but to the target neurons of that neuron. The amount of change

is proportional to the level of activity in the target neurons. This is in keeping with the Hebbian learning paradigm. One final assumption is that the membrane potential of individual neurons can be represented on the more coarse physical level of spike count within a region.

The results of this processing are shown in Figs. 5.44- 5.48. The X and Y axes represent the image plane and the amplitude along the Z axis is the relative number of spikes at each (x,y) location. The difference in the spike count for stimulation with and without learning are shown in Fig. 5.46. The maximum difference in the amplitudes are 10 for the square and circle, 11 for the cross, and 8 for the rectangle. In the figures, the amplitudes have been scaled for ease in viewing. The most prominant stimulus features encoded are shown in the peaks in each figure and the features that are emphasized in the learning process are shown in the difference between the two spike count inages. The change in the response profiles of E_c are shown in Figs. 5.47 and 5.48. There is no change in the response profiles for the circle and the rectangle. These two shapes correspond to the images in Fig. 5.46 with the smallest number of spikes after learning. The differences after learning for the square show a few spikes concentrated close to E_c. This information is shown in the large peak at the end of the response profile in Fig. 5.47. The differences after learning for the cross are the most numerous and this is reflected in the changes in the response profile after learning.

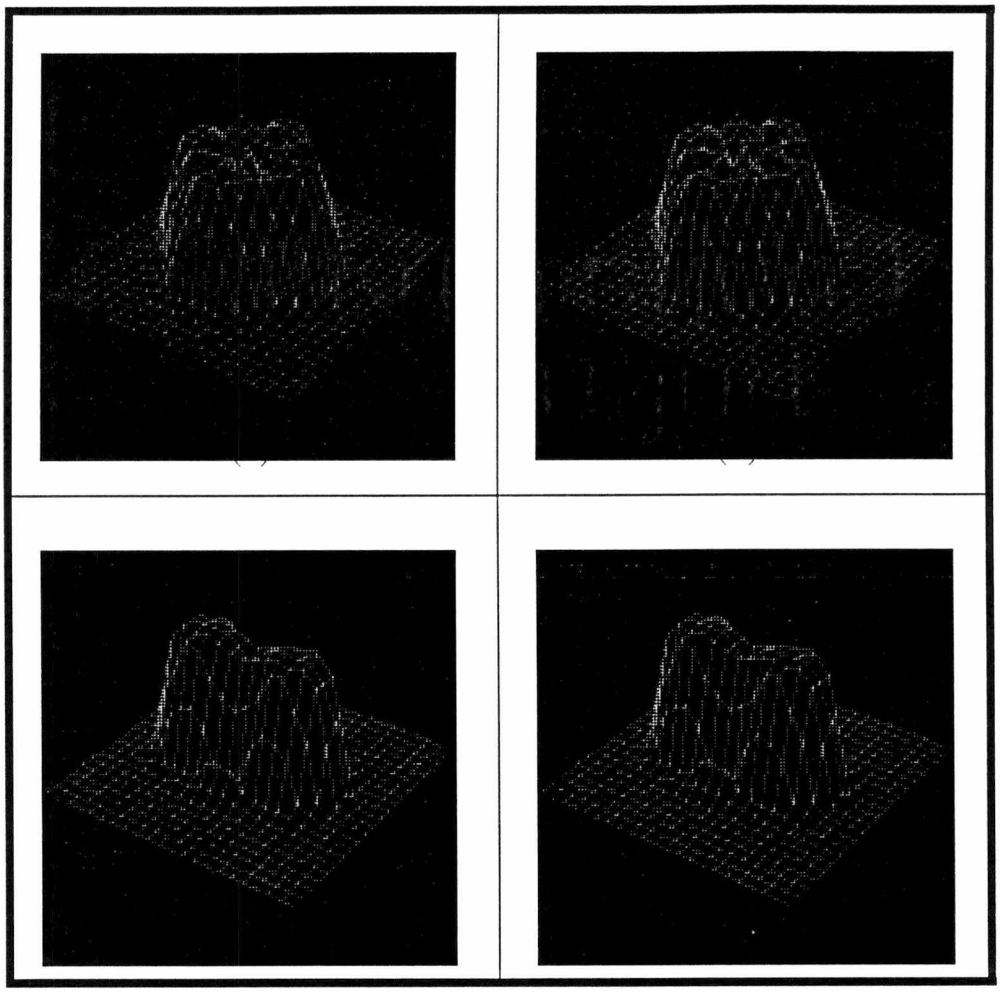


Figure 5.44: (a): Input–cross, Spikes in layer $E2$, no learning; (b): Input– cross, Spikes in layer $E2$, with learning; (c): Input–rectangle, Spikes in layer $E2$, no learning; (d): Input–rectangle, Spikes in layer $E2$, with learning

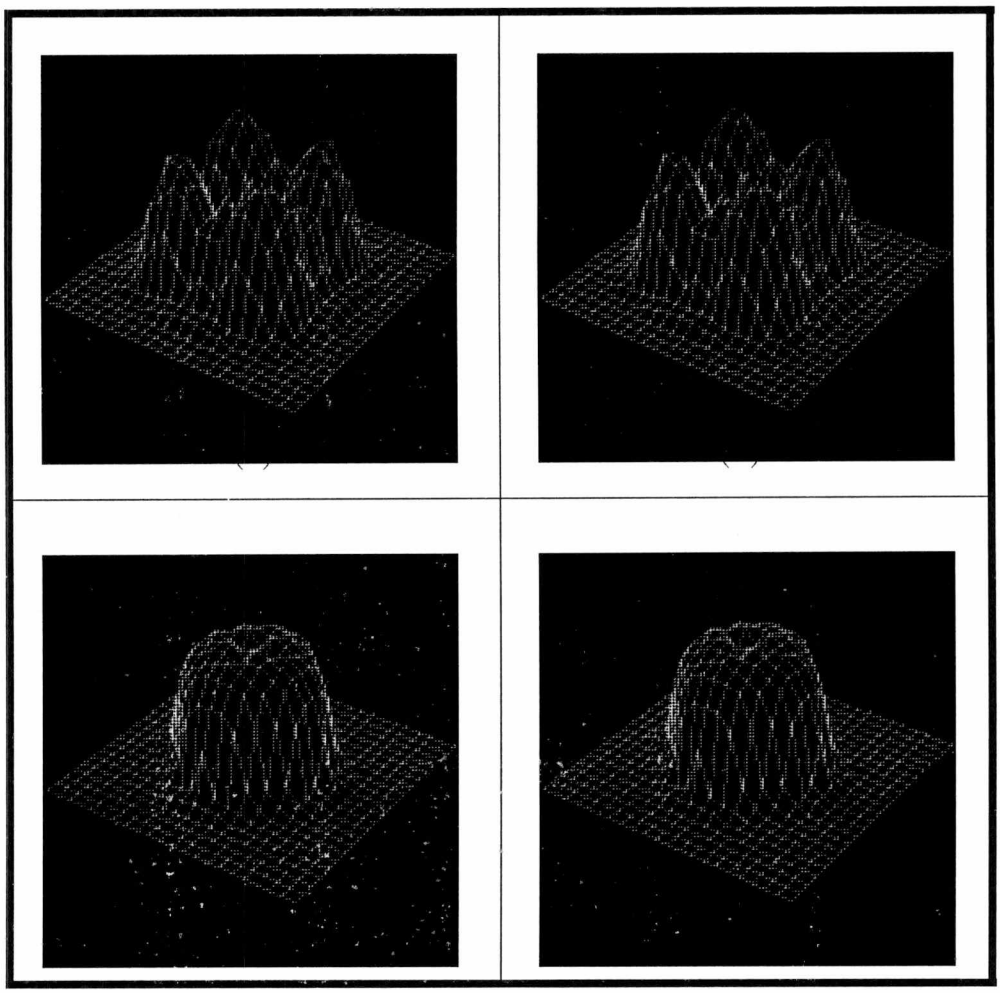


Figure 5.45: (a): Input–square, Spikes in layer $E2$, no learning; (b): Input–square, Spikes in layer $E2$, with learning; (c): Input–circle, Spikes in layer $E2$, no learning; (d): Input–circle, Spikes in layer $E2$, with learning

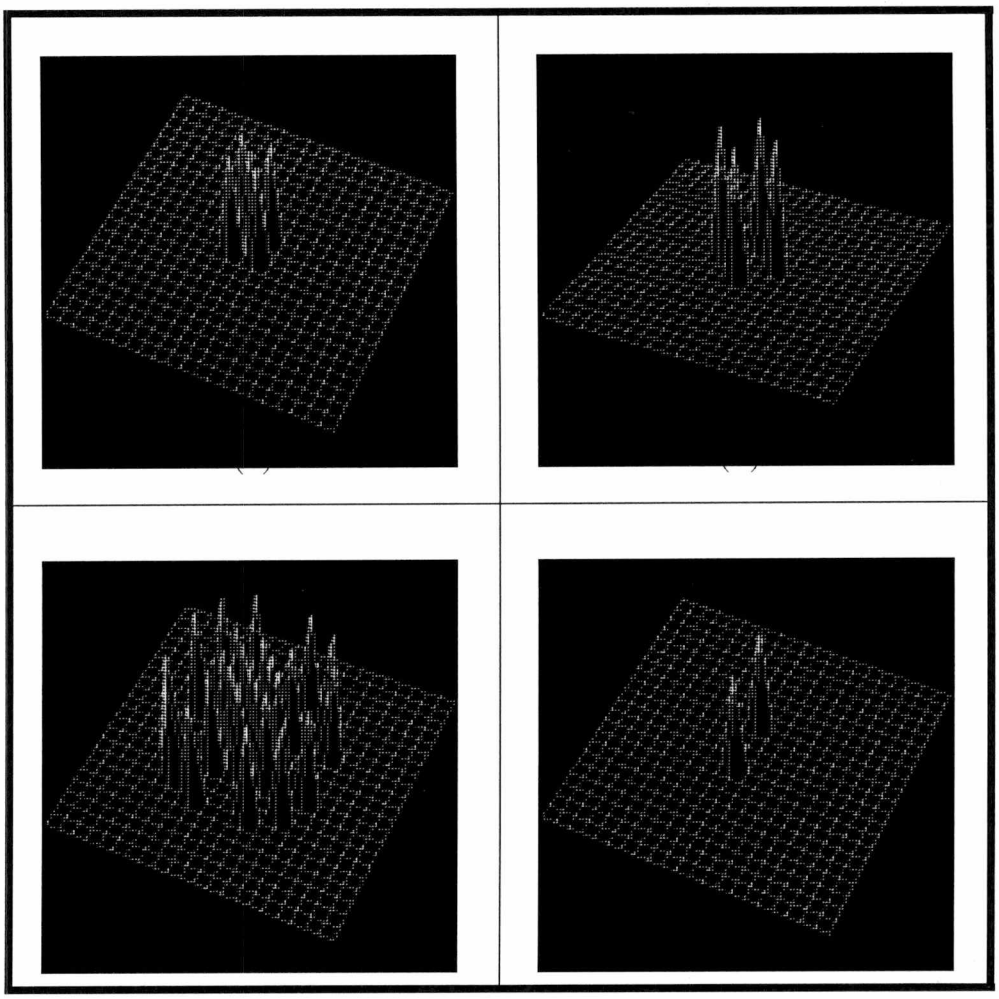


Figure 5.46: The Differences After Learning (a): Square: Max Difference=10; (b): Circle: Max Difference=10; (c): Cross: Max Difference=11; (d): Rectangle: Max Difference=8

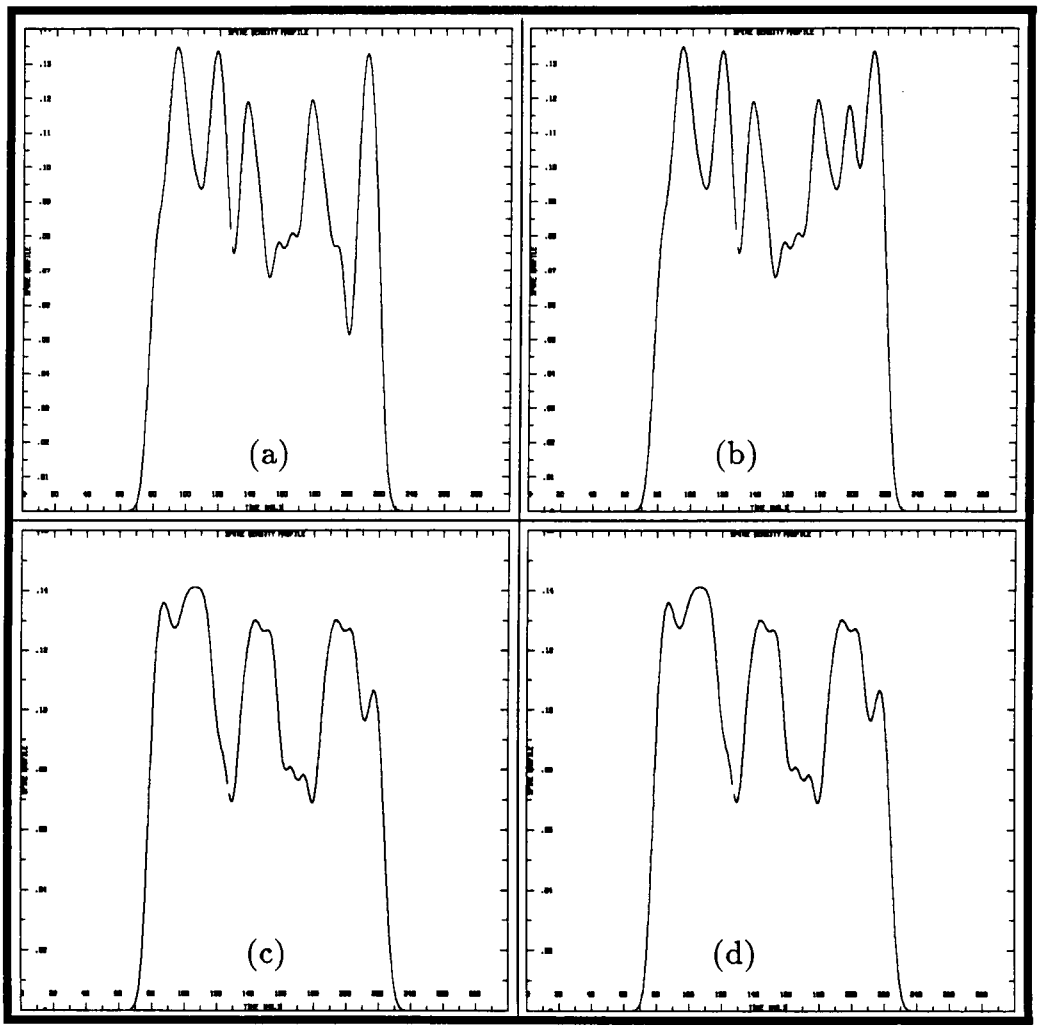


Figure 5.47: Response profiles of E_c (a): Cross no learning; (b): Cross with Learning; (c): Rectangle no learning; (d): Rectangle with Learning

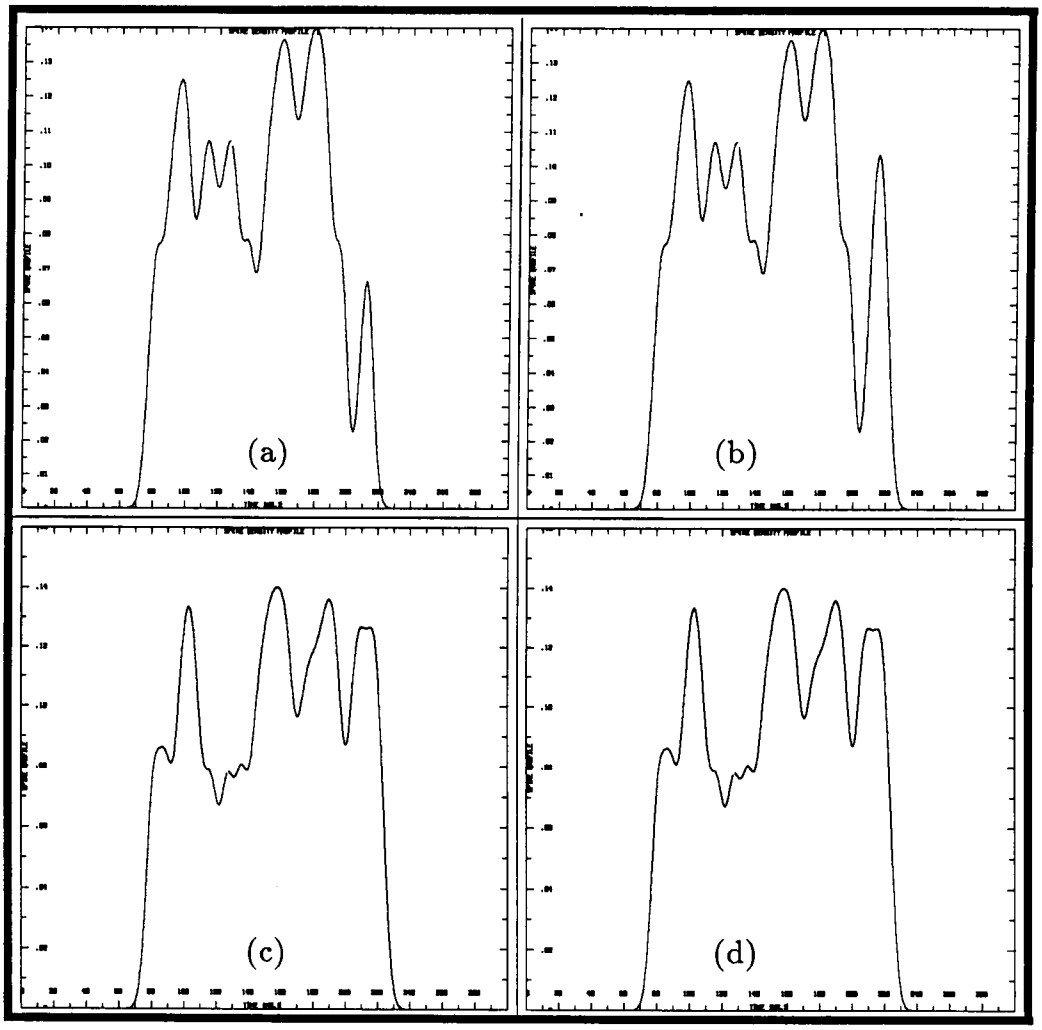


Figure 5.48: Response profiles of E_c (a): Square no learning; (b): Square with Learning; (c): Circle no learning; (d): Circle with Learning

5.5 Clustering Activity With Learning and Memory Mechanisms

The usefulness of any image processing or pattern recognition technique is dependent on a meaningful interpretation of the results by human beings. The simulations presented thus far, while hinting at potential extensions to applications , e.g., decomposing the profiles and computing the coefficients, they have not shown a clear strategy for interpreting the time-varying behaviors of either E_c's profile or the spatial patterns of $E2$. The following has been developed in an attempt to map the time-varying information back into a meaningful spatial domain through clustering in regions in $E2$ that may, with further development, lead to useful interpretations. In addition, learning and memory mechanisms are developed for clustering. The specific mechanisms developed are floating the membrane potentials and increasing the strengths of excitatory links.

5.5.1 The Architecture of the System

The basic architecture of the system is the same as before. There are some fundamental differences as discussed in the following. Since the ultimate goal of this simulation is to cluster regions of activity that reflect specific characteristics of the signal transmitted from the full field of $E2$, each of the changes is designed so that different regions in $E2$ are most sensitive to different stimulation.

Each neuron in $E2$ is centered over $E1$ so that every neuron is seeing exactly the same time-varying spatial pattern. The sizes of the receptive fields vary

randomly across $E2$ so that different regions are more sensitive to different time and spatial frequencies. For the same reason, the strength of the links between each neuron are also varied randomly and the sense of the C/S mechanism (excitatory/inhibitory or inhibitory/excitatory) is also varied randomly. The range of sizes of the receptive fields are: $SEI = 15$ and $CEI = 9$ (large), $SEI = 13$ and $CEI = 7$ (medium), and $SEI = 9$ and $CEI = 5$ (small) for the excitatory/inhibitory configurations; and $SEI = 15$ and $CEI = 7$ (large), $SEI = 13$ and $CEI = 5$ (medium), and $SEI = 9$ and $CEI = 3$ (small) for the inhibitory/excitatory configurations.

The intrayer receptive field dimensions, strengths, and sense of the C/S mechanisms are randomly assigned with a random number generator as with the interlayer connections. These values are set at a constant for all neurons and are relatively high to compensate for the fairly sparse initial activity in $E2$. The excitatory links in the intralayer receptive fields are the only modifiable links.

5.5.2 Learning and Memory For Clustering

The interlayer strengths are initially set to very low values and are allowed to float with stimulation. Learning at this initial stage is very similar to that discussed in Section (5.4). After a time interval if Δt_{learn}, or if a neuron in $E2$ fires prior to a period of Δt_{learn}, the neuron, N_{high}, with the highest average membrane potential, MEM_{high}, during the interval is located.

The average membrane potential of the neighborhood of every neuron with an

average membrane potential greater than or equal to $0.9*MEM_{high}$ is calculated. The neighborhood with the highest average neighborhood potential, MPN_{high}, has it's resting potential changed by an amount ΔMEM_{incr}, where

$$\Delta MEM_{incr} = \frac{MP_{ave}}{MEM_{high}} \frac{\Theta_2 - MEM_{high}}{INC}; \tag{5.3}$$

where Θ_2 is the membrane firing threshold, INC is a constant, and MP_{ave} is the average membrane potential of the neuron.

The resting membrane potential of each neuron in a $L \times L$ neighborhood with an average membrane potential greater than or equal to $0.9 * MEM_{high}$, at a distance greater than or equal to O_{learn} from the center of the neighborhood of every other neighborhood that has been updated is changed by a similar amount. A further constraint on the neurons whose membrane potentials are changed is that the average neighborhood membrane potential is greater than or equal to $0.95 * MPN_{high}$. This continues through each time interval Δt_{learn} until at least one neuron in $E2$ fires.

Once a neuron in $E2$ has fired, the second phase of the learning begins. The excitatory links within an $LS \times LS$ region with the highest spike count during a maximum time interval T_{spikes} are modified. The assumptions for modification are similar to those in Section (5.4); only excitatory links from the most active neurons in the region to other neuron within the region are modified according to

$$\omega_{ji} = \omega_{ji} + LM \frac{SP_i}{SP_J}, \tag{5.4}$$

where each term is defined in Section (5.4).

After a maximum time period of Δt_{PER}, the learning rules are disengaged and all floating membrane potentials and interlayer connection strengths, excluding the most active regions, are reset to their original values. The stimulus is presented for another Δt_{add} time steps to allow the neuron activity to cluster. Each cluster of activity is characterized by the receptive field size and receptive field configuration distributions reflecting the stimulus parameters transmitted from $E1$.

5.5.3 Clustering Activity

The results of incorporating these learning rules are discussed in the following for each of the four basic shapes (circle, square, cross, and rectangle) used throughout this work. The activity, in each case, is clustered around specific areas within layer $E2$. The clustering could be made more localized by further experimentation with the intralayer weights, the size of the region targeted for learnig, and the time interval over which the weights are modified. The reults of learning result in quite distinct regions within layer $E2$ and the receptive field characteristics pertaining to the cluster(s) associated with each shape are distinct. The distributions of the receptive field sizes and the signs of the center mechanisms for the receptive field structures for each of the clusters associated with each shape are given in Table (5.1). The distribution characterizes the information transmitted from $E1$, and, thus, from I.

Each cluster is characterized by a high level of small receptive field activity, corresponding to spatially centralized activity transmitted from the center of layer $E1$. The sign distribution is evenly distributed between excitatory $(+)$ and inhibitory $(-)$ central mechanisms, except in the case of the circle which has predominately inhibitory central mechanisms.

The cluster associated with the circle is also characterized by large and medium excitatory central mechanism receptive fields. The square is characterized by an even distribution of excitatory and inhibitory central mechanisms for the medium sized receptive fields and an inhibitory central mechanism for the large receptive fields.

The rectangle and the cross, each, have two associated clusters. The small receptive fields in both of the rectangle's clusters are evenly distributed between excitatory and inhibitory central mechanisms. One cluster has predominately inhibitory central mechanisms associated with the large receptive fields and predominately excitatory central mechanisms associated with the medium size receptive fields. The second cluster has predominately excitatory central mechanisms associated with the large receptive fields and has an even distribution of excitatory and inhibitory central mechanisms associated with the medium size receptive fields. The clusters associated with the cross have an even distribution of excitatory and inhibitory central mechanisms associated with the small receptive fields and have only excitatory central mechanisms associated with the medium size receptive fields. The difference between the two clusters is that

one has predominately excitatory central mechanisms associated with the large receptive fields while the other has predominately inhibitory central mechanisms associated with the large receptive fields.

The spike distribution after learning is shown in Fig. 5.49. The peaks in each correspond to the regions clustered during learning. The peak in Fig. 5.49 (a), corresponding to the circle, is in the lower left region of $E2$, centered at location $(17, 7)$. Layer $E2$ is a 21×21 array. The lower left peak in Fig. 5.49 (b), corresponding to the cross, is also located at location $(17, 7)$ in $E2$. The second peak is centrally location at $(3, 17)$ in $E2$. The peak in Fig. 5.49 (c), corresponding to the square, is centrally located at $(10, 15)$. The peaks in Fig. 5.49 (d), corresponding to the rectangle, are centrally located at $(12, 4)$ and $(5, 18)$.

For more exact clustering, assumptions could be made about the spatial frequency sensitivities in regions of $E2$ and the weighting and receptive field configurations could be appropriately initialized. It is of interest to note that striate cortex is composed of a columnar organization which is organized according to spatial frequency, in addition to orientation. The sensitivities of the clusters in $E2$ demonstrate that spatial frequency is a potentailly useful feature for clustering in physiological simulations.

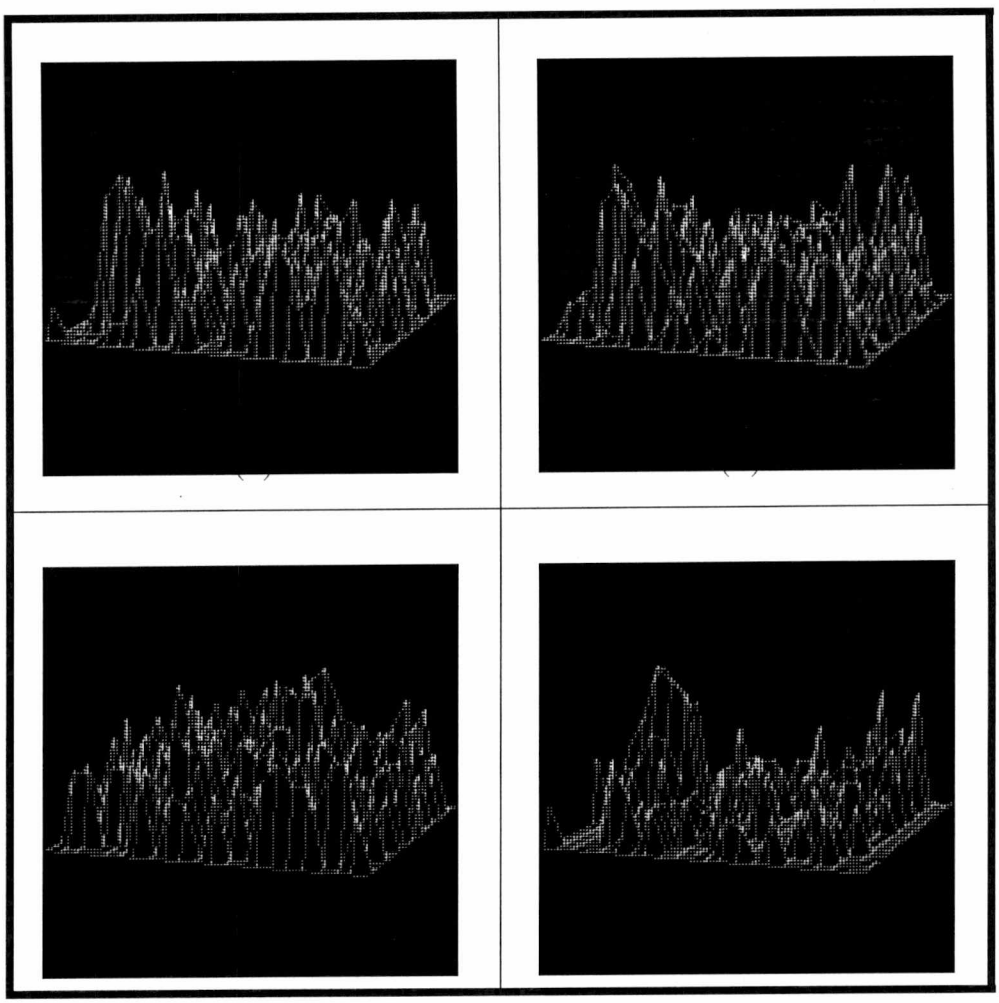


Figure 5.49: Spike distribution with clustering (a): Circle; (b): Cross; (c): Square; (d): Rectangle

CHAPTER 6

Conclusions

The main hypothesis of this thesis is the signal processing mechanisms of physiological neurons encode and transmit information through a temporal modulation of the neuron response spike train, and that software simulations of basic physiological neural mechanisms will result in a time-varying waveform that uniquely describes the information encoded by a model neuron unit. The work in this thesis has drawn from three sources to support this hypothesis: physiology, neural network classifiers, and the simulations developed in this work.

In Chapter 2, the structure of the primary visual pathway was discussed. The primary visual pathway was shown to be a highly structured system, whose structure suggests function in terms of visual processing. Signal flow was traced fom the etina to the lateral geniculate nucleus, midbrain, and, finally, to the visual cortex. The concept of *receptive field* was developed in terms of spatial parameters and was shown to be a basic structure throughout the visual pathway pertinent to signal processing.

In Chapter 3, the physiological visual system was discussed on finer scale: the the dynamics of signal processing for individual neuron units. The signal processing mechanisms were shown to be associated with dynamics along the

neuron membrane. Infomation was shown to be encoded by graded potentials at the neuron membrane and transmitted by both graded potentials and spikes – also at the neuron membane. Some basic neuron models and the structure associated with each model were discussed and it was shown that the dynamics of signal processing performed by a neuron could not be discussed independent of the structure of the ensemble. These models provided a background for the simulations developed in this thesis. Learning and memory mechanisms for each of the models was also discussed and, then, a recent physiologically based learning and memory mechanisms was introduced. This recent physiological mechanisms was shown to support a time-varying output paradigm.

In Chapters 4 and 5, the simulations developed in this thesis were presented. Chapter 4 presented the basic neuron model, designed to simulate physiological mechanisms associated with the time-varying output. The model was extended to an ensemble of neurons. The basic structure of the ensemble was the receptive field configuration of the individual neurons. The function of the receptive field was discussed in terms of a *center/surround* configuration. From this, the *tuning* of the receptive field was developed. The time-varying output behavior for various inputs was demonstrated.

In Chapter 5, some properties of the model were discussed and the behavior of the system under various parameter changes was demonstrated. The physiological visual system is known to process information at different levels of resolution. Simulations were presented to demonstrate coarse and fine resolution

processing. Rotation and shift invariant characteristics of the system were also discussed. Two leaning/memory mechanisms were discussed and the reult of the simulations was a modification of the output waveform, which did not necessarily include a change in the spike count during the peristimulus interval. This behavior was cited as a pertinent characteristic (Chapter 3) involved in quantifying information content of the physiological neuron output waveforms. The two learning/memory mechanisms were extended to a two-layered system that clustered activity in specific regions that were associated with specific inputs.

The main contribution of this thesis is the integration of known physiological signal processing mechanisms into a single model that suports a time-varying response model. The simulations demonstated that these mechanisms can be incorporated into a model that performs some potentially powerful image processing/pattern recognition tasks. In addition, a strong arguement for an interdiscplinary approach to image processing/pattern recognition has been presented. The time-varying output model provides a paradigm for incorporating feature extraction, information encoding and transmission, learning and memory, and recognition in the design of a single system.

BIBLIOGRAPHY

BIBLIOGRAPHY

[1] J. Stone, *Parallel Processing in the Visual System.* Plenum Press, New York, 1983.

[2] E. Wolff, *Anatomy of the Eye and Orbit.* W.B. Saunders Co.: Philadelphia, 7 ed., 1976. Revised by Roger Warwick.

[3] J. Dowling and M. Dublin, "The Vertebrate Retina," in *Handbook of Physiology. Sect. 1*, (J. Brookhart and V. Mountcastle, eds.), pp. 317–340, Waverly Press: Baltimore, 1984.

[4] R. H. Masland, "The Functional Architecture of the Retina," *Scientific American*, vol. 225, no. 6, December 1986.

[5] T. Saito, "Physiological and Morphological Differences Between On- and Off-Center Bipolar Cells in the Vertebrate Retina," *Vision Research*, vol. 27 no. 2, pp. 135–142, 1987.

[6] J. H. Kaas, "The Structural Basis for Information Processing in the Primate Visual System," in *Visual Neuroscience*, (J. Pettigrew, S. K.J., and W. Levick, eds.), pp. 315–340, Cambridge University Press, 1986.

[7] C. Youdelis and A. Hendrickson, "A Qualitative and Quantitative Analysis of the Human Fovea During Development," *Vision Research*, vol. 26 no. 6, pp. 847–855, 1986.

[8] J. I. Yellot, B. A. Wandell, and T. N. Cornsweet, "The Beginnings of Visual Perception: the Retinal Image and its Initial Encoding," in *Handbook of Physiology. Sect. 1*, (J. Brookhart and V. Mountcastle, eds.), pp. 257–316, Waverly Press: Baltimore, 1984.

[9] H. Deubel and T. Elsner, "Threshold Perceptin and Saccadic Eye Movements," *Biological Cybernetics*, vol. 54, pp. 351–358, 1986.

[10] H. Deubel and T. Elsner, "The Effect of Saccades on Threshold Perception - A Model Study," *Biological Cybernetics*, vol. 54, pp. 359–366, 1986.

[11] D. Kelly and C. A. Burbeck, "Motion and Vision .1. Stabilized Images of Stationary Gratings," *J. Opt. Soc. Am.*, vol. 69, no. 9, pp. 1266–1279, 1979.

[12] D. Kelly and C. A. Burbeck, "Motion and Vision.3. Stabilized Spatio-Temporal Threshold Surface," *J. Opt. Soc. Am.*, vol. 69, no. 9, pp. 1340–1349, 1979.

[13] D. Kelly and C. A. Burbeck, "Motion and Vision.3. Stabilized Pattern adaptation," *J. Opt. Soc. Am.*, vol. 70, no. 11, pp. 1283–1289, 1980.

[14] S. Dawis, R. Shapely, E. Kaplan, and D. Tranchina, "The Receptive Field Organization of X-Cells in the Cat: Spatiotemporal Coupling and Asymmetry," *Vision Research*, vol. 24, no. 6, pp. 549–564, 1984.

[15] J. Richter and S. Ullman, "A Model for the Temporal Organization Of X- and Y-Type Receptive Fields in the Primate Retina," *Biological Cybernetics*, vol. 43, pp. 127–145, 1982.

[16] L. Missotten, " Estimation of the Ratio of Cones to Neurons in the Fovea of the Human Retina," *Investigative Opthalmology*, vol. 13, no. 12, pp. 1045–1049, December 1974.

[17] J. G. Malpeli and F. H. Baker, "The Representations of the Visual Field in the Lateral Geniculate Nucleus of Mucaca Mulatta," *Journal of Comparative Neurophysiology*, vol. 161, pp. 569– 594, 1975.

[18] P. Bishop, "Processing of Visual Information Within the Retinostriate System," in *Handbook of Physiology. Sect. 1*, (J. Brookhart and V. Mountcastle, eds.), pp. 341–424, Waverly Press: Baltimore, 1984.

[19] J. Kaas, M. Heurta, J. Weber, and J. Harting, "Patterns of Retinal Terminations and Laminar Organization of the Lateral Geniculate Nucleus of Primates ," *Journal of Comparative Neurophysiology*, vol. 182, pp. 517–554, 1978.

[20] T. T. Norton, V. A. Casagrande, G. E. Irvin, M. A. Sesma, and H. M. Petry, "Contrast-Sensitivity Functions of W-, X-, and Y-Like Relay Cells in the Lateral Geniculate Nucleus of Bush Baby, Gulago crassicaudatus," *Journal of Neurophysiology*, vol. 59, no. 6, 1988.

[21] Beraradi, Nicoletta, and Morrone, "The Role of γ Aminobutryic Acid Mediated Inhibition in the Response Properties of Cat Lateral Geniculate Nucleus Neurones," *Journal of Physiology*, vol. 357, pp. 505–523, 1984.

[22] P. Hammond, "Contrasts in Spatial Organization of Receptive Fields at Geniculate and Retinal Levels: Centre, Surround and Outer Surround ," *Journal of Physiology*, vol. 228, pp. 115–137, 1973.

[23] P. H. Schiller, "The Connections of the Retinal On and Off Pathways to the Lateral Geniculate Nucleus of the Monkey," *Vision Research*, vol. 24, no. 9, pp. 923–932, 1984.

[24] F. D. Monasterio and P. Gouras, " Functional Properties of Ganglion cells of the Rhesus Monkey Retina," *Journal of Physiology*, vol. 251, pp. 167–195, 1975.

[25] J. Nordeen and J. Kaas, "The Identification of Relay Neurons in the Dorsal Lateral Geniculate Nucleus of Monkeys Using Horseradish Peroxidase," *Journal of Comparative Neurophysiology*, vol. 182, pp. 707–726, 1978.

[26] A. K. Sestokas and S. Lehmkuhle, "Visual Response Latency of X- and Y-cells in the Dorsal Lateral Geniculate Nucleaus of the Cat," *Vision Research*, vol. 26, no. 7, pp. 1041–1054, 1986.

[27] J. G. Daugman, "Complete 2-D Gabor Transforms by Neural Networks for Image Analysis and Compression ," *IEEE Transactions on Acoustics, Speech, and Signal Processing*, vol. 36, no. 7, 1988.

[28] C. Stevens, *Neurophysiology: A Primer.*
New York, John Wiley and Sons, 1966.

[29] A. Vander, J. Sherman, and D. Luciano, *Human Physiology: the Mechanics of Body Function.*
McGraw-Hill, New York, 4 ed., 1985.

[30] I. Segev and W. Rall, "Computational Study of an Excitable Dendritic Spine," *Journal of Neurophysiology*, vol. 60, no.2, pp. 499–523, 1988.

[31] A. Guyton, *Physiology of the Human Body.*
Sanders College Publishing, 6 ed., 1984.

[32] C. Vaughan, "A New View of Vision," *Science News*, vol. 134, Jul. 23, pp. 58–60, 1988.

[33] B. Richmond, L. Optican, M. Podell, and H. Spitzer, "Temporal Encoding of Two-Dimensional Patterns by Single Units in Primate Inferior Temporal Cortex. 1. Response Characteristics ," *Journal of Neurophysiology*, vol. 57, pp. 132–146, 1987.

[34] B. Richmond, L. Optican, M. Podell, and H. Spitzer, "Temporal Encoding of Two-Dimensional Patterns by Single Units in Primate Inferior Temporal Cortex. 2. Quantification of Response Waveform ," *Journal of Neurophysiology*, vol. 57, pp. 147–161, 1987.

[35] B. Richmond, L. Optican, M. Podell, and H. Spitzer, "Temporal Encoding of Two-Dimensional Patterns by Single Units in Primate Inferior Temporal Cortex. 3. Information Theoretic Analysis ," *Journal of Neurophysiology*, vol. 57, pp. 162–178, 1987.

[36] A. Hodgkin and A. Huxley, "A Quantitative Description of Membrane Current and its Application to Conduction and Excitation to Nerve ," *Journal of Physiology. London*, vol. 117, pp. 500–544, 1952.

[37] A. Hodgkin, *The Conduction of the Nervous Impulse.* Charles C. Thomas: Sprigfield, Ill, 1964.

[38] H. Tuckwell, *Introduction to Theoretical Neurobiology.* Cambridge University Press, Cambridge, 1988.

[39] R. F. Reiss, ed., *Neural Theory and Modeling.* Stanford University Press, Stanford, Cali., 1964.

[40] F. Hoppensteadt, *An Introduction to the Mathematics of Neurons.* An Introduction to the Mathematics of Neurons, 1986.

[41] F. G. Stremler, *Introduction to Communication Systems.* Addison-Wesley, 2 ed., 1982.

[42] D. Rumelhart, J. McClelland, and the PDP Research Group, *Parallel Distributed Processing: Explorations in the Microstructure of Cognition.* Vol. 1, Foundations, Cambridge, MA: MIT Press/Bradford Books, 1986.

[43] W. D.J. and M. von der C., "How Patterned Nerual Connections can be Set Up by Self-Organization ," *Proc. R. Soc. Lond.B.*, vol. 194, pp. 431–445, 1976.

[44] D. Hebb, *The Organization of Behavior.* Wiley: New York, 1949.

[45] G. Lynch, *Synapses, Circuits, and the Beginnings of Memory.* Cambridge: The MIT press, 1986.

[46] M. Bear, L. Cooper, and F. Ebner., "A Physiological Basis for a Theory of Synapse Modification," *Science*, vol. 237, 1987.

[47] J. Buhman and K. Schulten, "Associative Recognition and Storage in a Model Network of Physiological Neurons ," *Biological Cybernetics*, vol. 54, pp. 319–335, 1986.

[48] D. Marr, *Vision.* W. H. Freeman and Company, New York, 1982.

[49] W. Rall, "Time Constants and Electrotonic Length of Membrane Cylinders and Neurons," *Biophysical Journal*, vol. 9, pp. 1483–1508, 1969.

[50] W. Rall and J. Rinzell, "Branch Input Resistance and Steady Attenuation for Input to One Branch of a Dendritic Neuron model," *Biophysical Journal*, vol. 13, pp. 648–688, 1973.

[51] J. Rinzell, "Neuronal Plasticity (Learning)," *Lectures on Mathematics in the Life Sciences*, vol. 15, pp. 7–25, 1982.

VITA

Hal Beck was born in May of 1957 in Topeka, Kansas. He has a Bachelor of Arts in Psycholgy and a Bachelor of Science in Electrical Engineering. His research interests are physiological mechanisms associated with information processing in the human visual tract and image understanding.